TU/e EINDHOVEN UNIVERSITY OF TECHNOLOGY

The Shubnikov-de Haas effect in Cd3As2, CdSnAs2 and (Cd1-xMnX)3As2

Citation for published version (APA):
Neve, J. J. (1984). *The Shubnikov-de Haas effect in Cd3As2, CdSnAs2 and (Cd1-xMnX)3As2*. [Phd Thesis 1 (Research TU/e / Graduation TU/e), Applied Physics and Science Education]. Technische Hogeschool Eindhoven. https://doi.org/10.6100/IR137462

DOI:
10.6100/IR137462

Document status and date:
Published: 01/01/1984

Document Version:
Publisher's PDF, also known as Version of Record (includes final page, issue and volume numbers)

Please check the document version of this publication:

• A submitted manuscript is the version of the article upon submission and before peer-review. There can be important differences between the submitted version and the official published version of record. People interested in the research are advised to contact the author for the final version of the publication, or visit the DOI to the publisher's website.
• The final author version and the galley proof are versions of the publication after peer review.
• The final published version features the final layout of the paper including the volume, issue and page numbers.

Link to publication

General rights
Copyright and moral rights for the publications made accessible in the public portal are retained by the authors and/or other copyright owners and it is a condition of accessing publications that users recognise and abide by the legal requirements associated with these rights.

• Users may download and print one copy of any publication from the public portal for the purpose of private study or research.
• You may not further distribute the material or use it for any profit-making activity or commercial gain
• You may freely distribute the URL identifying the publication in the public portal.

If the publication is distributed under the terms of Article 25fa of the Dutch Copyright Act, indicated by the "Taverne" license above, please follow below link for the End User Agreement:

www.tue.nl/taverne

Take down policy
If you believe that this document breaches copyright please contact us at:

openaccess@tue.nl

providing details and we will investigate your claim.

Download date: 08. Jul. 2024

THE SHUBNIKOV-DE HAAS EFFECT IN Cd_3As_2, $CdSnAs_2$ AND $(Cd_{1-x}Mn_x)_3As_2$

J.J. NEVE

THE SHUBNIKOV-DE HAAS EFFECT IN Cd_3As_2, $CdSnAs_2$ AND $(Cd_{1-x}Mn_x)_3As_2$

PROEFSCHRIFT

ter verkrijging van de graad van doctor in de technische wetenschappen aan de Technische Hogeschool Eindhoven, op gezag van de rector magnificus, prof. dr. S.T.M. Ackermans, voor een commissie aangewezen door het college van dekanen in het openbaar te verdedigen op dinsdag 10 april 1984 te 16.00 uur

door

Johannes Jacobus Neve

geboren te Kloosterzande

1984

Offsetdrukkerij Kanters B.V.,
Alblasserdam

Dit proefschrift is goedgekeurd door de promotoren
Prof.dr. M.J. Steenland en Prof.dr. F. van der Maesen
Co-promotor: Dr.ir. F.A.P. Blom

Aan Maatje en Jos

TABLE OF CONTENTS

CHAPTER I INTRODUCTION

The work described in this thesis has been performed in the group Semiconductor Physics of the Solid State Division of the Department of Physics of the Eindhoven University of Technology. The research in this group is concentrated on electrical transport and optical properties of semiconducting compounds. A part of the interest is concentrated on the study of narrow gap semiconductors (NGSC) of II-V and II-IV-V_2 compounds, such as Cd_3As_2 and $CdSnAs_2$, respectively. Recently the study of the $(Cd_{1-x}Mn_x)_3As_2$ mixed crystal system has started. This thesis deals with an investigation of the geometry of the conduction band Fermi-surfaces as function of the electron concentration of degenerate n-type Cd_3As_2, $CdSnAs_2$ and $(Cd_{1-x}Mn_x)_3As_2$ by means of the Shubnikov-de Haas (SdH)-effect.

In the past two decades there has been a growing interest in the II-V compounds such as Cd_3As_2 and Cd_3P_2 because of their small energy gaps, low effective masses and high mobilities [1-3]. The investigations of the band structure of Cd_3As_2 have been hampered for a long time due to the difficulties appearing in the preparation of good quality single crystals and the ever present high electron concentration. In addition the crystal structure (Cd_3As_2 crystallizes in a body centered tetragonal structure with 160 atoms per unit cell, spacegroup C_{4v}^{12} [4,5]) makes direct calculation of the band structure extremely complicated.
In spite of the tetragonal crystal structure and the early observations by Rosenman [6] and Doi et al. [7] of the conduction band anisotropy, the experimental electrical transport and optical data have been interpreted in terms of an isotropic Kane-type band model throughout the years [8]. Aubin et al. [9,10] constructed in a phenomenological way a band model for Cd_3As_2 which was consistent with all relevant data available at that moment. In this Kane-type model an inverted band structure ($E_g<0$) was adopted and a small indirect gap between the conduction band and the heavy hole valence band was assumed. The acceptability of their main ideas was confirmed theoretically by pseudopotential calculations [11] as well as experimentally [12-14]. In the mean time Bodnar [15] developed

an improved model, incorporating the anisotropy of the interband momentum matrix elements and the crystal field splitting. From a reinterpretation of earlier SdH- and dHvA (de Haas - van Alphen)-data [6,7] Bodnar concluded that Cd_3As_2 has an inverted band structure and a positive crystal field splitting. He obtained values of the primary band-parameters from measurements which covered only a narrow range of electron concentrations beyond $1 * 10^{24}$ m^{-3}. Since the Bodnar-model predicts a considerable increase of the anisotropy with decreasing electron concentration, we started the investigations of the SdH-effect in low concentration samples, which could be obtained due to improvements in material technology [12].
The validity of the Bodnar-model and its extension to quantising magnetic fields [16] have been examined for Cd_3As_2 in a large electron concentration range. The experimental results of these investigations are presented in this thesis.

The model proposed by Bodnar in order to interpret the anisotropy of the conduction band of Cd_3As_2 is essentially the same as Kildal's band model [17] for $CdGeAs_2$, which seems applicable to chalcopyrite II-IV-V_2 compounds in general [18]. Out of this family $CdSnAs_2$ is an attractive compound to be studied by means of the SdH-effect because of its narrow bandgap and its relatively high electron mobility. $CdSnAs_2$ is believed to have the normal ordering of the energy levels ($E_g > 0$) and a negative crystal field splitting [18]. Data on the anisotropy of the conduction band of $CdSnAs_2$, however, are scarce. Moreover, the available data on the anisotropy of the effective mass [19,20] obtained from optical measurements indicated a considerably higher anisotropy of the conduction band than expected from the Bodnar (Kildal)-model by substituting the generally accepted values of the bandparameters [18]. The present study of the SdH-effect was undertaken in order to determine the anisotropy of the conduction band of $CdSnAs_2$ in more detail and to verify the applicability of the Bodnar (Kildal)-model for this material.

Recently, a new class of semiconducting materials has been attracting much attention [21]. Mixed crystals have been formed by alloying II-VI semiconducting compounds, such as CdSe and HgTe, and magnetic transition

metal compounds MnSe, MnTe [22,23]. Due to the exchange interaction between the mobile carriers and the electrons in the partly filled d-shell of the transition metal ion, the spin dependent electronic properties of these materials change drastically with temperature and magnetic field.

During the study in our group of transport and optical properties of Cd_3As_2, it was realised that an alloy of Cd_3As_2 with the magnetic compound Mn_3As_2 could be a potential new member of what is called the group of semimagnetic semiconductors (SMSC). Since Cd_3As_2 has a tetragonal crystal structure it was expected that the mixed crystal system $(Cd_{1-x}Mn_x)_3As_2$ would introduce anisotropic features of the spin dependent electronic properties into the research of SMSC. SdH-measurements have been performed on $(Cd_{1-x}Mn_x)_3As_2$ samples with a low magnetic ion content ($x \leq 0.05$) in order to check whether $(Cd_{1-x}Mn_x)_3As_2$ is indeed a SMSC and to verify the band model developed for this material. Due to the narrow electron concentration range of the measured samples we are not able to give an elaborate quantitative description of the temperature and field dependences of the band structure of this mixed crystal system. Therefore only a tentative interpretation of our measurements in the band model for tetragonal SMSC is presented in this thesis.

The thesis is organised as follows. In chapter II brief descriptions are given of the Bodnar-model, its extension in the presence of quantising magnetic fields and of the SMSC band model, i.e. including terms due to the exchange interaction. The theory of the SdH-effect is treated qualitatively from the motion of a free electron in a magnetic field in chapter III, while the experimental set-ups and data taking procedures are given in chapter IV. In chapter V the results of our SdH-measurements on Cd_3As_2-, $CdSnAs_2$- and $(Cd_{1-x}Mn_x)_3As_2$-samples are presented and interpreted in the models treated in chapter II. The main results and conclusions are summarised in chapter VI.
References are given at the end of each chapter.
§2.3 and parts of §5.1, §5.2 and §5.3 have already been published elsewhere [24-27].

REFERENCES

[1] W. Żdanowicz, L. Żdanowicz, Ann. Rev. of Material Science Vol. 5, (Ann. Reviews, Palo Alto, California, 1975), p. 301.

[2] D.N. Nasledov, V.Ya. Shevchenko, Phys. Stat. Solidi A15, 9 (1973).

[3] Proc. 1st. Int. Symposium on the Phys. and Chem. of II-V Compounds, Mogilany 1980, ed. M.J. Gelten, L. Żdanowicz, (Eindhoven University of Technology, 1981).

[4] G.A. Steigman, J. Goodyear, Acta Cryst. B24, 1062 (1968).

[5] P.J. Lin-Chung, Phys. Rev. 188, 1272 (1969).

[6] I. Rosenman, J. Phys. Chem. Solids 30, 1385 (1969).

[7] H. Doi, T. Fukuroi, T. Fukase, Y. Muto, K. Tanaka, Sci. Rep. Inst. Tohoku Univ. A20, 190 (1969).

[8] F.A.P. Blom, Narrow Gap Semiconductor Physics and Applications, ed. W. Zawadzki, (Springer Verlag, Berlin, 1980), p. 191.

[9] M.J. Aubin, L.G. Caron, J.P. Jay-Gérin, Phys. Rev. B15, 3872 (1977).

[10] L.G. Caron, J.P. Jay-Gérin, M.J. Aubin, Phys. Rev. B15, 3879 (1977).

[11] B. Dowgiallo-Plenkiewicz, P. Plenkiewicz, Phys. Stat. Solidi B87, 309 (1978).

[12] F.A.P. Blom, M.J. Gelten, Phys. Rev. B19, 2411 (1979).

[13] M.J. Gelten, C.M. van Es, F.A.P. Blom, J.W.F. Jongeneelen, Solid State Commun. 33, 833 (1980).

[14] J. Cisowski, E.K. Arushanov, J. Bodnar, K. Kloc, W. Żdanowicz, Proc. Int. Conf. Phys. Semicond., Edinburgh, 1978 (Institute of Physics, Bristol/London, 1979), p. 253.

[15] J. Bodnar, Proc. Int. Conf. Phys. Narrow-Gap Semicond., Warsaw, 1977 (Polish Scientific Publ. Warsaw, 1978), p. 311.

[16] P.R. Wallace, Phys. Stat. Solidi B92, 49 (1979).

[17] H. Kildal, Phys. Rev. B10, 5082 (1974).

[18] J.L. Shay, J.H. Wernick, Ternary Chalcopyrite Semicond., (Pergamon Press, Oxford, 1975), p. 85.

[19] R.K. Karymshakov, Yu. I. Ukhanov, Yu.V. Shmartsev, Sov. Phys.-Semicond. 4, 1702 (1971).

[20] T.A. Polyanskaya, I.N. Zimkin, V.M. Tuchkevich, Yu.V. Shmartsev, Sov. Phys.-Semicond. 2, 1215 (1969).

[21] R.R. Galazka, Proc. Int. Conf. Phys. Semicond., Edinburgh, 1978, (Institute of Physics, Bristol/London, 1979), p. 133.

[22] M. Jaczinsky, J. Kossut, R.R. Galazka, Phys. Stat. Solidi B88, 73 (1978).

[23] S. Takeyama, R.R. Galazka, Phys. Stat. Solidi B96, 413 (1979).

[24] J.J. Neve, J. Kossut, C.M. van Es, F.A.P. Blom, J. Phys. C: Solid State Phys. 15, 4795 (1982).

[25] F.A.P. Blom, J.W. Cremers, J.J. Neve, M.J. Gelten, Solid State Commun. 33, 69 (1980).

[26] J.J. Neve, C.F.J. de Meyer, F.A.P. Blom, J. Phys. Chem. Sol. 42, 975 (1981).

[27] J.J. Neve, C.J.R. Bouwens, F.A.P. Blom, Solid State Commun. 38, 27 (1981).

CHAPTER II BAND MODELS FOR TETRAGONAL SEMICONDUCTORS

In this chapter the four level band model developed by Bodnar [3] and Kildal [4] for a tetragonal semiconductor is described briefly (§2.1). Taking this model as a starting point Wallace [8] calculated the band structure of Cd_3As_2 in the presence of quantising magnetic fields. In §2.2 the main steps of his calculations are given. An extension of the calculation of Wallace to the case of $(Cd_{1-x}Mn_x)_3As_2$ is given in §2.3, where the terms due to the exchange interaction of conduction electrons with those in the 3d shells of Mn-ions have been taken into account.

2.1. The Bodnar-model

Using the proper symmetry in the Γ-point (pointgroup C_{4v}), Bodnar has calculated the influence of the tetragonal crystal field on the three level Kane-model [1,2] for tetragonal semiconductors with a narrow bandgap. Only a very small part of the results he obtained during the preparation of his Ph.D. thesis has been published. Unfortunately completion of his thesis and the rest he planned to, was not to be. In Bodnar's contribution on the band structure of Cd_3As_2 [3] at the Warsaw Conference, only a symplified version of the secular equation obtained from his calculations has been given. This symplified secular equation, was obtained by neglecting the lack of inversion symmetry as well as the anisotropy in the spin-orbit interaction [1]. It coincides with the results given by Kildal [4] for the band structure of the chalcopyrite $CdGeAs_2$. Following Hopfield [5] Kildal approximated the real field of $CdGeAs_2$ by a cubic field plus a tetragonal distortion.
A similar approach can be used to calculate the four level band model of Cd_3As_2 in the vicinity of the Γ-point. In that case the field of Cd_3As_2 is represented by adding a tetragonal distortion to the cubic field of fluorite. Following Van Doren et al. [6] a brief description of this approximation is given in this section.

Including spin-orbit coupling, the Schrödinger equation for an electron in the periodic potential $V(\vec{r})$ can be written as:

$$\{\frac{p^2}{2m_o} + V + \sum_j \frac{\hbar}{4m_o^2c^2} (\vec{\nabla}V \times \vec{p})_j \cdot \vec{\sigma}_j\} \psi_k = E_k \psi_k \quad , \tag{2.1}$$

where $\vec{p}$ is the momentum operator and the $\vec{\sigma}_j$ are the Pauli-spin matrices. Eq. 2.1 can be rewritten by introducing the Bloch-functions $\psi_k = u_k e^{i\vec{k}.\vec{r}}$, where u_k has the periodicity of the lattice. The following equation is obtained:

$$\{\frac{p^2}{2m_o} + V + \frac{\hbar}{m_o} \vec{k}.\vec{p} + \sum_j \frac{\hbar}{4m_o^2c^2} (\vec{\nabla}V \times \vec{p})_j \cdot \vec{\sigma}_j\} u_k$$

$$= (E_k - \frac{\hbar^2 k^2}{2m_o}) u_k \quad , \tag{2.2}$$

where the $\vec{k}$-dependent spin-orbit interaction term $\sum_j \frac{\hbar^2}{4m_o^2c^2} (\vec{\nabla}V \times \vec{k})_j . \vec{\sigma}_j u_k$ has been neglected since the spin-orbit coupling is more effective in the interior of the atom [2]. The real crystal potential V is written as $V=V_o+V_t$, where V_t represents the deviation of the crystal potential from the potential V_o with cubic symmetry. In order to calculate the band structure near $\vec{k}=0$, the unperturbed Hamiltonian $H_o = p^2/2m_o + V_o$ is considered to be solved exactly. The tetragonal distortion of the cubic potential [6,7], the $\vec{k}.\vec{p}$ term and the spin-orbit coupling are treated as first order perturbations.

Linear combinations of the wavefunctions S, X, Y, Z of the unperturbed eigenvalue problem have been used as basis functions for the matrix representation of the total Hamiltonian. The following set of basis states, which diagonalise the spin-orbit interaction is chosen [8,9]:

$$u_1 = |\, i\, S \downarrow\rangle \qquad u_5 = |-\frac{1}{\sqrt{6}} (X+iY) \downarrow + \frac{2}{\sqrt{6}} Z \uparrow\rangle$$

$$u_2 = |\, i\, S \uparrow\rangle \qquad u_6 = |\frac{1}{\sqrt{2}} (X+iY) \uparrow\rangle \tag{2.3}$$

$$u_3 = |\frac{1}{\sqrt{2}} (X-iY) \downarrow\rangle \qquad u_7 = |-\frac{1}{\sqrt{3}}(X-iY) \uparrow + \frac{1}{\sqrt{3}} Z \downarrow\rangle$$

$$u_4 = |\frac{1}{\sqrt{6}} (X-iY) \uparrow + \frac{2}{\sqrt{6}} Z \downarrow\rangle \qquad u_8 = |\frac{1}{\sqrt{3}} (X+iY) \downarrow + \frac{1}{\sqrt{3}} Z \uparrow\rangle \quad .$$

The symbols ↑ and ↓ mean spin-up and spin-down functions, respectively. The functions X, Y, Z and S refer to the unperturbed valence band and conduction band wave functions, respectively. They transform like atomic p and s functions under the operations of the cubic group at the Γ-point. In this basis the total 8 x 8 Hamiltonian-matrix can be written as

$$H = \begin{vmatrix} H_1 & H_2 \\ H_2^{\dagger} & H_3 \end{vmatrix} \tag{2.4}$$

with

$$H_1 = \begin{bmatrix} E_s & 0 & P_{\perp}k_- & \sqrt{\frac{2}{3}}\,P_{/\!/}k_z \\ 0 & E_s & 0 & \sqrt{\frac{1}{3}}\,P_{\perp}k_- \\ P_{\perp}k_+ & 0 & E_p + \frac{\Delta}{3} + \frac{\delta}{3} & 0 \\ \sqrt{\frac{2}{3}}\,P_{/\!/}k_z & \sqrt{\frac{1}{3}}\,P_{\perp}k_+ & 0 & E_p + \frac{\Delta}{3} + \frac{\delta}{3} \end{bmatrix}$$

$$H_2 = \begin{bmatrix} -\sqrt{\frac{1}{3}}\,P_{\perp}k_+ & 0 & \sqrt{\frac{1}{3}}\,P_{/\!/}k_z & \sqrt{\frac{2}{3}}\,P_{\perp}k_+ \\ \sqrt{\frac{2}{3}}\,P_{/\!/}k_z & P_{\perp}k_+ & -\sqrt{\frac{2}{3}}\,P_{\perp}k_- & \sqrt{\frac{1}{3}}\,P_{/\!/}k_z \\ 0 & 0 & 0 & 0 \\ 0 & 0 & \frac{-\sqrt{2}}{3}\,\delta & 0 \end{bmatrix} \tag{2.5}$$

$$H_3 = \begin{bmatrix} E_p + \frac{\Delta}{3} - \frac{\delta}{3} & 0 & 0 & -\frac{\sqrt{2}}{3}\,\delta \\ 0 & E_p + \frac{\Delta}{3} + \frac{\delta}{3} & 0 & 0 \\ 0 & 0 & E_p - \frac{2}{3}\,\Delta & 0 \\ -\frac{\sqrt{2}}{3}\,\delta & 0 & 0 & E_p - \frac{2}{3}\,\Delta \end{bmatrix}$$

In the matrices the eigenvalues of the unperturbed Hamiltonian have been denoted by E_s and E_p, while $k_\pm$ stands for $\frac{1}{\sqrt{2}}(k_x \pm i\,k_y)$. The quantities known as the interband momentum matrix elements ($P_{//}$, $P_\perp$), the spin-orbit splitting parameter (Δ) and the crystal field splitting parameter (δ) are defined as [4]:

$$P_{//} \equiv -\frac{i\hbar}{m_o}\langle S|p_x|X\rangle = -\frac{i\hbar}{m_o}\langle S|p_y|Y\rangle$$

$$P_\perp \equiv -\frac{i\hbar}{m_o}\langle S|p_z|Z\rangle$$

$$\Delta \equiv \frac{3i\hbar}{4m_o^2c^2}\langle X|\frac{\partial V_o}{\partial x}p_y - \frac{\partial V_o}{\partial y}p_x|Y\rangle = \frac{3i\hbar}{4m_o^2c^2}\langle X|\frac{\partial V_o}{\partial x}p_z - \frac{\partial V_o}{\partial z}p_x|Z\rangle =$$

$$\frac{3i\hbar}{4m_o^2c^2}\langle Y|\frac{\partial V_o}{\partial y}p_z - \frac{\partial V_o}{\partial z}p_y|Z\rangle \qquad (2.6)$$

$$\delta \equiv 3\langle X|V_t|X\rangle = 3\langle Y|V_t|Y\rangle = -\frac{3}{2}\langle Z|V_t|Z\rangle$$

The anisotropy of Δ has been neglected, since there exist no experimental data which justify such a refinement.
After diagonalisation of the matrix H, the following secular equation, which determines the eigenvalues, is obtained [3,4,6]:

$$\gamma(E') = f_1(E')\{k_x^2 + k_y^2\} + f_2(E')k_z^2 \qquad (2.7)$$

with

$$\gamma(E') = E'(E'-E_g)\{E'(E'+\Delta) + \delta(E'+\tfrac{2}{3}\Delta)\}$$

$$f_1(E') = P_\perp^2\{E'(E'+\tfrac{2}{3}\Delta) + \delta(E'+\tfrac{\Delta}{3})\} \qquad (2.8)$$

$$f_2(E') = P_{//}^2\{E'(E'+\tfrac{2}{3}\Delta)\} \quad ,$$

where

$$E' = E - \frac{\hbar^2k^2}{2m_o} \quad .$$

The $\frac{\hbar^2 k^2}{2m_o}$ term is the free electron term, which from now on will be neglected.

Equation 2.7 has been obtained by shifting the zero of energy i.e. by assuming $E_p + \frac{\Delta}{3} + \delta = 0$ and replacing E_s by the energy gap E_g. This relation reduces to the Kane-band model when $\delta = 0$ and $P_{//} = P_{\perp}$. Eg. 2.7 describes the four band model of tetragonal semiconductors with a narrow bandgap, i.e. normal as well as inverted bandstructure ($E_g > 0$ or $E_g < 0$) and with $\delta > 0$ as well as with $\delta < 0$. For $\vec{k} = 0$ the eigenvalues become 0, E_g, E_1 and E_2 with

$$E_{1,2} = -\frac{(\Delta+\delta)}{2} \pm \frac{1}{2}\left[(\Delta+\delta)^2 - \frac{8}{3}\Delta\delta\right]^{\frac{1}{2}}$$

The level $E = E_g$ originates from a non-degenerate s-like atomic level, while the levels $E = 0$, E_1 and E_2 originate from a triply degenerate p-like atomic level, splitted by the simultaneous influence of the spin-orbit interaction and the non-cubic crystal field. Due to the narrow bandgap the states at finite $\vec{k}$ will have a mixed s-p type character.

In fig. 2.1 the solutions of eq. 2.7 are shown as functions of k_x and k_z for the four possible combinations of E_g and δ. $E_g > 0$ and $\delta < 0$ applies to the chalcopyrite structure of $CdGeAs_2$ which results in the following ordering of the levels at $\vec{k} = 0$: $E_g > E_1 > E = 0 > E_2$ [4]. For Cd_3As_2 Bodnar [3] found $E_g < 0$ and $\delta > 0$ from fits of the anisotropies in the period of the SdH-oscillations and in the cyclotron effective mass. A negative bandgap and a positive crystal field splitting result in $E = 0 > E_1 > E_g > E_2$ at $\vec{k} = 0$ and $E = 0$ is the energy of the conduction band at $\vec{k} = 0$.

It should be noted that for $E_g < 0$, $\delta > 0$ the conduction band ($E = 0$ at $\vec{k} = 0$) and the heavy hole band ($E = E_1$ at $\vec{k} = 0$) and for $E_g > 0$, $\delta < 0$ the heavy hole band ($E = E_1$ at $\vec{k} = 0$) and light hole band ($E = 0$ at $\vec{k} = 0$) do not overlap, but touch at one point in the k_z-direction. These bands neither overlap nor touch for other directions of the wavevector. In the k_z-directions the bands will not touch any longer when the effect of higher and lower bands has been incorporated. Furthermore, taking into account these effects the flat parts of the conduction bands and heavy hole valence bands in fig. 2.1 obtain a finite curvature.

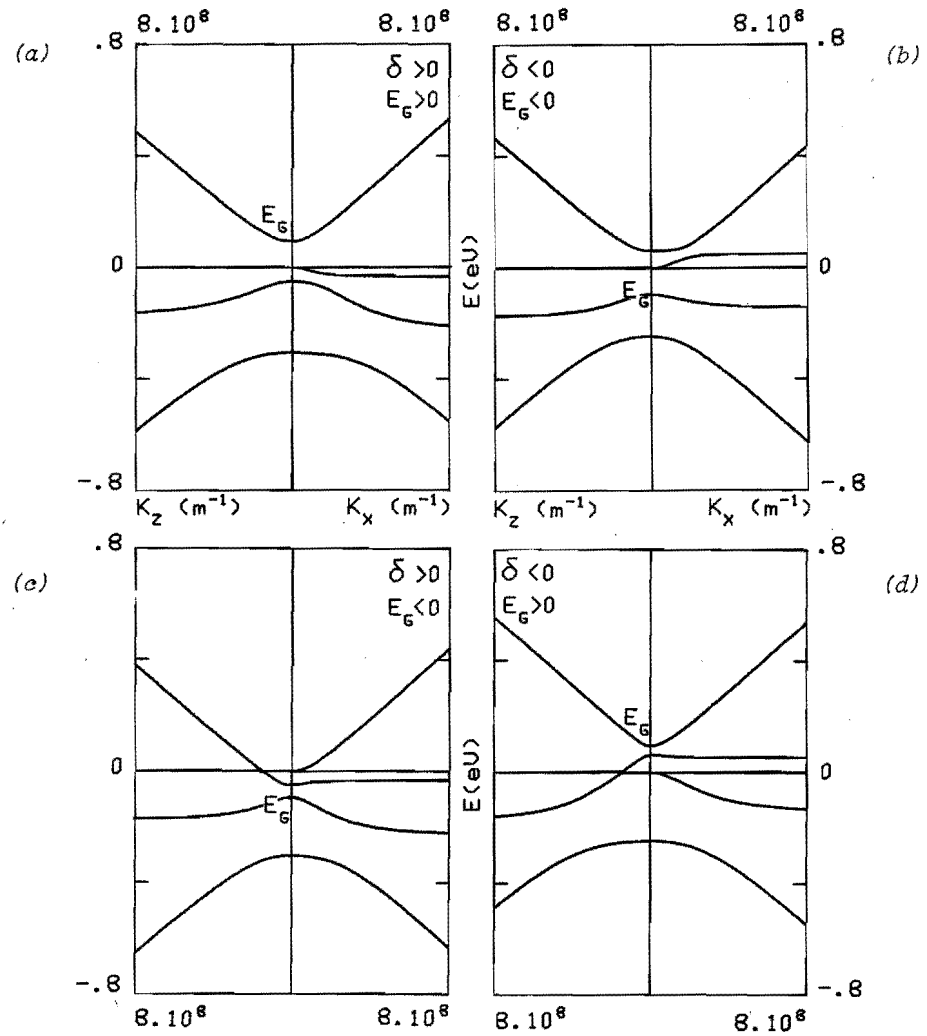

*Fig.2.1. Schematic diagrams of the energy band structures near $\vec{k} = 0$ resulting from the Bodnar-model. The parameters $P_{//}$, $P_{\perp}$ and Δ are 7.21 * 10^{-10} eVm, 7.43 * 10^{-10} eVm and 0.27 eV, respectively. The values of E_g are 0.095 eV (a,d) and -0.095 eV (b,c). The values of δ are 0.085 eV (a,c) and -0.085 eV (b,d). Fig.2.1.c represents the level ordering in Cd_3As_2 while fig.2.1.d gives the ordering in $CdSnAs_2$.*

2.2. The Bodnar-model in a magnetic field

A model which describes the band structure of Cd_3As_2 in the presence of quantising magnetic fields taking the Bodnar-model as a starting point, has been developed by Wallace [8]. This model plays an important role in the interpretation of our experimental data on Cd_3As_2 and $CdSnAs_2$, in particular concerning the cyclotron effective mass and the effective g-factor. The main steps of Wallace's extension of the Bodnar-model are given in this section.

In a magnetic field making an arbitrary angle θ with the c-axis (= z-direction) the Landau-levels are obtained by introducing the following coordinate transformation:

$$\begin{aligned} k_x' &= k_x \cos\theta - k_z \sin\theta \\ k_y' &= k_y \\ k_z' &= k_x \sin\theta + k_z \cos\theta \quad . \end{aligned} \tag{2.9}$$

With eq. 2.9 the secular equation 2.7 is written as:

$$\gamma(E) = Ak_x'^2 + Bk_y'^2 + Ck_z'^2 + 2Dk_x'k_z' \tag{2.10}$$

where

$$\begin{aligned} A &= f_1 \cos^2\theta + f_2 \sin^2\theta \\ B &= f_1 \\ C &= f_1 \sin^2\theta + f_2 \cos^2\theta \\ D &= (f_1 - f_2) \sin\theta \cos\theta \quad . \end{aligned} \tag{2.11}$$

The quantities γ, f_1 and f_2 are defined in eq. 2.8. Using the commutation relations

$$[k_x', k_y'] = -i/l^2$$

$$[k_x', k_z'] = [k_y', k_z'] = 0 \quad , \tag{2.12}$$

where l is the classical cyclotron radius $\sqrt{\hbar/eB}$ of the lowest oscillator orbit, Wallace obtained the following creation and annihilation operators:

$$\Lambda^{\pm} = \sqrt{A}k_x' \pm i\sqrt{B}k_y' + (D/\sqrt{A})k_z' \quad . \tag{2.13}$$

Making use of the commutation rules for the unprimed k's and the operators Λ^+ and Λ^-, the Landau-levels can be calculated from the diagonalisation of the Bodnar-Hamiltonian matrix. The secular equation then becomes:

$$\gamma(E) = \frac{2n+1}{l^2}\left[f_1(f_1\cos^2\theta + f_2\sin^2\theta)\right]^{\frac{1}{2}} + \frac{f_1 f_2 k_z'^2}{f_1\cos^2\theta + f_2\sin^2\theta}$$
$$\pm \frac{P_\perp \Delta}{3l^2}\left[(E+\delta)^2 P_\perp^2 \cos^2\theta + E^2 P_{/\!/}^2 \sin^2\theta\right]^{\frac{1}{2}} \quad , \tag{2.14}$$

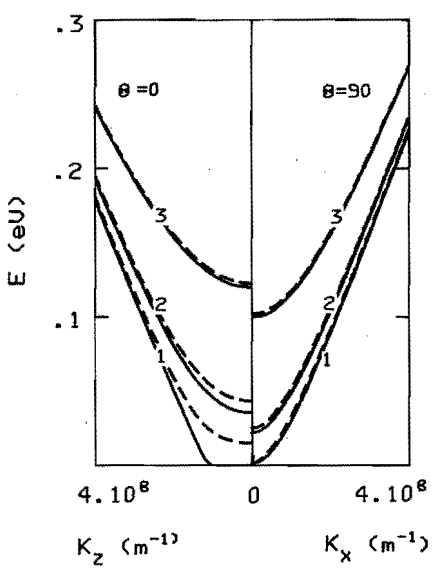

Fig. 2.2.
The conduction band Landau-levels calculated from eq. 2.14 for B parallel to the c-axis (B = 2 T, θ = 0) and B perpendicular to the c-axis (B = 2 T, θ = 90). The curves 1,2,3 correspond to the spin splitted Landau-levels 0^-, 0^+; 2^-, 2^+; 10^- and 10^+, respectively. The values of the parameters are $P_{/\!/} = 7.21 * 10^{-10}$ eVm, $P_\perp = 7.43 * 10^{-10}$ eVm, $\Delta = 0.27$ eV, $\delta = 0.085$ eV and $E_g = -0.095$ eV.

where all symbols have their usual meaning.
The first term on the right hand side of 2.14 represents the quantisation of $(k_x'^2 + k_y'^2)$, the second term is unaffected by the magnetic field since the field points in the z'-direction. The third term accounts for the spin-splitting of the Landau-levels. A plot of the lowest conduction band Landau-levels is given in fig. 2.2.
It is possible to calculate numerically a value of the effective g-factor for given B, θ and Landau number n by taking the difference between two solutions corresponding to the conduction band and dividing it by $\mu_B B$, where μ_B is the Bohr-magneton.
An analytical expression for the effective g-factor has been obtained by Wallace from eq. 2.14 under the condition $g^*\mu_B B \ll E_F$, thus for a large number of Landau-levels below the Fermi-level. The expression reads as follows:

$$g^*(\theta) = \left(\frac{2m_o}{3m_c^*(\theta)}\right) P_\perp \Delta \frac{[(E+\delta)^2 P_\perp^2 \cos^2\theta + E^2 P_{/\!/}^2 \sin^2\theta]^{\frac{1}{2}}}{[f_1(f_1\cos^2\theta + f_2\sin^2\theta)]^{\frac{1}{2}}} \quad . \qquad (2.15)$$

The effective cyclotron mass m_c^* used in this relation has been obtained from eq. 2.14 after neglecting the spin-splitting term and assuming the magnetic field to be low. The effective cyclotron mass then becomes:

$$\frac{m_c^*(\theta)}{m_o} = \frac{\hbar^2}{2}\frac{d}{dE}\left\{\frac{\gamma}{[f_1(f_1\cos^2\theta + f_2\sin^2\theta)]^{\frac{1}{2}}}\right\} \quad . \qquad (2.16)$$

2.3. The Bodnar-model including exchange interaction

In the case of semimagnetic semiconductors (SMSC), apart from the usual $\vec{k}.\vec{p}$, spin-orbit and crystal field terms in the Hamiltonian, one has to account for the terms due to the exchange interaction of free carriers and electrons in the 3d shells of magnetic ions [10]. The exchange interaction may be represented by

$$H_i = \sum_{R_n} J(\vec{r} - \vec{R}_n)\vec{\sigma} \cdot \vec{S}_n \quad , \qquad (2.17)$$

where J, $\vec{\sigma}$ and $\vec{S}_n$ stand for the exchange integral, the electron spin

operator and the total spin operator of the Mn-ion at $\vec{R}_n$, respectively [11]. In this section we present the Bodnar-model in quantising magnetic fields including the exchange interaction of this type.

In the basis states given by eq. 2.3 the total matrix, including the contribution of H_i, has the following form: (see next page).

Due to the lower symmetry of the crystal we have now three independent quantities describing the exchange interaction (instead of two for $Hg_{1-x}Mn_xTe$ [12]). These are defined as

$$\alpha = \langle S|J|S\rangle/\Omega_o$$

$$\beta_{//} = \langle Z|J|Z\rangle/\Omega_o \qquad (2.19)$$

$$\beta_{\perp} = \langle X|J|X\rangle/\Omega_o = \langle Y|J|Y\rangle/\Omega_o \quad ,$$

where Ω_o is the unit cell volume.
The other symbols used in 2.18 read as follows:

$$a = \frac{1}{2}\alpha \times \langle S_z\rangle \qquad a_{\pm} = \frac{1}{2}\alpha \times \langle S_{\pm}\rangle$$

$$b = \frac{1}{2}\beta_{\perp} \times \langle S_z\rangle \qquad d_{\pm} = \frac{1}{2}\beta_{\perp} \times \langle S_{\pm}\rangle \qquad (2.20)$$

$$b' = \frac{1}{2}\beta_{//} \times \langle S_z\rangle \qquad c_{\pm} = \frac{1}{2}\beta_{//} \times \langle S_{\pm}\rangle \quad ,$$

where x is the molar fraction of Mn, $\langle S_z\rangle$ and $\langle S_{\pm}\rangle \equiv \langle S_x \pm iS_y\rangle$ are the thermal averages of the components of Mn-spins.
In case of non-interacting magnetic moments the component of $\langle\vec{S}\rangle$ along the magnetic field does not vanish, so we may write

$$\langle S_z\rangle = \langle S\rangle_B \cos\theta$$

$$\langle S_{\pm}\rangle = \langle S\rangle_B \sin\theta \quad , \qquad (2.21)$$

where θ is the angle between an external magnetic field and the crystallographic c-axis.

$$
H = \begin{bmatrix}
E_g - a & a_+ & P_\perp k_- & \sqrt{\frac{2}{3}}\, P_{/\!/} k_z & -\sqrt{\frac{1}{3}}\, P_\perp k_+ & 0 & \sqrt{\frac{1}{3}}\, P_{/\!/} k_z & \sqrt{\frac{2}{3}}\, P_\perp k_+ \\
a_- & E_g + a & 0 & \sqrt{\frac{1}{3}}\, P_\perp k_- & \sqrt{\frac{2}{3}}\, P_{/\!/} k_z & P_\perp k_+ & -\sqrt{\frac{2}{3}}\, P_\perp k_- & \sqrt{\frac{1}{3}}\, P_{/\!/} k_z \\
P_\perp k_+ & 0 & -b & \sqrt{\frac{1}{3}}\, d_+ & 0 & 0 & -\sqrt{\frac{2}{3}}\, d_+ & 0 \\
\sqrt{\frac{2}{3}}\, P_{/\!/} k_z & \sqrt{\frac{1}{3}}\, P_\perp k_+ & \sqrt{\frac{1}{3}}\, d_- & -\frac{1}{3}(2\delta + 2b' - b) & \frac{2}{3}\, c_+ & 0 & -\frac{\sqrt{2}}{3}\,(\delta + b' + b) & \frac{\sqrt{2}}{3}\, c_+ \\
-\sqrt{\frac{1}{3}}\, P_\perp k_- & \sqrt{\frac{2}{3}}\, P_{/\!/} k_z & 0 & \frac{2}{3}\, c_- & -\frac{1}{3}(2\delta + b - 2b') & -\sqrt{\frac{1}{3}}\, d_+ & \frac{\sqrt{2}}{3}\, c_- & \frac{\sqrt{2}}{3}(b + b' - \delta) \\
0 & P_\perp k_- & 0 & 0 & -\sqrt{\frac{1}{3}}\, d_- & b & 0 & \sqrt{\frac{2}{3}}\, d_- \\
\sqrt{\frac{1}{3}}\, P_{/\!/} k_z & -\sqrt{\frac{2}{3}}\, P_\perp k_+ & -\sqrt{\frac{2}{3}}\, d_- & -\frac{\sqrt{2}}{3}(\delta + b + b') & \frac{\sqrt{2}}{3}\, c_+ & 0 & -\Delta - \frac{1}{3}(\delta + b' - 2b) & \frac{1}{3}\, c_+ \\
\sqrt{\frac{2}{3}}\, P_\perp k_- & \sqrt{\frac{1}{3}}\, P_{/\!/} k_z & 0 & \frac{\sqrt{2}}{3}\, c_- & \frac{\sqrt{2}}{3}\,(b + b' - \delta) & \sqrt{\frac{2}{3}}\, d_+ & \frac{1}{3}\, c_- & \Delta - \frac{1}{3}(\delta + 2b - b')
\end{bmatrix}
\tag{2.18}
$$

For low magnetic ion contents the component of $\langle \vec{S} \rangle$ along the magnetic field is assumed to be given by [13]:

$$\langle S \rangle_B = S_{eff} \cdot B_{5/2} \left(5\mu_B B / k_B (T+T_o) \right) \quad , \tag{2.22}$$

where $B_{5/2}$ is the Brillouin-function and S_{eff} and $T_{eff} = T + T_o$ are effective values for the saturation and temperature, respectively.

2.3.1. Magnetic field parallel to the c-axis

When $\theta = 0$ the terms in eq. 2.18 involving $a_{\pm}$, $c_{\pm}$ and $d_{\pm}$ vanish. In that case the following creation and annihilation operators can be introduced:

$$\Lambda^{\pm} = 1\, k_{\pm} \tag{2.23}$$

with $1/1^2 = eB/\hbar$.
Then, for $k_z=0$, the 8x8 matrix given by eq. 2.18 decouples into two 4x4 matrices

$$H = \begin{vmatrix} H_a & 0 \\ 0 & H_b \end{vmatrix} \quad . \tag{2.24}$$

The eigenvectors of H_a and H_b may be expressed in terms of harmonic oscillator functions Φ_n:

$$\begin{bmatrix} a_1 & \Phi_n \\ a_2 & \Phi_{n+1} \\ a_3 & \Phi_{n-1} \\ a_4 & \Phi_{n-1} \end{bmatrix}, \begin{bmatrix} b_1 & \Phi_n \\ b_2 & \Phi_{n+1} \\ b_3 & \Phi_{n-1} \\ b_4 & \Phi_{n+1} \end{bmatrix} \tag{2.25}$$

for H_a and H_b, respectively.

Then H_a and H_b become

$$H_a = \begin{bmatrix} E_g - a & \sqrt{n+1}\,\frac{P_\perp}{1} & -\sqrt{\frac{n}{3}}\,\frac{P_\perp}{1} & \sqrt{\frac{2}{3}n}\,\frac{P_\perp}{1} \\ \sqrt{n+1}\,\frac{P_\perp}{1} & -b & 0 & 0 \\ -\sqrt{\frac{n}{3}}\,\frac{P_\perp}{1} & 0 & -\frac{1}{3}(2\delta+b-2b') & \frac{\sqrt{2}}{3}(b+b'-\delta) \\ \sqrt{\frac{2}{3}n}\,\frac{P_\perp}{1} & 0 & \frac{\sqrt{2}}{3}(b+b'-\delta) & -\Delta-\frac{1}{3}(\delta+2b-b') \end{bmatrix} \tag{2.26}$$

(basis functions u_1, u_3, u_5, u_8 see eq. 2.3).

$$H_b = \begin{bmatrix} E_g + a & \sqrt{\frac{1}{3}(n+1)}\,\frac{P_\perp}{1} & \sqrt{n}\,\frac{P_\perp}{1} & -\sqrt{\frac{2}{3}(n+1)}\,\frac{P_\perp}{1} \\ \sqrt{\frac{1}{3}(n+1)}\,\frac{P_\perp}{1} & \frac{1}{3}(b-2b'-2\delta) & 0 & -\frac{\sqrt{2}}{3}(b+b'+\delta) \\ \sqrt{n}\,\frac{P_\perp}{1} & 0 & b & 0 \\ -\sqrt{\frac{2}{3}(n+1)}\,\frac{P_\perp}{1} & -\frac{\sqrt{2}}{3}(b+b'+\delta) & 0 & -\Delta-\frac{1}{3}(\delta+b'-2b) \end{bmatrix} \tag{2.27}$$

(basis functions u_2, u_4, u_6, u_7 see eq. 2.3).

The secular equations corresponding to eqs. 2.26 and 2.27 are generally of the fourth order. Fig. 2.3,a presents the results of diagonalisation of eqs. 2.26 and 2.27 in the form of the Landau-levels at $k_z=0$ as function of the magnetic field. For the sake of comparison the magnetic levels of Cd_3As_2 are plotted in fig. 2.3.b. One can see that the a(-1) level is no longer the lowest one in case of $(Cd_{0.99}Mn_{0.01})_3As_2$ below 4 T. Above this value of the field the a(-1) level becomes again the lowest one and the sequence of a(-1) and b(1) levels is that of Cd_3As_2. This characteristic feature of SMSC is shown also by the crossings of the other Landau-levels.

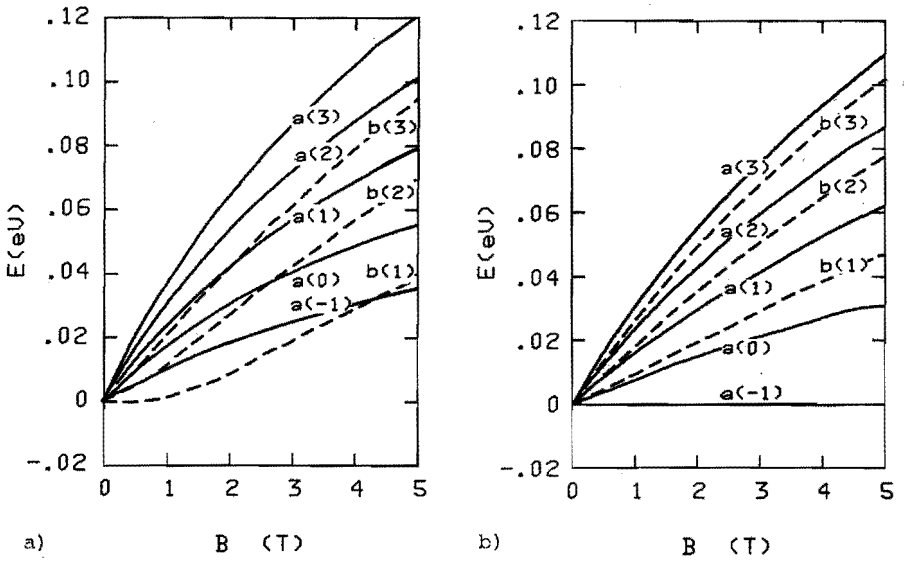

Fig. 2.3. Lowest conduction band Landau-levels in $(Cd_{0.99}Mn_{0.01})_3As_2$ (a) and Cd_3As_2 (b) at T = 4 K calculated as a function of the magnetic field parallel to the c-axis. The used values of α, $\beta_{//}$, $\beta_{\perp}$, S_{eff} and T_o are -3.4 eV, 4.9 eV, 4.9 eV, 1.6 and 1.9 K, respectively. The values of the other bandparameters are given in fig. 2.2. The levels a(-1), a(0), b(2) and a(2) in fig. 2.3.b correspond to the 0^-, 0^+, 2^- and 2^+ levels in fig. 2.2 for θ = 0.

2.3.2. Arbitrary direction of the magnetic field

Two difficulties arise when the magnetic field is not parallel to the c-axis. Firstly, the operators $\Lambda^{\pm}$ defined in eq. 2.23 are no longer proper Landau-quanta since they do not fulfil usual commutation relations. Secondly, the off-diagonal terms $a_{\pm}$, $c_{\pm}$ and $d_{\pm}$ in eq. 2.18 are no longer equal to zero. When $\theta \neq 0$ the eigenvalue problem cannot be split into two 4x4 problems, but its dimension is 8x8 even in the k_z=0 case.

Here the main steps of Wallace's paper [8] have been adopted in order to handle the problem of Landau-levels in anisotropic $(Cd_{1-x}Mn_x)_3As_2$ alloys. Using the primed system of coordinates (see eq. 2.9), one may look for new creation and annihilation operators in terms of these

primed variables. It is possible to define them analogous to Wallace (see eq. 2.13):

$$\overline{\Lambda}^{\pm} = (4\,\overline{A}\;\overline{B})^{-\frac{1}{4}}\{\sqrt{\overline{A}}\,k_x' \pm i\sqrt{\overline{B}}\,k_y' + \frac{\overline{D}}{\sqrt{\overline{A}}}k_z'\} \qquad (2.28)$$

where $[\overline{\Lambda}^{+}, \overline{\Lambda}^{-}] = 1/l^2$ because $[k_x', k_y'] = -i/l^2$ and $[k_x', k_z'] = [k_y', k_z'] = 0$.
The quantities $\overline{A}$, $\overline{B}$, $\overline{D}$ are defined as:

$$\begin{aligned}\overline{A} &= \bar{f}_1\cos^2\theta + \bar{f}_2\sin^2\theta \\ \overline{B} &= \bar{f}_1 \\ \overline{D} &= (\bar{f}_1-\bar{f}_2)\sin\theta\cos\theta\end{aligned} \qquad (2.29)$$

where

$$\bar{f}_1 = P_{\perp}^{\,2}\{E(E+\tfrac{2}{3}\Delta) + \delta(E+\tfrac{\Delta}{3}) - b^2\}$$

$$\bar{f}_2 = P_{/\!/}^{\,2}\{E(E+\tfrac{2}{3}\Delta) - b^2\}\ .$$

However, one also finds that the Hamiltonian contains terms quadratic in $\Lambda^{\pm}$. This means that simple vector columns, as defined in eq. 2.25, cannot serve as eigenvectors of our problem.
A difficulty of this kind is often met in the problem of magnetic energy levels in semiconductors [14-16]. A way out of this difficulty is to use vector columns which contain infinite series of harmonic oscillator functions in each row. Then, if a certain cut-off of the expansion is assumed, it is possible to find the eigenvalues by means of a lengthly computer calculation [16]. Such an approach is necessary when one is interested in very accurate values of the eigenenergies in the heavy hole band. However, when dealing with the conduction band it is often found that the terms quadratic in the Landau-quanta do not contribute largely to the actual values of the eigenenergies and it is allowed to neglect them [14, 15]. Following this procedure, one obtains a Hamiltonian-matrix, which eigenvectors can be written in the form of a vector column containing only one harmonic oscillator in each row.
Neglecting the terms quadratic in $\overline{\Lambda}^{\pm}$, it is possible to derive a secular

equation (eighth degree) and solve it numerically.
Taking the difference between the two solutions corresponding to the conduction band and dividing it by $\mu_B B$ one obtains the value of the effective g-factor for a given B, θ and Landau-quantum number n.
Figure 2.4 shows the results of such a calculation as function of the angle θ between the magnetic field and the c-axis for x=0.01 and different combinations of α, $\beta_{//}$ and $\beta_{\perp}$.

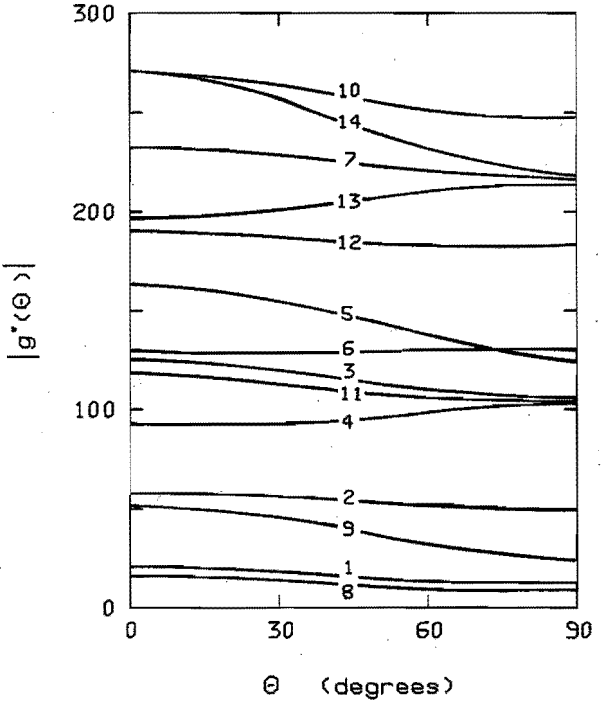

	α	$\beta_{//}$	$\beta_{\perp}$
1	0	0	0
2	0	2	2
3	0	4	4
4	4	0	0
5	0	-4	-4
6	-4	0	0
7	4	4	4
8	-4	4	4
9	4	-4	-4
10	-4	-4	-4
11	4	4	4
12	4	4	4
13	4	3	5
14	4	5	3

Fig. 2.4. The values of the effective g-factor of $(Cd_{0.99}Mn_{0.01})_3As_2$ for different orientations of the magnetic field, calculated including the off-diagonal $\langle S_{\pm} \rangle$ terms at T = 4 K, B = 2 T and n = 15. The different values of α (eV), $\beta_{//}$ (eV), $\beta_{\perp}$ (eV) are given in the figure. S_{eff} and T_o were kept at the values 1.6 and 1.9 K, respectively. The values of the other bandparameters are given in fig 2.2. Curve 1 corresponds to the case of Cd_3As_2. The curves 11 and 12 are calculated for B = 2 T, T =10 K and B = 4 T, T = 4 K, respectively.

2.3.3 Analytical expression for the effective g-factor

In the case that the magnetic field is parallel to the c-axis it is possible to derive an analytical expression for the effective g-factor. Restricting ourselves to $k_z=0$ and b'=b the following secular equation is obtained:

$$\bar{\gamma} = \frac{(2n+1)}{l^2}\bar{f}_1 \pm\left[G + (E+\delta)\frac{P_\perp^2}{3l^2}\Delta\right] \quad , \tag{2.30}$$

where

$$\bar{\gamma} = [E(E-E_g) + ab][E(E+\Delta) + \delta(E+\tfrac{2}{3}\Delta) - b^2] + b(\delta-\tfrac{\Delta}{3})\ [aE + b(E-E_g)] + b\frac{\Delta}{3}\frac{P_\perp^2}{l^2} \tag{2.31}$$

$$\bar{f}_1 = P_\perp^2\ [E(E+\tfrac{2}{3}\Delta) + \delta(E+\tfrac{\Delta}{3}) - b^2] \tag{2.32}$$

$$G = (2n+1)b\delta\frac{P_\perp^2}{l^2} - b(\delta-\tfrac{\Delta}{3})[E(E-E_g) + ab] - [aE + b(E-E_g)][E(E+\Delta) + \delta(E+\tfrac{2}{3}\Delta) - b^2] \ . \tag{2.33}$$

The first term on the right hand side of eq. 2.30 gives the orbital quantisation while the second term describes the splitting of the Landau-levels. For a=b=0 eq. 2.30 reduces to the result of Wallace for Cd_3As_2 (see eq. 2.14 for $\theta=0$). From eq. 2.30 it is possible to derive analytical expressions for the cyclotron effective mass and the g-factor of the conduction electrons.
Following Wallace (see §2.2) we obtain

$$m_c^*(\theta=0) = \frac{\hbar^2}{2}\frac{d}{dE}\left[\frac{\bar{\gamma}}{\bar{f}_1}\right] \tag{2.34}$$

and

$$g^*(\theta=0) = \frac{m_o}{m_c^*(\theta=0)}\frac{[2Gl^2 + \frac{2}{3}\Delta P_\perp^2(E+\delta)]}{\bar{f}_1} \ , \tag{2.35}$$

where m_o is the free electron mass.
It turns out that the value of $m_c^*(\theta = 0)$ given by eq. 2.34 is practically the same as for Cd_3As_2, although the formulae for $\bar{\gamma}$ and $\bar{f}_1$ contain the terms due to the exchange interaction. For instance, taking the previously mentioned bandparameters (see fig. 2.3.a) and $E_F = 0.15$ eV, we find $m_c^*(\theta = 0) = 0.03256\, m_o$ while for Cd_3As_2 one gets $m_c^*(\theta = 0) = 0.03260\, m_o$. The effective g-factor however, depends strongly on the exchange interaction, as can be seen from fig. 2.4. It should be noted that $g^*(\theta = 0)$ given by eq. 2.35 depends explicitly on B and n.
From eqs. 2.34 and 2.35 a linear relation in a and b is obtained when the small terms proportional to ab^2, b^2, b^3 are neglected. This expression reads as follows:

$$\nu[E(E + \tfrac{2}{3}\Delta) + \delta(E + \tfrac{\Delta}{3})]\frac{P_\perp^2}{1^2} - \tfrac{\Delta}{3}(E+\delta)\frac{P_\perp^2}{1^2} =$$

$$b\{(2n+1)\frac{\delta P_\perp^2}{1^2} - (E-E_g)[E(E + \tfrac{2}{3}\Delta) + 2\delta(E + \tfrac{\Delta}{3})]\} -$$

$$aE[E(E+\Delta) + \delta(E + \tfrac{2}{3}\Delta)] \quad , \qquad (2.36)$$

where $\nu = \frac{1}{2}\frac{m_c^*}{m_o} g^*$.
Under these assumptions a constant value of ν corresponds to a linear relation in a and b and therefore a straight line in the (α,β) plane is obtained.

REFERENCES

[1] W. Zawadzki, private communication.

[2] E.O. Kane, J. Phys. Chem. Solids 1, 249 (1957).

[3] J. Bodnar, Proc. Int. Conf. Phys. Narrow-Gap Semicond., Warsaw, 1977 (Polish Scientific Publ., Warsaw, 1978), p. 311.

[4] H. Kildal, Phys. Rev. B10, 5082 (1974).

[5] J.J. Hopfield, J. Phys. Chem. Solids 15, 97 (1960).

[6] V.E. Van Doren, P.E. Van Camp, J.T. Devreese, internal report Esis, 1979 (unpubl.).

[7] G.L. Bir, G.E. Pikus, Symmetry and Strain-Induced Effects in Semiconductors, (John Wiley and Sons, New-York/Toronto 1974).

[8] P.R. Wallace, Phys. Stat. Solidi B92, 49 (1979).

[9] W. Zawadzki, Narrow Gap Semiconductor Physics and Applications, ed. W. Zawadzki, (Springer-Verlag, Berlin, 1980), p. 85.

[10] R.R. Galazka, Proc. 14th Int. Conf. Phys. Semicond., Edinburgh 1978, ed. B.L.H. Wilson, Conf. Series 43, (Inst. of Physics, London, 1979), p. 133.

[11] J. Kossut, Phys. Stat. Solidi B78, 537 (1976).

[12] M. Jaczynski, J. Kossut, R.R. Galazka, Phys. Stat. Solidi B88, 73 (1978).

[13] J.A. Gaj, R. Planel, G. Fishman, Solid State Commun. 29, 435 (1979).

[14] W. Leung, L. Liu, Phys. Rev. B8, 3811 (1973).

[15] M.S. Adler, C.R. Hewes, S.D. Senturia, Phys. Rev. B7, 5186 (1973).

[16] R. Stepniewski, K. Pastor, M. Grynberg, J. Phys. C: Solid State Phys. 13, 5783 (1980).

CHAPTER III MAGNETORESISTANCE OSCILLATIONS: THE SHUBNIKOV-DE HAAS EFFECT

Oscillations in the electrical resistivity as function of the magnetic field were first observed in bismuth by Shubnikov and de Haas [1] in 1930. There has been a renewed interest in this effect as a tool for the investigation of the band structure of semiconductors. Reviews on theory and experimental results were presented by Landwehr, by Kahn and Frederikse, by Adams and Keyes and by Roth and Argyres [2-5].

In this chapter the SdH-effect is qualitatively described from the motion of a free electron in a magnetic field (see §3.1). General expressions for the amplitude and phase of the SdH-oscillations and for the oscillation period and the cyclotron effective mass of charge carriers are given in §3.2. These expressions are applied to the Bodnar-band model in §3.3. The influence of a magnetic field dependent Fermi-energy on the periodicity, the effective mass and the spin-splitting of the SdH-signal is discussed in §3.4. In §3.5 we treat the SdH-effect in a SMSC by taking into account the exchange interaction.

3.1. The free electron model for the SdH-oscillations

The oscillatory magnetoresistance or Shubnikov-de Haas-effect is a direct result of the quantisation of electron states by a magnetic field and can be qualitatively understood from the motion of a free electron in a magnetic field [6]. In case of an n-type semiconductor with a parabolic conduction band and a spherical Fermi-surface the free electron model can be used by replacing the free electron mass m_o by an isotropic effective mass m^* [5].

By applying a magnetic field in the z-direction, the motion of the free electron is disturbed. Under influence of the Lorentz-force the particle will follow a cyclotron motion in a plane perpendicular to the field direction, while the motion parallel to the field is unaffected. The original free electron conduction band

$$E = \frac{\hbar^2}{2m^*} (k_x^2 + k_y^2 + k_z^2) \tag{3.1}$$

is split into magnetic subbands or Landau-levels, which are labelled

with the quantumnumber n and differ in energy by an amount $\hbar\omega_c$, where $\omega_c = eB/m^*$ is the cyclotron frequency.

The energy values are given by

$$E_n = (n+\tfrac{1}{2})\hbar\omega_c + \frac{\hbar^2 k_z^2}{2m^*} \pm \tfrac{1}{2} g^*\mu_B B \qquad n = 0,1,2,..... \quad , \qquad (3.2)$$

where g^* and μ_B stand for the effective spectroscopic splitting factor and the Bohr-magneton, respectively. The last term in eq. 3.2 represents the lifting of the spin degeneracy.

The uniform distribution of quantum states in $\vec{k}$-space for the electron-gas in the absence of a magnetic field is broken up and replaced by a series of interlocking Landau-cylinders on which surfaces the electron states are quantised [7]. Due to the bunching of states at the energy levels $(n+\tfrac{1}{2})\hbar\omega_c$ the density of states per unit volume, neglecting collision broadening and spin-splitting, becomes

$$d_s(E) = \frac{1}{4\pi^2}\left(\frac{2m^*}{\hbar^2}\right)^{3/2} \sum_{n=0}^{\infty} \frac{\hbar\omega_c}{(E-(n+\tfrac{1}{2})\hbar\omega_c)^{\frac{1}{2}}} \quad . \qquad (3.3)$$

A plot of the density of states $d_s(E)$ versus $E/\hbar\omega_c$ is shown in fig. 3.1. The curves with $\omega_c\tau = 10$ and $\omega_c\tau = 1$, where τ is the relaxation time, illustrate the effect of a Lorentzian shaped level broadening on the density of states.

The discrete nature of the Landau-levels fades away unless their energy separation $\hbar\omega_c$ is much larger than the thermal broadening k_BT. Furthermore

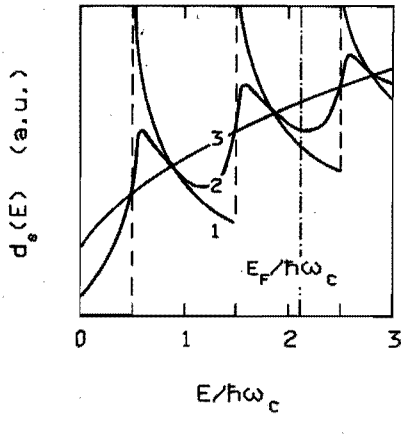

Fig. 3.1.
Density of states $d_s(E)$ in arbitrary units as function of $E/\hbar\omega_c$ for various degrees of level broadening. The numbers 1,2,3 represent the cases $\omega_c\tau = \infty$, 10 and 1, respectively. The Fermi-energy is indicated in the figure. After Landwehr [2].

the electrons must perform complete cyclotron orbits in $\vec{k}$-space before being scattered, in order to observe quantum effects. This requirement can be formulated as $\omega_c\tau \gg 1$. From fig. 3.1 it can be seen that when the energy coincides with a Landau-level the density of states diverges in case $\omega_c\tau = \infty$. For increasing magnetic fields the Landau-levels will successively pass the Fermi-level. This produces periodic fluctuations in the density of states at the Fermi-energy E_F. These fluctuations strongly affect the scattering rates of electrons [4] and consequently periodic oscillations in the resistance as function of the magnetic field are produced.
If the Fermi-energy is assumed to be independent of the magnetic field, the oscillations in the resistivity are periodic in 1/B [2]. In addition to the conditions formulated above ($\hbar\omega_c > k_BT$, $\omega_c\tau \gg 1$), the Fermi-energy E_F must be larger than $\hbar\omega_c$. In general these requirements are fulfilled in case of a degenerate n-type semiconductor with a high electron mobility at low temperatures and high magnetic fields.

3.2. The analytical expression for SdH-oscillations

A theory for the transverse magnetoresistance oscillations has been given by Adams and Holstein [9]. This theory, developed for a simple electrongas, has been generalised including effects of anisotropic and non-parabolic bands [9], collision broadening [10] and spin-splitting [11]. The resulting expression for the transverse magnetoresistance oscillation becomes

$$\frac{\Delta\rho}{\rho_o} = \frac{ck_BTm_c^*}{\hbar e\, m_o}\left(\frac{P}{B}\right)^{\frac{1}{2}} \sum_{r=1}^{\infty}\left[\frac{r^{\frac{1}{2}}e^{-r\beta m_c^*T_d/m_oB}}{\sinh(r\beta m_c^*T/m_oB)}\cos(r\pi\nu) * \cos\left(\frac{2\pi}{PB}r - \frac{\pi}{4} - 2\pi r\gamma\right)\right] \qquad (3.4)$$

$$= \sum_{r=1}^{\infty} A_r(B,T)\cos\left(\frac{2\pi}{PB}r - \frac{\pi}{4} - 2\pi r\gamma\right) ,$$

where ρ_o is the classical magnetoresistance,

$$\beta = \frac{2\pi^2 m_o k_B}{\hbar e} = 14.693\,(T/K), \quad c = \frac{5\pi^2\sqrt{2}}{2} \quad \text{and} \quad T_d = \frac{\hbar}{\pi k_B \tau}\ (K)$$

is the Dingle-temperature, m_c^* is the cyclotron effective mass, P is the SdH-oscillation period, $\nu = (m_c^*/2m_o)g^* = (\mu_B B/\hbar\omega_c)g^*$, g^* is the effective g-factor and γ is a phase factor.

Expression 3.4 is derived under the conditions $E_F \gg \hbar\omega_c$, $\hbar\omega_c > k_B T$ and $\omega_c \tau \gg 1$. The exponential factor represents the energy level broadening due to ionised impurity scattering introduced by Dingle [10]. Argyres [14] obtained a similar expression for the longitudinal magnetoresistance oscillations. The constant c has the value $\pi^2\sqrt{2}/2$ in the longitudinal case.

Although eq. 3.4 is derived for an isotropic spherical Fermi-surface, it is applicable to arbitrary shaped closed Fermi-surfaces. In that case the oscillation period P and the cyclotron effective mass m_c^* are directly related to the Fermi-surface by the relations [13]

$$P = \left(\frac{2\pi e}{\hbar S_m}\right)_{E=E_F} \tag{3.5}$$

$$m_c^* = \frac{\hbar^2}{2\pi}\left(\frac{dS_m}{dE}\right)_{E=E_F}, \tag{3.6}$$

where S_m is the extremal cross sectional area of the Fermi-surface perpendicular to the magnetic field direction (see fig. 3.2).

3.3. Period and effective mass according to the Bodnar-model

In case of the Bodnar-model, it follows from eq. 2.7 and eq. 2.8 that the Fermi-surface is a single ellipsoid of revolution, with semi-axes depending on energy. Rewriting eq. 2.7 into

$$1 = \frac{(k_x^2 + k_y^2)}{a^2} + \frac{k_z^2}{c^2} \tag{3.7}$$

we obtain for the principal semi-axes of the ellipsoid

$$a = \left(\frac{\gamma}{f_1}\right)^{\frac{1}{2}} \tag{3.8}$$

$$c = \left(\frac{\gamma}{f_2} \right)^{\frac{1}{2}} \quad . \tag{3.8}$$

Due to the fact that the coefficients $f_1(E)$ and $f_2(E)$ have different energy dependences if $\delta \neq 0$, the ellipsoid changes shape with varying Fermi-energy.

The extremal cross sectional area S_m of the ellipsoid in the plane perpendicular to the applied magnetic field is given by

$$S_m = \pi \gamma(E) \; [f_1(E)\cos^2\theta + f_2(E)\sin^2\theta]^{-\frac{1}{2}} [f_1(E)]^{-\frac{1}{2}} \; , \tag{3.9}$$

where θ is the angle between $\vec{B}$ and the tetragonal c-axis (see fig. 3.2).. The directional dependences of the SdH-oscillation period and the cyclotron effective mass, according to the Bodnar-model, can be determined directly from eqs. 3.5, 3.6 and 3.9.

From eqs. 3.5 and 3.9 it follows that

$$P(\theta) = [P(\theta = 0)\cos^2\theta + P(\theta = 90)\sin^2\theta]^{\frac{1}{2}} \quad . \tag{3.10}$$

In case of high degeneracy one can calculate the electron concentration

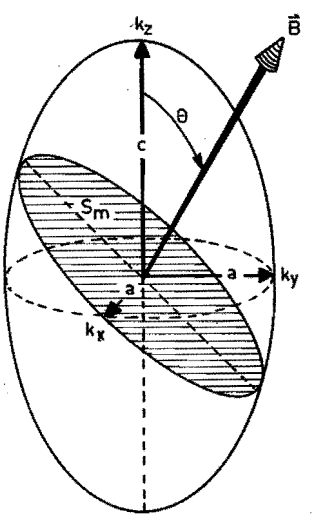

Fig.3.2.
The cross sectional area S_m of the Fermi-surface perpendicular to $\vec{B}$. Prolate ellipsoid of revolution: c>a. Oblate ellipsoid of revolution: c<a.

from the volume of the Fermi-ellipsoid. The electron concentration N equals

$$N = \frac{a^2 c}{3\pi^2} = \frac{1}{3\pi^2}\left(\frac{2e}{\hbar}\right)^{3/2}\left[P(\theta=0)\,P^2(\theta=90)\right]^{-\frac{1}{2}} \quad , \tag{3.11}$$

where a and c are defined in fig. 3.2 and eq. 3.8.
The analytical expression for the effective g-factor is given in eq. 2.15.
Defining the anisotropy factors of the period (K_p), the cyclotron effective mass (K_m) and the effective g-factor (K_g), one finds [14]:

$$K_p = \frac{P(\theta=0)}{P(\theta=90)} = \frac{c}{a} = \left[\frac{f_1(E)}{f_2(E)}\right]^{\frac{1}{2}}_{E=E_F} \tag{3.12}$$

$$K_m = \frac{m_c^*(\theta=90)}{m_c^*(\theta=0)} = \left[\frac{\frac{d}{dE}\left(\frac{\gamma}{f_1^{\frac{1}{2}} f_2^{\frac{1}{2}}}\right)}{\frac{d}{dE}\left(\frac{\gamma}{f_1}\right)}\right]_{E=E_F} \tag{3.13}$$

$$K_g = \frac{g^*(\theta=0)}{g^*(\theta=90)} = \frac{K_m}{K_p} \cdot \frac{P_\perp}{P_{//}} \left[\frac{E+\delta}{E}\right]_{E=E_F} \quad . \tag{3.14}$$

3.4. The influence of a field dependent Fermi-energy

Thus far it has been assumed that the Fermi-energy E_F is independent of the magnetic field. When the field dependence of E_F is not negligible the SdH-signal will no longer be perfectly periodic in 1/B and the cyclotron effective mass and effective g-factor will depend on the order of Landau-level passing through the Fermi-energy. In the following the influence of a field dependent Fermi-energy on the SdH-oscillation period, the cyclotron effective mass and the effective g-factor is described for the Bodnar-model on the basis of extreme degeneracy.

Deviations in periodicity

In case of a field independent Fermi-energy, the distance $\left(\Delta\frac{1}{B}\right)_n = (1/B_{n+1} - 1/B_n)$ between two SdH-oscillation peaks of the fundamental (r=1 in eq. 3.4) is independent of n.
Kahn and Frederikse [3] calculated the field dependence of E_F for

isotropic energy surfaces, neglecting spin-splitting and collision broadening at T=0 K. Their results for $(\Delta\frac{1}{B})_n$ expressed in terms of a field independent period P are given in the second column of table 3.1. A similar calculation can be made starting from the Bodnar-model in a magnetic field (see eq. 2.14). Since the Bodnar-model describes an anisotropic Fermi-surface with anisotropy depending on energy, the deviations in periodicity will depend on the Landau-number n, the electron concentration and the orientation of the magnetic field. This is illustrated in table 3.1. From this table it follows that the deviations in periodicity are of the order of a few percent as well for the isotropic energy surfaces as for the Bodnar-model. Furthermore the energy dependent anisotropy in the Bodnar-model does not affect the deviation in periodicity seriously. For low quantumnumbers

n	isotropic	Bodnar $N=0.47*10^{24}$ m^{-3}		Bodnar $N=2*10^{24}$ m^{-3}	
		$\theta=0$	$\theta=90$	$\theta=0$	$\theta=90$
1	1.048 P	1.051 P	1.047 P	1.050 P	1.047 P
2	1.024 P	1.025 P	1.023 P	1.025 P	1.023 P
3	1.015 P	1.016 P	1.014 P	1.016 P	1.015 P
4	1.010 P	1.011 P	1.010 P	1.011 P	1.010 P
5	1.008 P	1.008 P	1.008 P	1.008 P	1.008 P

Table 3.1. Deviations in periodicity due to a field dependent Fermi-energy as function of the Landau-number n, calculated for isotropic energy surfaces and energy surfaces according to the Bodnar-model. The results are expressed in the field independent periods P corresponding to the respective cases. Calculations are performed for T = 0 K. The deviations in periodicity for the Bodnar-model are calculated for $E_g = -0.095$ *eV,* $\Delta = 0.27$ *eV,* $\delta = 0.085$ *eV,* $P_{//} = 7.21 * 10^{-10}$ *eVm and* $P_{\perp} = 7.43 * 10^{-10}$ *eVm (see eq. 2.7).*

the deviations in periodicity should be observable. However, in experiments the collision broadening tends to obscure the differences.

Deviations in the effective mass

A field dependent Fermi-energy changes the effective mass values calculated from eq. 3.6. The deviations depend on the Landau-number n, the electron concentration and the orientation of the magnetic field. It can be calculated that only for the lowest Landau-numbers ($n \leq 3$) the deviation in the effective mass becomes of the order of a few percent.

Influence on the effective g-factor

Due to the spin-splitting the degeneracy of each Landau-level is lifted. The spin splitted oscillation peaks belonging to the Landau-number n will occur at fields B_n^+ and B_n^-, respectively. If one neglects the field dependence of E_F, one obtains for a simple parabolic dispersion relation (see eq. 3.2):

$$|\nu| = \left|\frac{m^*}{2m_o} g^*\right| = \frac{1}{P}\left|\frac{1}{B_n^+} - \frac{1}{B_n^-}\right| \quad , \tag{3.15}$$

where P represents the oscillation period at low magnetic fields. Taking into account the field dependence of E_F at T=0 K, one obtains for a parabolic dispersion relation and $|\nu| < 1$ [2]:

$$\begin{aligned} \frac{1}{B_n^+} &= 0.825P\left[\sum_{k=0}^{n}(\sqrt{k} + \sqrt{k+\nu})\right]^{2/3} \\ \frac{1}{B_n^-} &= 0.825P\left[\sum_{k=1}^{n}(\sqrt{k} + \sqrt{k-\nu})\right]^{2/3} \quad . \end{aligned} \tag{3.16}$$

This expression coincides with eq. 3.15 only in the limit $n \gg 1$ and leads for low quantumnumbers to smaller values of $|\nu|$ compared with those obtained from eq. 3.15. In case of the Bodnar model one finds

$$\begin{aligned} \frac{1}{B_n^+} &= 0.825A_n^+(N,\theta)P(\theta)\left[\sum_{k=0}^{n}(\sqrt{k} + \sqrt{k+\nu})\right]^{2/3} \\ \frac{1}{B_n^-} &= 0.825A_n^-(N,\theta)P(\theta)\left[\sum_{k=1}^{n}(\sqrt{k} + \sqrt{k-\nu})\right]^{2/3} \quad , \end{aligned} \tag{3.17}$$

where the factors A_n^+ and A_n^- are functions of the electron concentration, the Landau-level and the magnetic field orientation. It can be calculated that eq. 3.17 differs only slightly (less than 1%) from eq. 3.16.

3.5. The influence of the exchange interaction

For semimagnetic semiconductors the SdH-oscillation period, the cyclotron effective mass and the electronic effective g-factor become field and temperature dependent due to the magnetisation. However, for a low magnetic ion content ($x \leq 0.05$), the period and cyclotron effective mass depend only weakly on the exchange interaction. On the other hand the g*-factor is strongly influenced by the exchange interaction since this interaction couples the conduction electron spins and the localised magnetic moments of the magnetic ions. Therefore the temperature and field dependences of the g*-factor in SMSC reflect the modification of the spin properties in the presence of magnetic ions, while the "orbital properties" given by m_c^* and P remain practically unchanged with respect to their non-magnetic counterparts.

The field and temperature dependences of $g^*(\theta)$ result in an anomalous behaviour of the SdH-oscillation amplitude. For normal semiconductors the amplitude is a monotonically decreasing function of temperature at fixed magnetic field, while in SMSC the amplitude can go to zero at certain combinations of field and temperature, as is illustrated in fig. 3.3. This can be understood from the Adams-

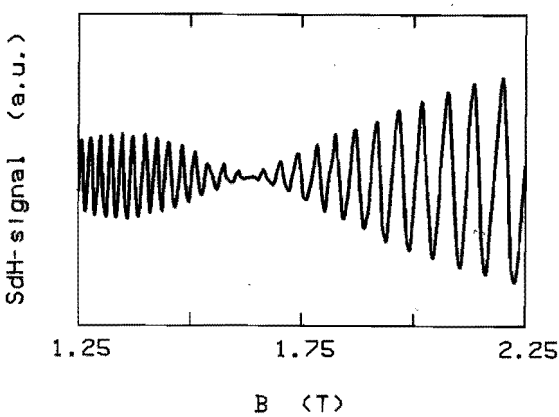

Fig.3.3. Experimental recording of SdH-oscillations at T = 1.8 K, showing the occurrence of a spin-splitting zero for a $(Cd_{1-x}Mn_x)_3As_2$ sample with x = 0.01 and $N = 3.65 * 10^{24}\ m^{-3}$.

Holstein expression for the oscillatory magnetoresistance given in eq. 3.4. When the Dingle-temperature T_d has such a value that only the first harmonic (r=1) is observed experimentally, the SdH-oscillation amplitude may go to zero whenever the quantity ν satifies [15]

$$\nu = \frac{m_c^*}{2m_o} g^* = k + \frac{1}{2} \qquad k = 0,1,2,..... \qquad (3.18)$$

In that case $\cos\pi\nu$ in eq. 3.4 becomes zero.

Under certain conditions the contributions of higher harmonics in the SdH-signal will be visible. This is illustrated in the fig. 3.4, where Γ indicates the level broadening. The amplitude of the fundamental passes zero for approximately 3 T. Due to the small level broadening ($\Gamma < \frac{1}{2}\hbar\omega_c$)

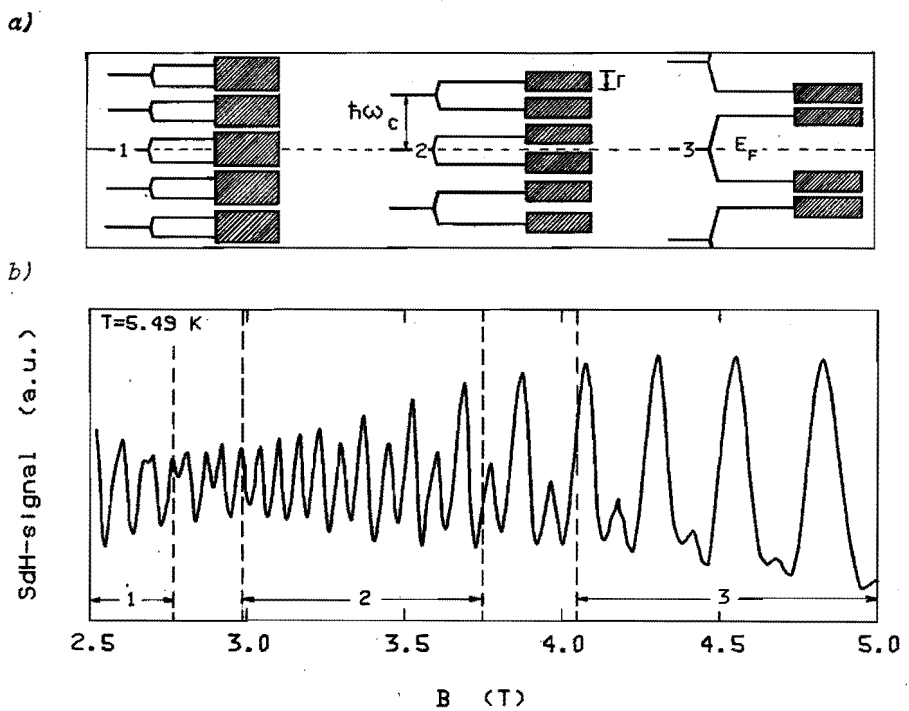

Fig.3.4. a) Landau-level scheme illustrating the appearance of higher harmonics. The level broadening is indicated with Γ.
b) Recorder trace of a SdH-signal showing the presence of higher harmonics.

the second harmonic (r=2) appears and the total signal amplitude is no longer zero. This phenomenon has been predicted by Kossut [16]. With further increase of the field the spin-splitting changes faster than the Landau-splitting. The energy distance between the spin down and spin up levels of neighbouring Landau-levels becomes smaller than the level broadening, therefore the second harmonic disappears again.

REFERENCES

[1] L. Shubnikov, W.J. de Haas, Leiden Commun. 207a, 207c, 207d, 210a, (1930).

[2] G. Landwehr, Physics of Solids in Intense Magnetic Fields, ed. E. Haidemenakis, (Plenum Press, New-York, 1969), p. 145.

[3] A.H. Kahn, M.P.R. Frederikse, Solid State Phys. 9, 257 (1959).

[4] E.N. Adams, R.W. Keyes, Progr. Semicond. 6, 87 (1962).

[5] L.M. Roth, P.N. Argyres, Semiconductors and Semimetals 1, ed. R.K. Willardson, A.C. Beer, (Ac. Press, New-York, 1966), p. 159.

[6] W. Zawadzki, Physics of Solids in Intense Magnetic Fields, ed. E. Haidemenakis, (Plenum Press, New-York, 1969), p. 301.

[7] J.S. Blakemore, Solid State Physics, (W.B. Saunders comp., London, 1970), p. 223.

[8] E.N. Adams, T.D. Holstein, J. Phys. Chem. Solids 10, 254 (1959).

[9] I.M. Lifshitz, A.M. Kosevich, Sov. Phys. JETP 2, 636 (1956).

[10] R.B. Dingle, Proc. Roy. Soc. A211, 517 (1952).

[11] M.H. Cohen, E.I. Blount, Phil. Mag. 5, 115 (1960).

[12] P.N. Argyres, J. Phys. Chem. Solids 4, 19 (1958).

[13] L. Onsager, Phil. Mag. 43, 1006 (1952).

[14] F.A.P. Blom, J.W. Cremers, J.J. Neve, M.J. Gelten, Solid State Commun. 33, 69 (1980).

[15] M. Jaczynski, J. Kossut, R.R. Galazka, Phys. Stat. Solidi B96, 413 (1979).

[16] J. Kossut, Solid State Commun. 27, 1237 (1978).

CHAPTER IV EXPERIMENTAL TECHNIQUE

In this chapter the sample preparation and characterisation (§4.1), the experimental set-ups (§4.2) and the data taking procedures (§4.3) are described.

4.1. Sample preparation and characterisation

Cd_3As_2

Cd_3As_2 polycrystalline starting material is obtained by directly melting stoichiometric amounts of spectrographically pure Cd and As in carbon coated quartz ampoules. The ingots are slowly cooled down through the $\beta \rightarrow \alpha$" phase transition at T=578°C [1]. A closed-tube sublimation technique at temperatures below the phase transition temperature is adopted to grow single crystals [1]. In this technique an evacuated quartz ampoule with special geometry is slowly pulled (speed: 1 mm/day) through a temperature gradient of about 5°C/cm at 460°C. Single crystals of 6 mm in diameter and 30 mm in length were obtained after about 4 weeks of growth.

$(Cd_{1-x}Mn_x)_3As_2$ and $CdSnAs_2$

$(Cd_{1-x}Mn_x)_3As_2$ and $CdSnAs_2$ single crystals are grown by a modified Bridgman-process in carbon coated quartz ampoules containing the proper amounts of spectrographically pure Cd, As, Mn and Cd, As and Sn, respectively. The pulling speed is about 20 mm/day.
In spite of the phase transitions at approximately 140°C and 10°C below the melting points for Cd_3As_2 (T_m=721°C) [1] and $CdSnAs_2$ (T_m=595°C) [2] respectively, crackfree single crystalline ingots of $(Cd_{1-x}Mn_x)_3As_2$ and $CdSnAs_2$ have been obtained in a reasonable number of attemps. After four days the Bridgman-process resulted in boules containing single crystalline parts of about 1 cm^3.

Characterisation

The obtained Cd_3As_2, $(Cd_{1-x}Mn_x)_3As_2$ and $CdSnAs_2$ crystals are degenerated n-type. The electron concentration N and Hall-mobility μ_H were measured by standard d.c.-techniques (v.d. Pauw-method [3]).

For Cd_3As_2 typical room temperature values of the electron concentration N and the mobility μ_H of the as-grown samples are $2 * 10^{24}$ m^{-3} and 1.6 m^2/Vs, respectively. By heating in an As atmosphere at 250° - 300°C for several days, followed by a long-term annealing at 100°C, we obtained samples with N as low as $0.5 * 10^{24}$ m^{-3} with a maximum μ_H of 2.6 m^2/Vs at 300K ($N=0.2 * 10^{24}$ m^{-3} and μ_H=30 m^2/Vs at 4.2 K).
Typical room temperature values of N and μ_H for $CdSnAs_2$ are $2 * 10^{24}$ m^{-3} and 0.7 m^2/Vs, respectively. For $(Cd_{1-x}Mn_x)_3As_2$ with x=0.01 these values are $N=5 * 10^{24}$ m^{-3} and μ_H=0.9 m^2/Vs. Annealing treatments of the $CdSnAs_2$ and $(Cd_{1-x}Mn_x)_3As_2$ crystals under different atmospheres did not affect the electron concentrations and mobilities appreciably. Examples of the temperature dependences of N and μ_H of Cd_3As_2, $CdSnAs_2$ and $(Cd_{1-x}Mn_x)_3As_2$ samples are given in fig. 4.1.

After orientation by the von Laue-back reflection method, the crystals

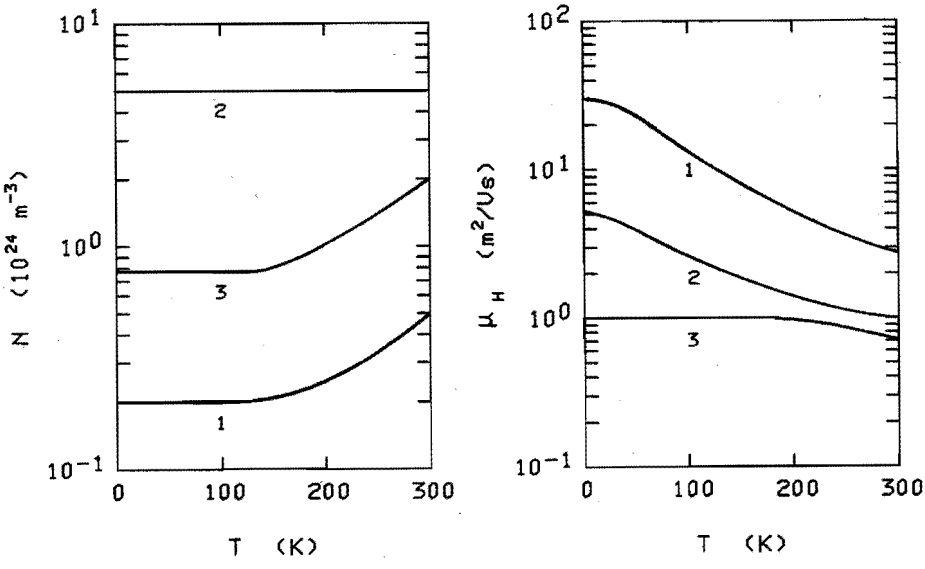

Fig.4.1. Temperature dependences of N and μ_H. For Cd_3As_2 (1) the values of N and μ_H are given for the sample with the lowest electron concentration. For $(Cd_{1-x}Mn_x)_3As_2$ (2) and $CdSnAs_2$ (3) characteristic samples have been chosen.

were cut with a wire saw into samples with final dimensions of $6 * 1 * 1$ mm^3. In order to perform SdH-measurements in different configurations, samples with the crystallographic c-axis parallel and perpendicular to the long edge were prepared. Copper current and potential leads were soldered directly onto the samples with Woods-metal.

4.2. Experimental set-up

Following the general block scheme, given in fig. 4.2, the various parts of our measuring system will be described. In §4.2.1 and §4.2.2 the detection and field modulation techniques are described. A description of the used magnets, dewars and sample holders is given in §4.2.3.

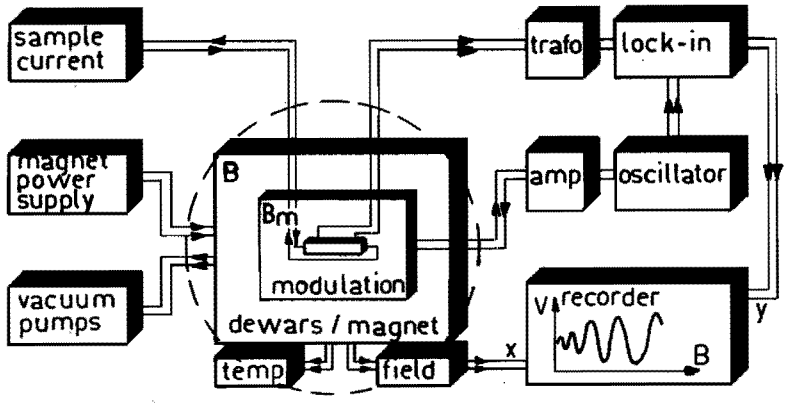

Fig.4.2. The general block scheme of the experimental set-up. The encircled part is shown in more detail in fig.4.5 and fig.4.6.

4.2.1. The main measuring circuitry

For the measurements the sample has to be placed in a magnetic field B. A constant d.c.-current (I=100 mA) is passed through the sample. The voltage drop V across the sample which varies when sweeping the magnetic field B is directly proportional to the resistivity of the sample. The oscillatory component of the voltage (V_{osc}) exhibits a small

amplitude and is superimposed on a large nonoscillatory background V_o ($V_{osc} \ll V_o$). Magnetic field modulation and phase sensitive detection [4] are used to eliminate this background.
The voltage drop is sent to a lock-in amplifier via a matching transformer. The lock-in amplifier selects a particular frequency (ω or 2ω) and phase relative to the reference signal from the oscillator ($f = \frac{\omega}{2\pi} = 33$ Hz). After being amplified the oscillator signal also drives the modulation coils. In the lock-in amplifier the selected signal is rectified and filtered. Plotting the resulting d.c.-signal versus the Hall-probe voltage on the x-y-recorder gives the desired magnetoresistance oscillations as function of B (see for instance fig. 4.7).

In order to avoid deformation of the SdH-signal the time constant of the detection system must be at least 10 times smaller than the time required for one complete SdH-oscillation. This time can be varied by varying the sweep speed of the d.c.-magnetic field [5].

4.2.2. *Magnetic field modulation* [4]

The modulation coils superimpose a small harmonic field $\hat{B}_m \cos \omega t$ on the slowly increasing main field B. The harmonic field influences the total voltage V measured across the potential contacts of the sample. The total voltage becomes $V=V_o+V_{osc}$, where V_o represents the classical magnetoresistance while V_{osc} is the oscillatory component due to the SdH-effect. For small modulation fields ($\hat{B}_m \ll B$) the voltage V_{osc} can be written as

$$V_{osc} \sim \sum_r A_r(B,T)\{\cos(2\pi r/PB - \phi_r')\cos(r\alpha\cos\omega t) - \cos(2\pi r/PB - \phi_r')\sin(r\alpha\cos\omega t)\} . \qquad (4.1)$$

Here $A_r(B,T)$ and ϕ_r' are short notations for the amplitude and phase factors, which are defined in eq. 3.4. The quantity α is defined as

$$\alpha = 2\pi\hat{B}_m/PB^2 . \qquad (4.2)$$

The factors $\cos(r\alpha\cos\omega t)$ and $\sin(r\alpha\cos\omega t)$ can be expanded in series of Besselfunctions. One obtains

$$\cos(r\alpha\cos\omega t) = J_o(r\alpha) + 2\sum_{n=1}^{\infty}(-1)^n J_{2n}(r\alpha)\cos(2n\omega t)$$
$$\sin(r\alpha\cos\omega t) = 2\sum_{n=0}^{\infty}(-1)^n J_{2n+1}(r\alpha)\sin((2n+1)\omega t) \quad . \tag{4.3}$$

Substitution of eq. 4.3 in eq. 4.1 clearly shows that modulation of the main field B with a frequency ω introduces higher harmonics of ω in V_{osc} which are weighted with their corresponding Besselfunctions. Detection of V_{osc} on the first (ω) or second (2ω) harmonic of the modulation field frequency results in d.c.-voltages given by

$$V_{osc1} \sim 2\sum_r A_r(B,T)\sin\left(\frac{2\pi r}{PB} - \phi_r'\right) J_1(r\alpha) \tag{4.4}$$

$$V_{osc2} \sim -2\sum_r A_r(B,T)\cos\left(\frac{2\pi r}{PB} - \phi_r'\right) J_2(r\alpha) \quad , \tag{4.5}$$

respectively. The resulting signals are first - or second derivative-like with respect to the original signal given by eq. 3.4.

The component V_o of the sample voltage is also influenced by the modulation field and contains harmonic terms $\cos\omega t$, $\cos 2\omega t$, $\cos 3\omega t$, etc. The relative contributions of these modulation harmonics depend on the actual behaviour of the classical magnetoresistance as function of the main field B. Since the classical magnetoresistance is only a slowly varying function of B, we are able to suppress the classical contribution by detecting on the second harmonic. A signal detected on the first harmonic or fundamental frequency will still contain a considerable background since the classical magnetoresistance is not linear in B. Therefore most of the data in this thesis are taken at the second harmonic of the modulation field. In this way we have a constant base line for the oscillations and the inductive voltages are minimised.

Observing the signal at the second harmonic of the modulation frequency, it is important to keep the harmonic distortion of the modulation field as low as possible [5]. The used oscillator, audio-

amplifier and modulation coil combination produce a total harmonic distortion of less than 1%.

The functions $J_2(\alpha)$ and $J_2(2\alpha)$ versus the main field B are given in fig. 4.3. The respective Besselfunctions exhibit several zeros in the low field region. The zeros in $J_2(\alpha)$ at $\alpha = 5.13$ etc. are used to calibrate the modulation field. This is illustrated in fig. 4.4 for an experimental SdH-recorder track.

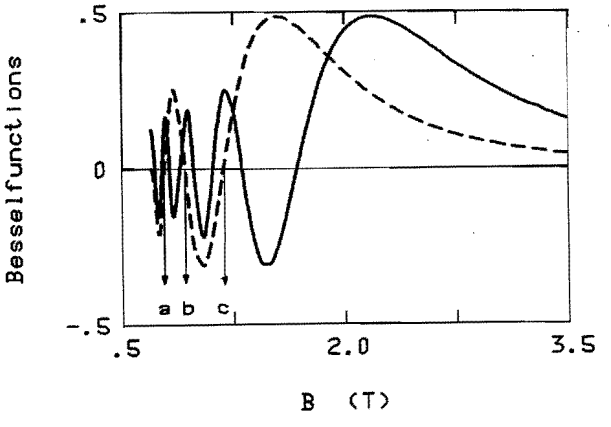

Fig.4.3. The Besselfunctions $J_2(\alpha)$ (dashed curve) and $J_2(2\alpha)$ (solid curve) as function of the main field B. For the calculations we used $P = 0.0275\ T^{-1}$ and $\hat{B}m = 0.0317$ T. The three zeros in $J_2(\alpha)$ indicated by a, b and c correspond to $\alpha = 11.62$, $\alpha = 8.42$ and $\alpha = 5.13$, respectively.

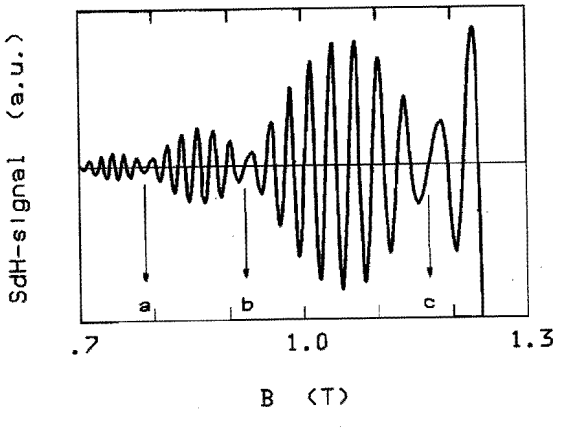

Fig.4.4. An experimental SdH-signal ($P = 0.0275\ T^{-1}$, $\hat{B}_m = 0.0317$ T) showing the zeros in $J_2(\alpha)$, which are used to calibrate the modulation field $\hat{B}_m$. The zeros indicated by a, b and c correspond to those shown in fig.4.3.

4.2.3. Magnets, cryostats and sampleholders

The SdH-experiments were performed in two almost identical experimental set-ups. The low field set-up (see fig. 4.5) consists of a nitrogen jacketed glass dewar (1) mounted between the poles of a water cooled electromagnet (B up to 2.1 T). The magnet is driven by a field regulated power supply. The main field is measured with a Hall-probe (2). To generate a modulation field ($\hat{B}_m$ up to 0.03 T) a pair of Helmholtz-type coils (3) are attached to the tapered magnet poles (4). The generated modulation field depends on the main field due to the saturation of the electromagnet iron core. The sampleholder (5) can be rotated about a vertical axis. The temperature of the sample (6), measured by a carbon-glass resistor (7), can be varied between 4.2 K and 1.6 K by pumping the He-vapour.

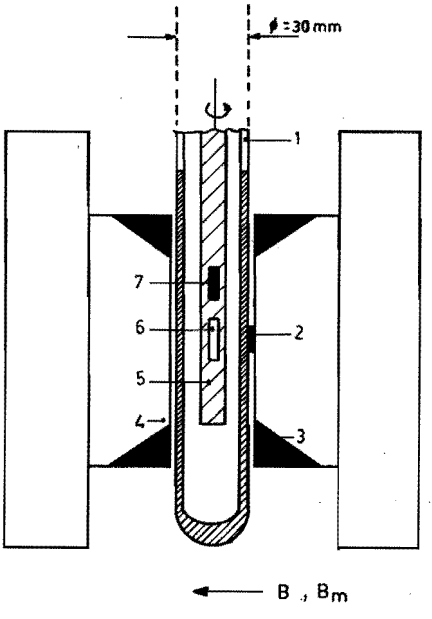

Fig.4.5.
The low field set-up.
The numbers are explained in the text.

The high field set-up consists of a stainless steel dewar system and a LHe-cooled superconducting solenoid. The system is capable of producing linearly increasing fields up to 6 T. Two types of stainless

steel insert-dewars and sampleholders are used to cover a temperature range between 2 K and 25 K.

For measurements below 4.2 K (see fig. 4.6.a) we use an insert-dewar (1) with an inner tail diameter of 35 mm, in which a motor-driven rotatable sampleholder (2) and a pair of copper Helmholtz-type modulation coils (3) ($\hat{B}_m$ up to 0.015 T) are mounted. Temperatures below 4.2 K are obtained by pumping the He-bath (4) and are measured by a carbon-glass resistor on the sampleholder (5).

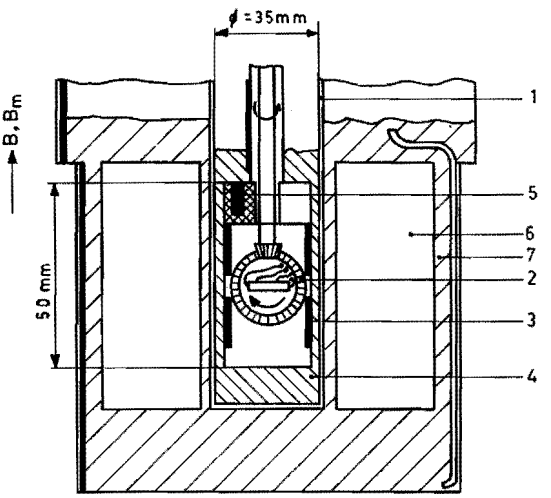

Fig. 4.6.
The high field set up.
a) Insert-dewar for measurements below 4.2 K. The numbers 6 and 7 are the superconducting solenoid and the main LHe-bath, respectively. The remaining numbers are explained in the text.

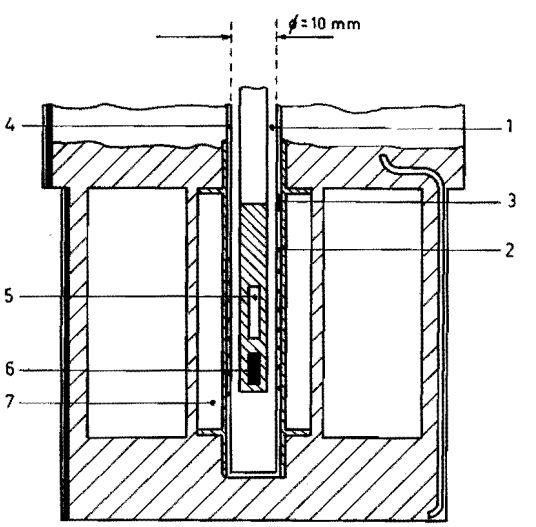

b) Insert-dewar for measurements in the region 4.2 K ≤ T ≤ 25 K . The numbers are explained in the text.

For measurements in the temperature region from 4.2 K up to about 25 K we make use of an other type of insert-dewar. This dewar consists of two vessels (see fig. 4.6.b). The inner vessel (1) of the dewar, which contains the sampleholder, is filled with He-contact gas at 1 atm. A heater (2) is mounted on the outside of the inner vessel. A small stainless steel heat-bridge (3) connects the inner with the outer vessel (4). The contact gas pressure in the outer vessel can be varied. By changing both the pressure of the contact gas in the outer vessel and the heat dissipation of the heater, the temperature of the sample (5) can be varied. When equilibrium in heat input and output is established, the sample temperature is constant within 0.01 K. The temperature of the sample is measured by means of a carbon-glass resistor (6). The orientation of the sample can only be changed by removing the sampleholder from the insert-dewar. A copper modulation coil (7) ($\hat{B}_m$ up to 0.02 T) is attached to the outside of the dewar tail which is immersed in the LHe of the main bath.

4.3. Data taking procedures

The angular dependences of the SdH-oscillation period, the effective cyclotron mass and the effective g-factor give direct information about the geometry of the Fermi-surface. In the following sections the methods used to extract the SdH-period (§4.3.1), the cyclotron effective mass (§4.3.2) and the effective g-factor (§4.3.3) from the experimental SdH-traces are described. Section 4.3.4 describes these methods in case of a SMSC.

4.3.1. The SdH-oscillation period

Usually only the first harmonic (r=1 in eq. 3.4) can be observed experimentally and the oscillations appear to be exponentially damped cosine functions. For these oscillations the spin is not resolvable and contributes only to the amplitude of the oscillations. In this case eq. 3.4 may be written as

$$\frac{\Delta\rho}{\rho_o} = A(B,T)\cos\left(\frac{2\pi}{PB} - 2\pi\gamma - \frac{\pi}{4}\right) \qquad (4.6)$$

From this equation it follows that extrema in the oscillatory behaviour for a given field orientation θ occur when

$$\frac{2\pi}{P(\theta)B} - 2\pi\gamma - \frac{\pi}{4} = m\pi \quad , \qquad (4.7)$$

where m is an integer. The phasefactor $2\pi\gamma$ is independent of the magnitude and orientation of the magnetic field, at least in the available field range. Plotting integers versus the $\frac{1}{B}$ -values of the low field oscillation extrema, one obtains a straight line of which the slope gives the period $P(\theta)$. The angular dependence of the period is obtained by repeating this procedure for different magnetic field directions θ.

A more accurate method to determine small angular dependences of the period is the following [6]. The relative change in period as function of the field direction is obtained by measuring the shift in field position of points of equal phase (m is constant in eq. 4.7). From relation 4.7 one obtains

$$\frac{P_o - P(\theta)}{P_o} = \frac{B - B_o}{B} \quad , \qquad (4.8)$$

where P_o and B_o are the reference period and field, respectively. Thus a simple measurement of the shift in the magnetic field of a constant phase point as function of θ gives directly the relative change of the period.

4.3.2. The cyclotron effective mass

The cyclotron effective masses as function of the field direction θ are determined by means of a standard procedure of measuring the temperature dependence of the peak-to-peak amplitude of the oscillations at fixed magnetic fields, for which the signal is purely periodic.

According to eqs. 3.4 and 4.6 the ratio $A(T_i)/A(T_j)$ of the oscillation

amplitudes at temperatures T_i and T_j for a fixed magnetic field B becomes

$$\frac{A(T_i)}{A(T_j)} = \frac{T_i \sinh(\beta m_c^*(\theta) T_j / m_o B)}{T_j \sinh(\beta m_c^*(\theta) T_i / m_o B)} \quad . \tag{4.9}$$

The value of $m_c^*(\theta)$ is then obtained by fitting the theoretical expression on the right handside of eq. 4.9 to the experimental amplitude ratios $A(T_i)/A(T_j)$ at fixed magnetic fields.
The accuracy of the fitted cyclotron effective mass values can be considerably increased by measuring several peak-to-peak amplitudes at different temperatures and fields (see fig. 4.7) and by applying a least squares fit to the obtained $A(B_k, T_j)$ amplitude matrices.

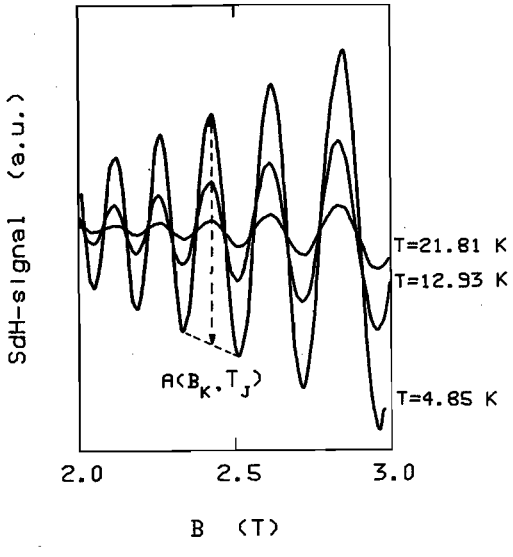

Fig.4.7. Example of SdH-recorder tracks at different temperatures measured on a $CdSnAs_2$ sample with $N = 0.95 * 10^{24}\ m^{-3}$. In the figure the data taking procedure for the cyclotron effective mass is indicated.

4.3.3. The effective g-factor

Due to the spin-splitting the degeneracy of Landau-level n is lifted and spin-splitted oscillation peaks may occur in the SdH-signal. Measured values of the period and the field positions B_n^+ and B_n^- of sharply defined spin-splitted peaks can be used in eqs. 3.15 and 3.16 to calculate $|\nu|$ rather than the absolute value

of the effective g-factor. Unfortunately mostly the thermal- and collision broadening smear out the discrete nature of the spin-splitted oscillation peaks, so that B_n^+ and B_n^- are less resolved in the available field range and a determination of g* from eqs. 3.15 and 3.16 becomes very inaccurate or even impossible (see for instance fig. 4.8).

However, from signals as shown in fig. 4.8 we determine the g*-values by a fitting procedure which uses the SdH-harmonics. It can be seen from eq. 3.4 that spin-splitted peaks appear as a result of superposition of different harmonics ($r \geq 2$). The ratio of the relative terms contains the information on the value of the effective g-factor.

Furthermore, an enhancement of the higher harmonic amplitudes relative to the fundamental amplitude can be achieved by detecting the signal with a low field modulation technique at the second harmonic of the field modulating frequency since $\lim_{\alpha \to 0} J_2(2\alpha)/J_2(\alpha) = 4$ (see fig. 4.3) [4]. The value of $|\nu|$ is determined from these SdH-signals by fitting them to the theoretical expression for the SdH-effect given in eq. 3.4, additionally taking into account the weighting of each harmonic by the Besselfunction with its proper argument. Our non linear least squares fitting routine is quite similar to that used by Stephens et al. [7]. However, Stephens et al. only use the periodic parts of the oscillations to fit the parameters, while in our method we use the relative amplitudes of the several harmonic terms. The fitting routine

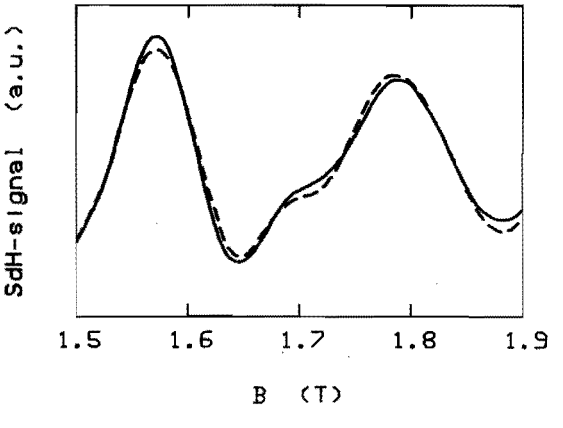

Fig.4.8. SdH-signal for a Cd_3As_2 sample with $N = 0.35 * 10^{24}\ m^{-3}$, showing a non-periodic shape due to the rise of higher harmonics. The dashed curve is obtained with our fitting routine.

takes into account the first 3 or 4 harmonics of the SdH-effect and determines the value of $|\nu|$, m_c^*, P, T_d and γ simultaneously.

4.3.4. Data taking procedures in SMSC

Measurements of the SdH-effect and the magnetisation on SMSC can provide information on the geometry of the Fermi-surface and the exchange interaction constants α, $\beta_{//}$ and $\beta_{\perp}$ which are defined in eq. 2.19. In the following we describe these measurements in more detail.

The magnetisation

Magnetisation measurements have been performed with a Foner-magnetometer on $(Cd_{1-x}Mn_x)_3As_2$ samples with a low Mn-ion content ($x \leq 0.05$). It was found that in the same temperature- and field range in which we perform the SdH-measurements, the magnetisation M can be described by the Brillouin function for a spin value of 5/2, adjusting the saturation value to an effective value $S_{eff}(x)$ and introducing an effective temperature $T_{eff}(x) = T + T_o(x)$ [8,9]:

$$M \sim \langle S \rangle = S_{eff}(x) B_{5/2}(B,\ T+T_o(x)). \qquad (4.10)$$

The results for S_{eff} and T_o as function of x are given in §5.3.1.

The SdH-oscillation period and the cyclotron effective mass

Since the period is depending only weakly on the magnetisation (see §3.5), one may use the method described in §4.3.1 to obtain the SdH-oscillation period.

The procedure (see §4.3.2) to obtain the cyclotron effective mass is only valid when the $\cos\pi\nu$-factor in eq. 4.6 is nearly constant. For SMSC this is not true in general (see eq. 2.36). However for temperatures above the temperature of the last amplitude zero (k=0 in eq. 3.18) the quantity ν will vary only slowly with temperature and approaches the value of the non-magnetic narrow-gap semiconductors. At those temperatures eq. 4.9 becomes applicable again if $|T_i - T_j|$ is small ($\leq$3 K)

[10]. Unfortunately, the small absolute value of the total SdH-oscillation amplitude at those temperatures (T ≈ 25 K) makes it impossible to perform reliable m_c^* measurements.

We adopted the Cd_3As_2-value for m_c^* for our investigated $(Cd_{1-x}Mn_x)_3As_2$ samples. Although in general in SMSC the primary band parameters change with the magnetic ion content x, the effective mass value for high electron concentrations ($N = 4 * 10^{24}$ m^{-3} in case of the $(Cd_{1-x}Mn_x)_3As_2$ samples) is expected to vary only slightly [11]. This is illustrated in fig. 4.9, which gives m_c^* (θ=0) and m_c^* (θ=90) as function of the energy gap E_g (fig. 4.9.a) and the crystal field splitting parameter δ (fig. 4.9.b) for several electron concentrations.

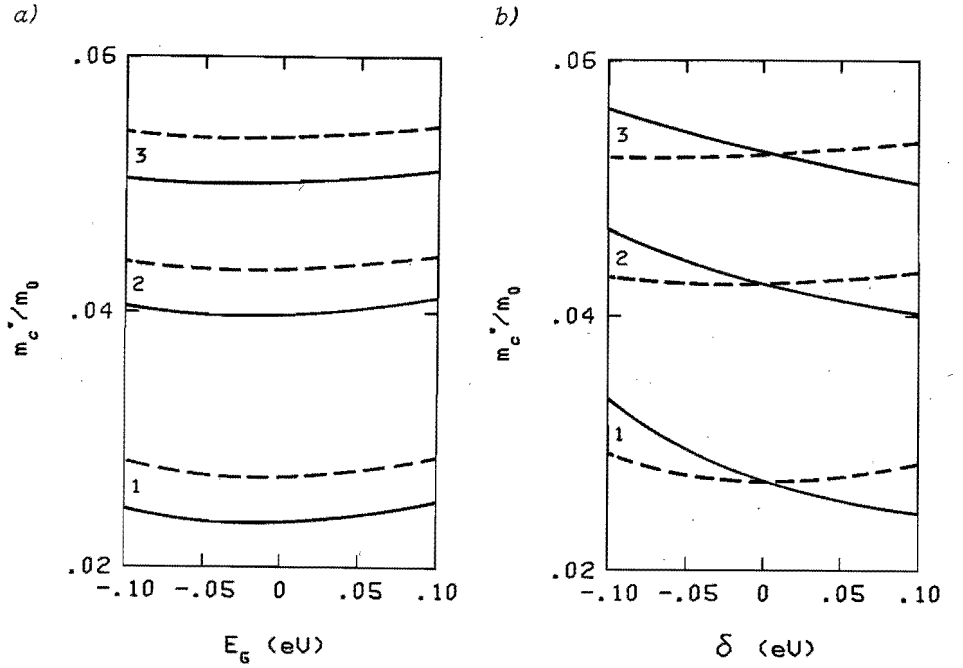

Fig.4.9 The E_g and δ dependences (4.9.a and 4.9.b, respectively) of $m_c^*(\theta = 0)$ (solid curve) and $m_c^*(\theta = 90)$ (dashed curve) for $N = 0.4 * 10^{24}$ m^{-3} (1), $2 * 10^{24}$ m^{-3} (2) and $4 * 10^{24}$ m^{-3} (3), respectively. The parameter values $\Delta = 0.27$ eV and $P_{//} = P_{\perp} = 7.3 * 10^{-10}$ eVm have been used in the calculations.

The effective g-factor

The value of the effective g-factor at temperatures and fields for which a pronounced zero in the SdH-oscillation amplitude occurs, can be obtained from eq. 3.18. However, the values of m_c^* and ν at the given temperature and field must be known. In principle the proper value of ν (or k) can be selected from the positions of the successive zeros on the temperature scale. This can be illustrated by using fig. 5.20. If the zero at T=2K corresponds to ν=5/2 or 3/2 respectively, then the zero at T=6K must correspond to ν=3/2 or 1/2 respectively. With increasing temperature the value of ν will decrease and finally reach the value corresponding to the case in which the influence of the exchange interaction on ν can be neglected. Knowing this value one can easily find the correct values of ν belonging to the spin-splitting zeros in amplitude by simply counting the numbers of zeros.

Furthermore, the existence of well defined amplitude zeros in B and T is crucial in order to obtain accurate g*-values from eq. 3.18. For some samples, as shown in fig. 3.4, the total signal does not become zero at a specific value of B and T, but a minimum in amplitude is observed over a wide range of B. In that case the spin-splitting zero procedure fails. A harmonic content analysis (see §4.3.3), similar to that used for normal semiconductor SdH-signals, does not lead to reliable results since it is based on eq. 3.4 with ν independent of B and T. One might include these dependences by introducing an analytical expression for g*, such as given in eq. 2.35 for θ=0 and fit the signal by varying α, $\beta_{//}$ and $\beta_{\perp}$ instead of g*. However, in that case the validity of the analytical g*-expression has to be checked first by other methods like for instance magneto-absorption measurements.

REFERENCES

[1] R. Koltirine, M. Chaumereuil, Phys. Stat. Solidi 13, K1 (1966).

[2] D.B. Gasson, P.J. Holmes, I.C. Jennings, B.R. Marathe, J.F. Parrot, J. Phys. Chem. Solids 23, 1291 (1962).

[3] L. v.d. Pauw, Philips Res. Rep. 13, 1 (1958).

[4] A. Goldstein, S.J. Williamson, S. Foner, Rev. Sci. Instrum. 36, 1356 (1965).

[5] B.L. Booth, Ph.D. Thesis, Northwestern Univ., Evanston 1967.

[6] D. G. Seiler, Phys. Rev. B1, 2824 (1970).

[7] A.E. Stephens, R.E. Miller, J.R. Sybert, D.G. Seiler, Phys. Rev. B18, 4394 (1978).

[8] W.J.M. de Jonge, M. Otto, C.J.M. Denissen, F.A.P. Blom, C. van der Steen, K. Kopinga, J. Magn. & Magn. Mat. 31-34, 1373 (1983).

[9] Only very recently it was found that a Mn-ion spin value of 3/2 has to be used in eq. 4.10. This leads to different experimental values of $S_{eff}(x)$ and $T_o(x)$. The actual value of <S> remains unchanged.
W.J.M. de Jonge, private communication.

[10] M. Jaczynski, W. Dobrowolski, Phys. Stat. Solidi B102, 195 (1980).

[11] R. Dornhaus, G. Nimtz, Springer Tracts in Modern Physics 78: Solide State Physics, (Springer Verlag, Berlin 1976), p. 36.

CHAPTER V THE RESULTS AND INTERPRETATION OF SdH-MEASUREMENTS ON Cd_3As_2, $CdSnAs_2$ AND $(Cd_{1-x}Mn_x)_3As_2$ SAMPLES

In this chapter the results of our SdH-measurements are presented and interpreted in the models given in chapter II. It should be noted that we performed SdH-measurements on far more samples than presented in this chapter. The SdH-effect provides a very sensitive check of the quality of the samples [1]. Therefore we carefully examined the SdH-patterns of all samples on irregularities and excluded samples with very noisy SdH-oscillations or beating patterns due to inhomogeneities from further investigations.

For Cd_3As_2 the results and interpretation are given in § 5.1. For $CdSnAs_2$ the results and interpretation are presented in § 5.2. The results on mono- and polycrystalline $(Cd_{1-x}Mn_x)_3As_2$ material and the interpretation of these results in the band model for SMSC are given in §5.3. In contrast to our results on Cd_3As_2 and $CdSnAs_2$ we are only able to give a tentative interpretation of our results on $(Cd_{1-x}Mn_x)_3As_2$. This is mainly caused by difficulties in material technology.

5.1. Cd_3As_2: Results and Interpretation

5.1.1. Introduction

We have investigated the shape of the conduction band Fermi-surface of Cd_3As_2 by measuring the angular dependences of the SdH-oscillation period, the cyclotron effective mass and the effective g-factor for several samples with electron concentrations in the range from $0.19 * 10^{24}$ m^{-3} to $7.75 * 10^{24}$ m^{-3} at 4.2 K.

The configurations in which measurements have been performed are defined in fig. 5.1. In these configurations the magnetic field $\vec{B}$ rotates about the [100]-axis (conf. I), the [$1\bar{1}0$]-direction (conf. II) and the [001]-axis (conf. III), respectively. A survey of the samples ordered with increasing electron concentration is given in table 5.1. The columns give the sample-code, the electron concentration and the configuration in which measurements have been performed. For all samples P(Θ) has been determined in conf. I. Cyclotron effective mass measurements

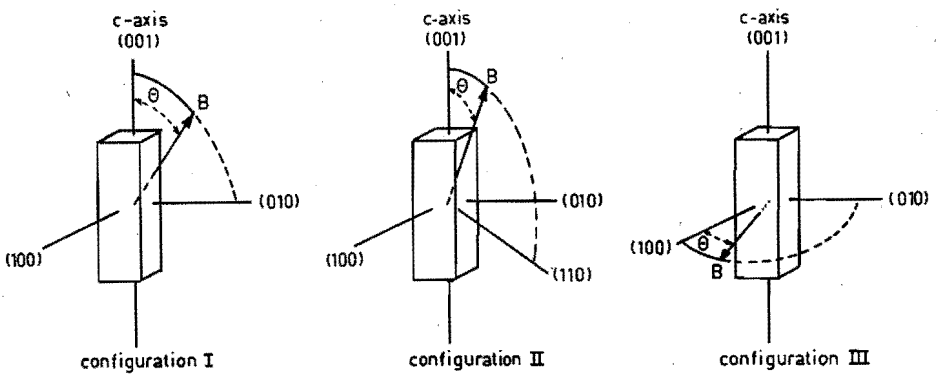

Fig.5.1. Definition of the configurations.

	sample	N (10^{24} m^{-3})	conf.	P(θ)	$m_c^*(\theta)$	$g^*(\theta)$
1	As-64-3-B	0.19	I	A	+	-
2	AS-64-7-1	0.33	I	A	-	-
3	As-35-18-2	0.35	I	A	+	+
4	As-35-15-1	0.40	I	A	-	-
5	As-64-2-A	0.53	I,II,III	R	-	-
6	As-64-2-B	0.69	I,II,III	R	-	-
7	As-38-7-1	0.78	I	A	+	+
8	As-38-3-4	0.80	I	A	+	-
9	As-35-3-1	0.84	I	A	+	-
10	As-64-15-1	1.12	I,II,III	R	+	-
11	As-55-4-3	1.60	I	A	+	+
12	As-61-3-1	1.90	I,II,III	R	-	-
13	As-61-3-3	2.70	I,II,III	R	-	-
14	As-61-3-2	7.75	I,II,III	R	-	-

Table 5.1. Survey of the measured Cd_3As_2 samples.
The absolute (see eq. 4.7) and relative (see eq. 4.8) period measurements are indicated with A and R, respectively.

have been performed on 7 of these samples, while for the samples with $N = 0.35 * 10^{24} m^{-3}$, $0.78 * 10^{24} m^{-3}$ and $1.60 * 10^{24} m^{-3}$ we were able to fit $g^*(\theta)$ in conf. I. The results of these period-, cyclotron effective mass- and effective g-factor measurements are given in § 5.1.2 and interpreted in § 5.1.3. For some samples $P(\theta)$ has been determined in configurations I, II and III by means of the relative method. The results of these measurements are presented and discussed in § 5.1.4.

5.1.2. Results on $P(\theta)$, $m_c^*(\theta)$ and $g^*(\theta)$

Fig. 5.2 shows the angular dependences of the period for some of our samples. The curves are least square fits using eq. 3.10. From the fitted values of $P(\theta = 0)$ and $P(\theta = 90)$, which are plotted in fig. 5.3, the electron concentration N (see eq. 3.11) and the anisotropy coefficient K_p (eq. 3.12) have been calculated. The values of N agree within a few percent with those obtained from Hall-effect measurements at 4.2 K. The results for K_p as function of the electron concentration are given in fig. 5.5.

Effective cyclotron mass measurements have been performed in the field region from 0.5 T to 1.5 T. An example of the angular dependences

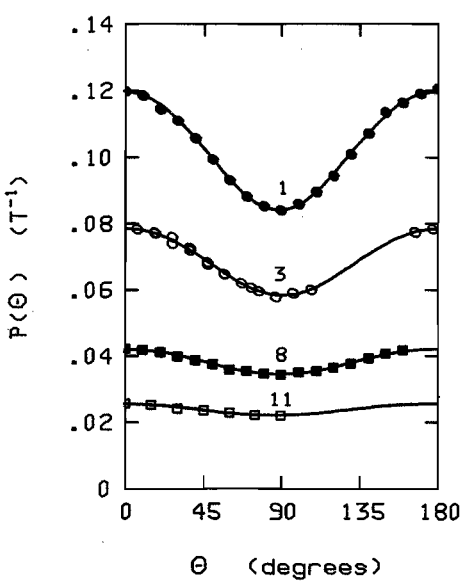

Fig.5.2.
The angular dependences of the SdH-oscillation period for several samples. The numbers refer to samples listed in table 5.1. The curves are the best fits according to eq. 3.10.

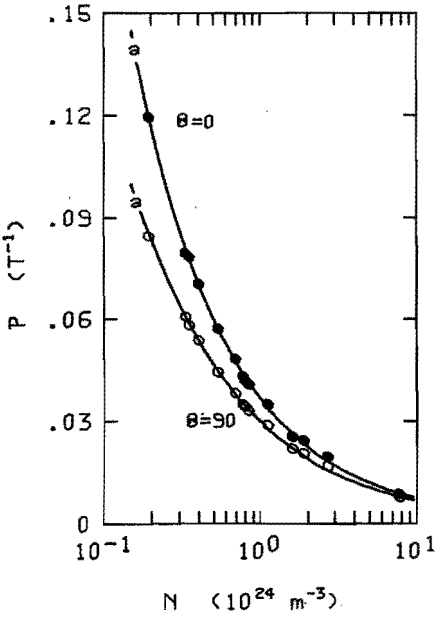

Fig. 5.3.
The electron concentration dependences of the periods P(θ = 0) and P(θ = 90). The curves (a) have been calculated with E_g = −0.095 eV, Δ = 0.27 eV, δ = 0.085 eV, $P_{//} = 7.21 * 10^{-10}$ eVm and $P_{\perp} = 7.43 * 10^{-10}$ eVm.

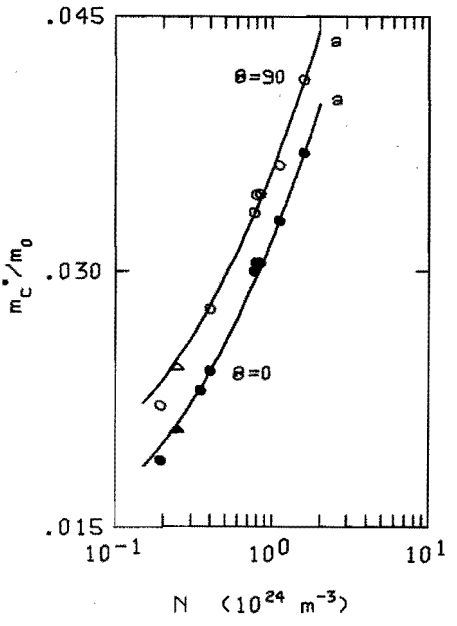

Fig. 5.4.
The electron concentration dependences of the cyclotron effective masses $m_c^*(\theta = 0)$ and $m_c^*(\theta = 90)$. The symbols Δ and ▲ refer to [6]. The curves (a) have been calculated with the parameters given in the caption to fig. 5.3.

of m_c^* is given in fig. 5.7. The experimental $m_c^*(\theta = 0)$ and $m_c^*(\theta = 90)$ values are shown in fig. 5.4. The resulting values for the anisotropy coefficient K_m (eq. 3.13) are given in fig. 5.6. The figures 5.3 to 5.6 clearly show that for all our samples $P(\theta = 0) > P(\theta = 90)$, $m_c^*(\theta = 0) < m_c^*(\theta = 90)$ and $K_p > K_m$. Furthermore it can be seen that K_p and K_m decrease with increasing electron concentration.

In combination with accurate measurements of $P(\theta)$ and $m_c^*(\theta)$, the anisotropy of the effective g-factor could be determined for the samples with $N = 0.35 * 10^{24}\ m^{-3}$ $0.78 * 10^{24}\ m^{-3}$ and $1.60 * 10^{24}\ m^{-3}$. An example of the experimental SdH-patterns is shown in fig. 5.8 for the sample

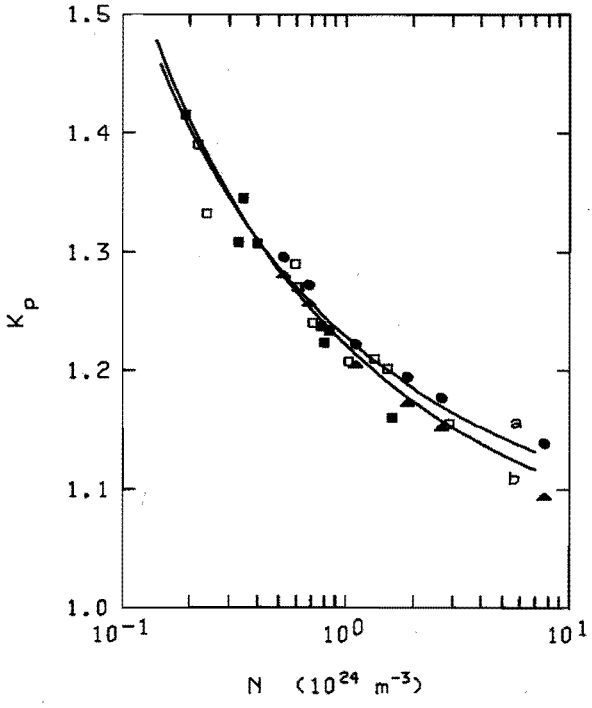

Fig.5.5.
The electron concentration dependences of the anisotropy coefficient of the period. The symbols read as follows:
■ *: absolute period measurements in conf. I.*
● *: relative period measurements in conf. II.*
▲ *: relative period measurements in conf. I.*
□ *: [5,6].*
Curve a is calculated with the parameters given in the caption to fig.5.3, curve b is obtained with $E_g = -0.095eV$, $\Delta = 0.027eV$, $\delta = 0.095eV$, $P_{//} = 7.35 * 10^{-10} eVm$ *and* $P_{\perp} = 7.40 * 10^{-10} eVm$.

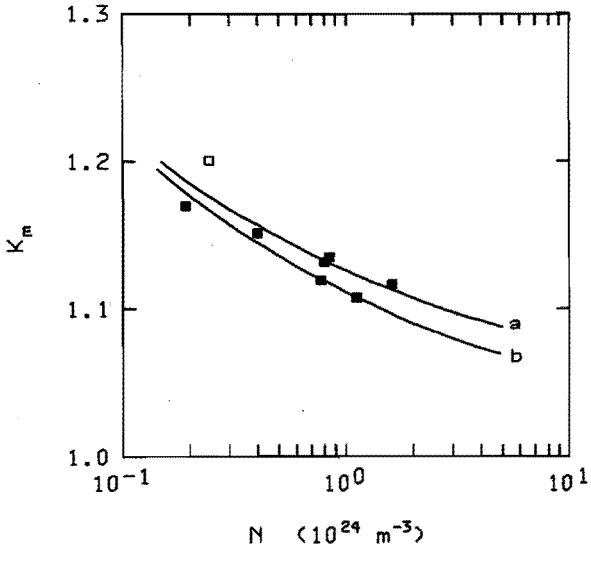

Fig.5.6.
The electron concentration dependences of the anisotropy coefficient of the cyclotron effective mass. The symbol □ refers to [6]. The curves a and b are obtained for the same parameter sets as in fig. 5.5.

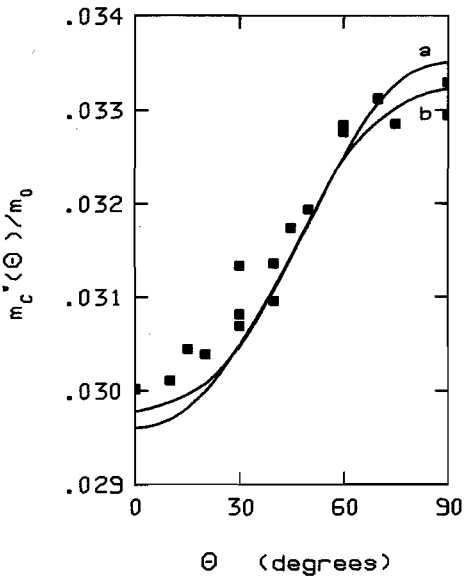

Fig.5.7.
Directional dependences of m_c^*/m_0 *for sample 7 (* $N = 0.78 * 10^{24}\ m^{-3}$ *). The curves correspond to the same parameter sets as in fig. 5.5.*

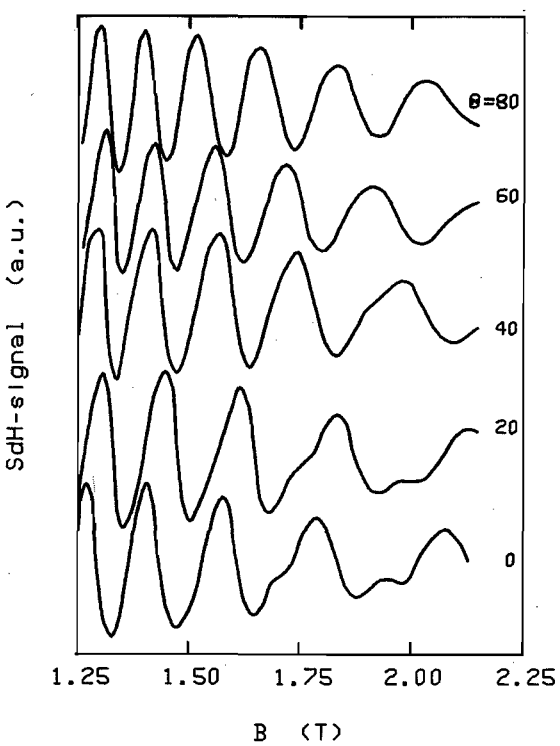

Fig.5.8.
Reproductions of the recorder graphs of sample 7 ($N = 0.78 * 10^{24}\ m^{-3}$*) for different field orientations. Second harmonic detection at* $T = 2.20$ *K.*

with N = 0.78 * 10^{24} m^{-3}. We fitted the experimental SdH-oscillations to the expression given by eq. 3.4 by means of our curve fitting routine (§ 4.3.3) As fitting parameters we used the period P, the Dingle-temperature T_d, the phase factor γ, the cyclotron effective mass m_c^* and the g*-factor. An example of such a fit is given in fig. 4.8 for the sample with N = 0.35 * $10^{24} m^{-3}$.

In this case the following values of the parameters were obtained for $\theta = 0$: $P(\theta = 0) = 0.0782\,T^{-1}$, $T_d = 11.2$ K, $\gamma = 0.533$, $m_c^*(\theta = 0) = 0.023 m_o$ and $g^*(\theta = 0) = 30.2$. As a check the values of P, T_d, γ and m_c^* have also been determined for each angle θ by analysing the pure periodic oscillations in a low field range (0.6T-0.8T) at different temperatures between 2.1 K and 4.2 K. The values of P, T_d, γ and m_c^* obtained in this way correspond within a few percent with those obtained from the g*-fit routine.

In fig. 5.9 we show the directional dependences of the g*-factor for the 3 investigated samples. It should be remarked that experimental data are

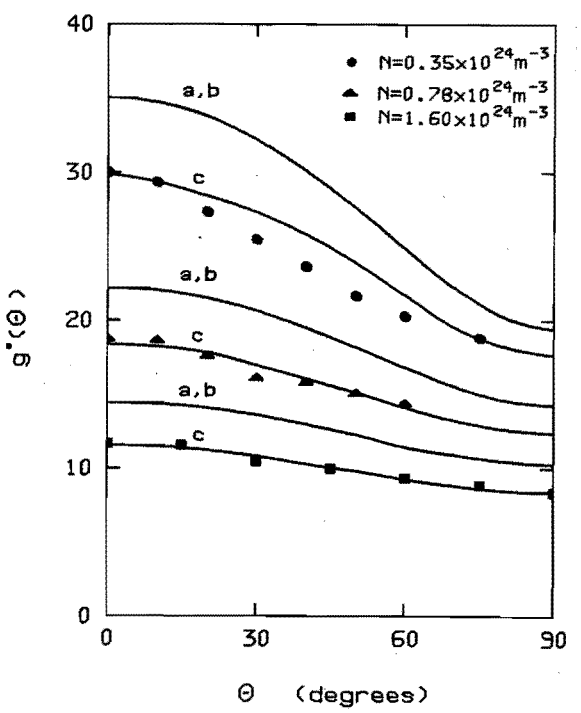

Fig.5.9.
The effective g-factor as function of θ for different electron concentrations. Curve c is obtained by taking into account the influence of the quantised free electron contribution. Curves a and b have been calculated for the parameter sets used for the fig.5.3 and fig.5.5.

missing at large angles for the samples with $N = 0.35 * 10^{24}\ m^{-3}$ and $N = 0.78 * 10^{24}\ m^{-3}$. This is caused by the fact that in this region the value of $\nu (= m_c^*(\theta) g^*(\theta)/2m_o)$ passes through $\nu = 0.25$, so that the second harmonic almost completely disappears and hence our method becomes very insensitive.

5.1.3. Interpretation of the $P(\theta)$-, $m_c^*(\theta)$- and $g^*(\theta)$ data

Analysing the experimental data of Rosenman [2] and Doi et al. [3], concerning SdH- and DHvA-effects, Bodnar [4] determined numerical values of the bandparameters for Cd_3As_2 i.e.

$$Eg = (-0.095 \pm 0.010)\ eV$$

$$\Delta = (0.027 \pm 0.03)\ eV$$

$$\delta = (0.085 \pm 0.010)\ eV$$

$$P_{//} = (7.21 \pm 0.05) * 10^{-10}\ eVm$$

$$P_{\perp} = (7.43 \pm 0.05) * 10^{-10}\ eVm$$

In these experiments the electron concentration covered only a small range around $2 * 10^{24} m^{-3}$. Our measurements on the SdH-oscillation period together with those reported by Monen [5] and Blom and Gelten [6], show that $P(\theta = 0)$, $P(\theta = 90)$ and K_p as functions of N can be correctly described by using the above given parameters down to $N = 0.2 * 10^{24}\ m^{-3}$. This can be seen from the figures 5.3 and 5.5 where the curves (a) have been calculated with the original Bodnar parameters. The agreement between points and curves is good, keeping in mind that the parameter values have been determined by Bodnar from samples with considerably smaller anisotropy.
The anisotropy of the SdH-period proves to be not very sensitive to variation of the parameters. Cyclotron effective mass and effective g-factor measurements as function of the field orientation and the electron concentration provide an additional and more sensitive check of Bodnar's conduction band and its parameter values. The Bodnar parameter set also describes our m_c^* measurements reasonably well. This can be

seen from the figures 5.4, 5.6 and 5.7 (curves a). Over a wide range of electron concentrations the experimental values of K_m deviate less than 2% from those given by the curve (a). Since the experimental values of $m_c^*(\theta = 0)$ and $m_c^*(\theta = 90)$ are accurate up to 3% the agreement for both K_m and $m_c^*(\theta = 0)$, $m_c^*(\theta = 90)$ is satisfactory. Only for the lowest electron concentration the theoretical values of $m_c^*(\theta = 0)$ and $m_c^*(\theta = 90)$ are somewhat too high.

Although the Bodnar-set of bandparameters describes our period and effective mass measurements reasonably well, we have tried to obtain even better values of the parameters. Keeping E_g and Δ fixed at -0.095eV and 0.27eV respectively, we have fitted $P(\theta)$ and $m_c^*(\theta)$ for several samples with different N. The averaged values of $P_{//}$, $P_\perp$ and δ turned out to be

$$P_{//} = (7.35 \pm 0.05) * 10^{-10} \text{ eVm}$$

$$P_\perp = (7.40 \pm 0.10) * 10^{-10} \text{ eVm}$$

$$\delta = (0.095 \pm 0.010) \text{ eV}$$

A 10 percent change of E_g and Δ did not alter the fitted values of $P_{//}$, $P_\perp$ and δ by more than 5%. In figures 5.5, 5.6 and 5.7 the curves (b) have been calculated with the fitted values of the parameters. The difference between these bandparameters and the Bodnar set of parameters is only marginal. An interesting aspect is the very small difference between $P_{//}$ and $P_\perp$, which indicates that the introduction of a crystal field splitting parameter alone seems to be sufficient to describe the anisotropy of the conduction band at this stage.

The effective g-factor is the third quantity which is sensitive to the conduction band structure. Previous reports [6-8] on g*-values were roughly in agreement with theoretical calculations for an isotropic band model [9]. However, these measurements are too incidental to give information about a possible anisotropy of g*. Our measurements of $g^*(\theta)$ given in fig. 5.9 clearly show an anisotropy which is considerably larger than the anisotropy in $P(\theta)$ and $m_c^*(\theta)$ and which strongly decreases with increasing N.

The curves (b) in fig. 5.9 are obtained with the Wallace formula for $g^*(\theta)$ (see eq. 2.15), substituting the values of the bandparameters previously determined from the best fits to period and effective mass data. The theoretical curves (a) of $g^*(\theta)$ calculated with the original Bodnar values practically coincide with these curves. The curves describe satisfactorily the observed angular dependences, but the absolute values of the theoretical curves and the experimental points still differ about 20 percent. A fit of the data points of $g^*(\theta)$ resulted in the following values for E_g, $P_{//}$, $P_{\perp}$, δ and Δ: $E_g = -0.10$ eV, $P_{//} = P_{\perp} = 7.3 * 10^{-10}$ eVm, $\delta = 0.087$eV and $\Delta = 0.18$ eV. The resulting value for Δ is far too low as compared to those reported in literature ($\Delta = 0.27$ eV- 0.30 eV)[10-12]. For this reason we do not feel convinced that this set of bandparameters is more favourable than the afore mentioned one.

The discrepancy between the calculated curves (a,b) and the experimental values of g^* might be attributed to neglecting the corrections for the free electron term and/or the influence of higher bands [13]. An incorporation of the free electron term into the expression of the g^*-factor, in conformity with the method suggested by Zawadzki [14] does indeed lower the theoretical g^*-values. However, as shown by Singh and Wallace [15], the Zawadzki method neglects the quantisation of the free electron term in the presence of a field. The calculations of Singh and Wallace give an essential improvement of the agreement between experimental and theoretical values of the g^*-factor as is shown in fig. 5.9 (curves c).

Various authors [13, 16, 17] consider the influence of higher bands on the g^*-factor in narrow gap semiconductors (NGSC) to be more important than the free electron contribution. The introduction of higher bands for Cd_3As_2 is complicated and adds several new unknown parameters to the set of basic bandparameters Eg, Δ, δ, $P_{//}$ and $P_{\perp}$. A fit of all our data with an enlarged number of parameters will give more doubtful results than the incorporation of the free electron term.
With the introduction of the quantised free electron contribution, it is possible to fit the $g^*(\theta)$-data with the same parameters which are consistent with the experimental $P(\theta)$- and $m_c^*(\theta)$-data. From this it

seems that the influence of higher bands on the effective g-factor is much smaller than has been expected, at least for Cd_3As_2.

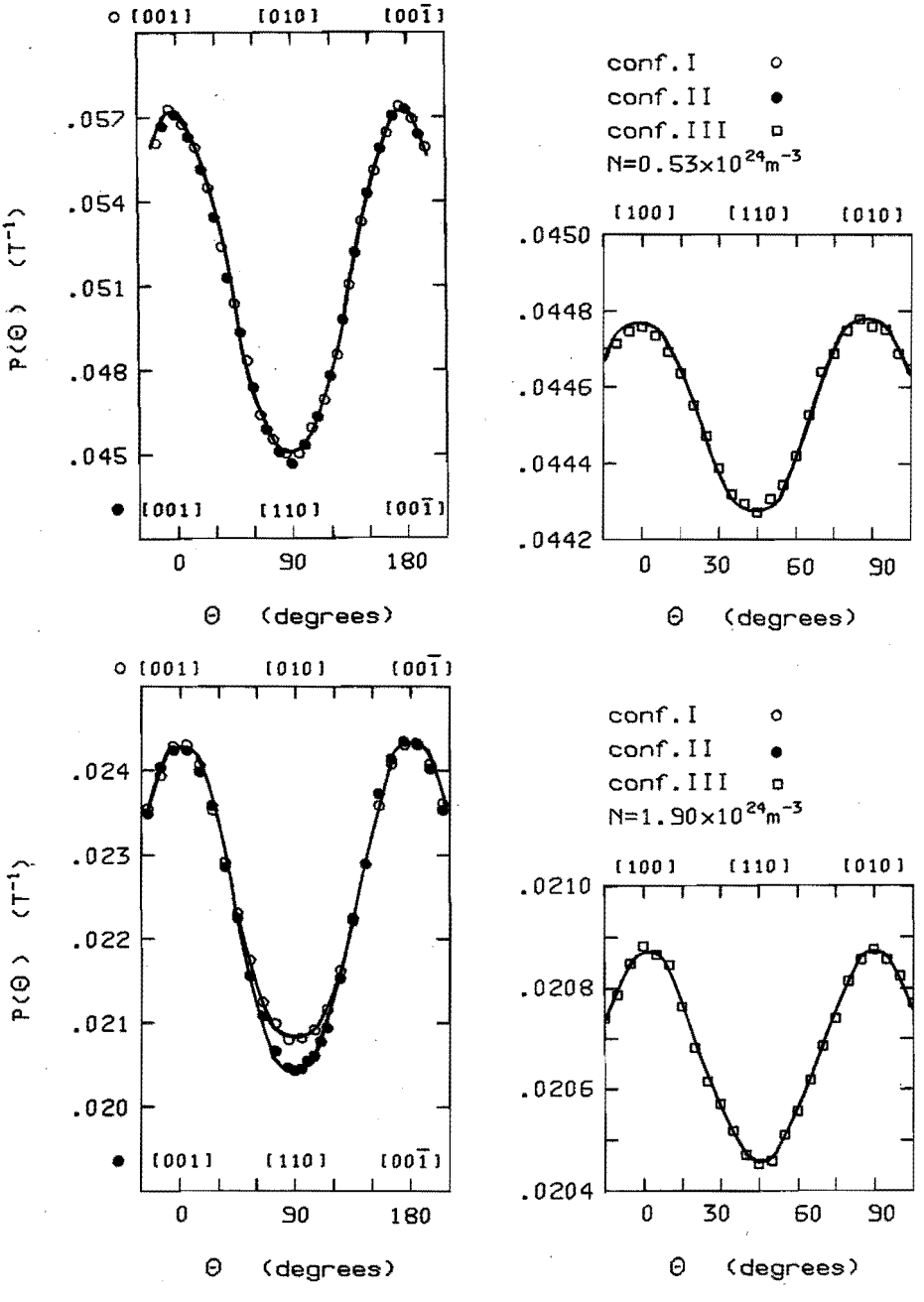

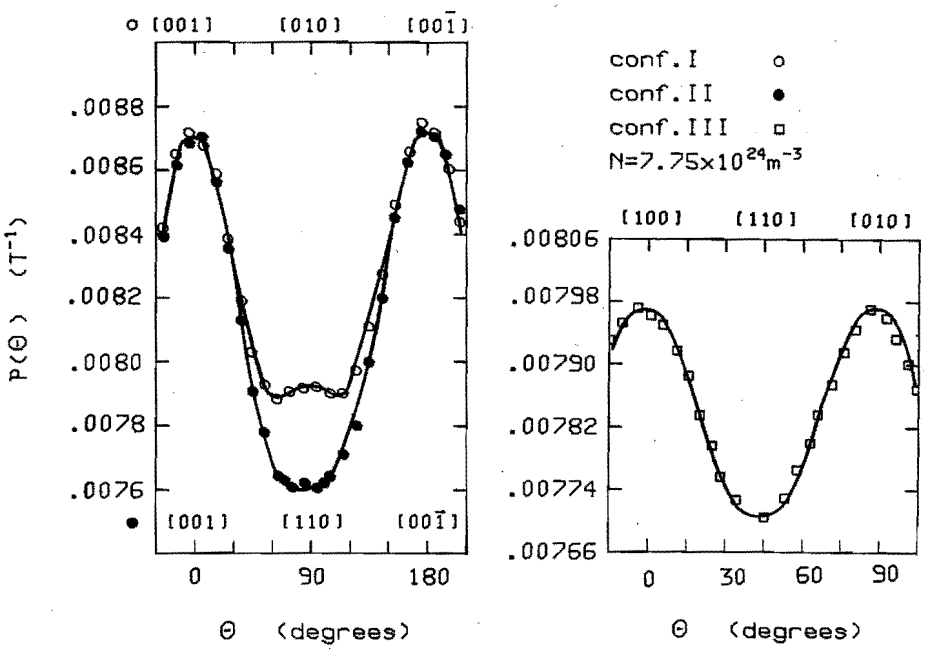

Fig.5.10. The angular dependences of the period for several samples in conf.I,II and III.
The curves have been obtained with the values of u_B and v_B given in table 5.2.

5.1.4. Deviations from the Bodnar-model for Cd_3As_2

During our measurements of P(θ) in the different configurations we discovered a small anisotropy of the period in configuration III for samples with relatively high electron concentrations. This anisotropy indicates a deviation of the Fermi-surface, which should be an ellipsoid of revolution about the k_z-axis according to Bodnar. We systematically investigated the angular dependences of the period in the configurations I, II and III for 6 samples with $0.5 * 10^{24}m^{-3} < N < 8.0 * 10^{24}m^{-3}$. The P(θ)-data for these samples are taken according to eq. 4.8.
Fig. 5.10 presents the angular variations of the period (conf. I, II and III) which are typical for the 6 samples. The dominant anisotropy

in conf. I and II is of the Bodnar-type. The ratios $P(\theta = 0)/P(\theta = 90)$ in these configurations are indicated in fig. 5.5 by the symbols ▲ (conf. I) and ● (conf. II). The observed angular behaviour in conf. III, which does not agree with the Bodnar-model, is quite similar to that observed in the cubic narrow gap semiconductors HgSe [18] and GaSb [19] in shape as well as in increase of the ratio $P(\theta = 0)/P(\theta = 45)$ with increasing electron concentration.

As a first approximation we treated the observed deviations from the Bodnar-model with the model for warped Fermi-surfaces of cubic NGSC [18,19] (see appendix). By introducing the quantities u_B and v_B which are expected to depend on the primary bandparameters, the higher bandparameters and the electron concentration we are able to describe the complete observed angular dependences in the given configurations as is shown by the curves in fig. 5.10.

The agreement between the experimental data and the corresponding calculated curves is almost perfect in each case. The obtained values of u_B and v_B for the 6 Cd_3As_2 samples are given in table 5.2.

The value of u_B turns out to increase with increasing N while v_B remains practically constant. The values of u_B and v_B are comparable to those found for HgSe and GaSb in absolute value as well as in sign. However, conclusions about the actual values of higher bandparameters can not be drawn from the obtained values of u_B and v_B since we do not know in which way u_B and v_B depend on these higher bandparameters for our case.

Attemps have been made fo fit higher bandparameters for Cd_3As_2 by calculating numerically $P(\theta)$ in the three configurations directly from a second order $\vec{k}.\vec{p}$ perturbation Hamiltonian [20] added to the Bodnar Hamiltonian. In this procedure the primary bandparameters were fixed

sample	N (10^{24} m^{-3})	u_B	v_B
As-64-2-A	0.53	0.35	-2.89
As-64-2-B	0.69	0.45	-2.80
As-64-15-1	1.12	1.07	-2.53
As-61-3-1	1.90	1.06	-2.64
As-61-3-3	2.70	1.24	-2.71
As-61-3-2	7.75	1.43	-2.65

Table 5.2.
The values of the warping parameters u_B and v_B for different electron concentrations.

at the values given in § 5.1.3., while the higher bandparameters were varied successively in order to fit the experimentally observed P(θ) behaviour. Up to now this procedure did not give satisfactory results.

5.2. *$CdSnAs_2$: Results and Interpretation*

5.2.1. *Introduction*

The angular dependences of the period and cyclotron effective mass have been measured for several $CdSnAs_2$-samples with electron concentrations in the range from $0.19 * 10^{24} m^{-3}$ to $3.97 * 10^{24} m^{-3}$ at 4.2 K. Table 5.3 gives a survey of the samples and the performed measurements. On 11 samples the period P(θ) has been measured by the absolute method (A), that is taking the data according to eq. 4.7. For the remaining samples the P(θ)-data were taken by the relative method (R), according to eq. 4.8. The cyclotron effective mass as function of the field orientation is obtained for 7 samples in configuration II. Only for the sample with the lowest electron concentration we were able to determine the g*(θ)-behaviour in configuration II.

The results of the period, effective mass and effective g-factor measurements are given in § 5.2.2 and interpreted in terms of the Bodnar-model in § 5.2.3. Deviations of the Bodnar-model are discussed in § 5.2.4.

5.2.2. *Results on P(θ), m_c*(θ) and g*(θ)*

The angular dependences of the period are shown in fig. 5.11 for some of our samples. The values of P(θ = 0), P(θ = 90) and the anisotropy coefficient K_p have been determined more accurately by a least squares fit of the experimental P(θ) data with eq. 3.10. The fitted values of P(θ = 0) and P(θ = 90) were used to calculate the electron concentration N by means of eq. 3.11 for an ellipsoid of revolution. They agree within a few percent with those obtained from Hall-effect measurements at 4.2 K. This proves, within the investigated range of electron concentrations, that we are dealing with a single ellipsoid.

	sample	N (10^{24} m^{-3})	conf.	P(θ)	$m_c^*(\theta)$	$g^*(\theta)$
1	CSA-6-2	0.19	II	A	+	+
2	CSA-6-3	0.27	II	A	-	-
3	CSA-6-12	0.32	II	A	+	-
4	CSA-6-13	0.43	II	A	+	-
5	CSA-6-6	0.44	II	A	-	-
6	CSA-6-4-1	0.45	II	A	-	-
7	CSA-6-4-2	0.46	II	A	+	-
8	CSA-6-4-A	0.47	II	A	+	-
9	CSA-22-2-1	0.71	I,III	R	-	-
10	CSA-8-3	0.75	II	R	-	-
11	CSA-22-1-1	0.93	I	R	-	-
12	CSA-8-9	0.95	II	A	+	-
13	CSA-8-A-1	0.96	II	A	-	-
14	CSA-8-A-4	1.04	II	R	-	-
15	CSA-8-A-6	1.06	II	R	-	-
16	CSA-8-A-3	1.09	II	R	-	-
17	CSA-8-A-2	1.10	II	R	-	-
18	CSA-8-A-7	1.13	II	R	-	-
19	CSA-1-8	1.38	II	A	+	-
20	CSA-10-3-2	1.68	I	R	-	-
21	CSA-9-6-5	2.72	I,III	R	-	-
22	CSA-9-16-4	3.97	I,III	R	-	-

Table 5.3. Survey of the measured $CdSnAs_2$ samples. A= absolute period, R= relative period.

For all samples we find $P(\theta = 90) > P(\theta = 0)$ in conf. I and II. This can be seen from fig. 5.12, which shows the electron concentration dependences of $P(\theta = 0)$ and $P(\theta = 90)$. The anisotropy in the period is quite small so that an accurate determination of the values of K_p in the respective configurations is difficult. Nevertheless, our results show that K_p increases with increasing electron concentrations, as can be seen from fig. 5.14.

Here it should be noted that the K_p values obtained from relative

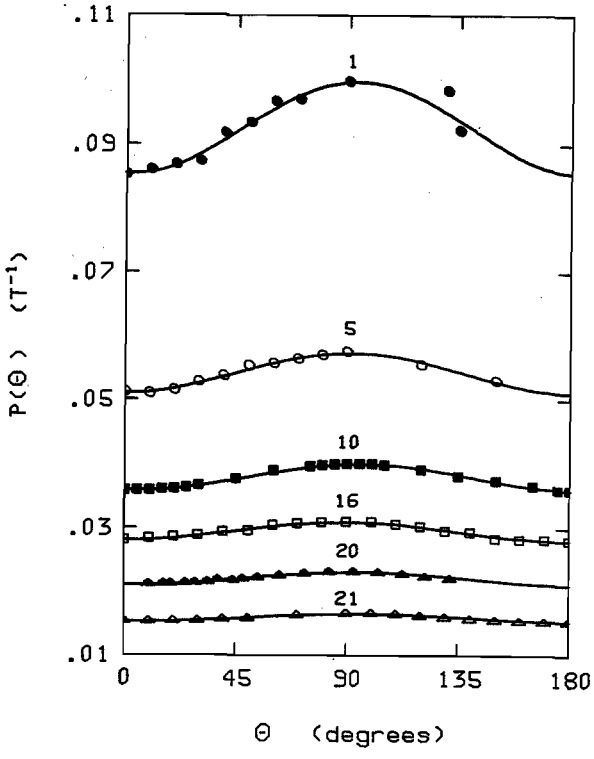

Fig.5.11.
The angular dependences of the SdH-oscillation period for several samples.
The numbers refer to samples listed in table 5.3.
The curves are the best fits according to eq.3.10.

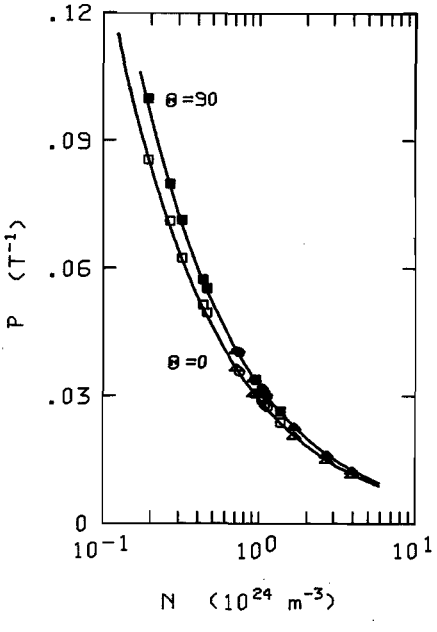

Fig.5.12.
The electron concentration dependences of the periods P(θ=0) and P(θ=90). The results for the samples with codes 4,5;6,7,8;12,13; 14,15 and 16,17 have been averaged.
The symbols read as follows:
□ , ■ *absolute period in conf.II.*
○ , ● *relative period in conf.II.*
△ , ▲ *relative period in conf.I.*
The curves have been calculated with E_g*=0.26 eV,*Δ*=0.5 eV,*δ*=-0.1 eV,* $P_{//}=P_{\perp}=8.5*10^{-10}$ *eVm.*

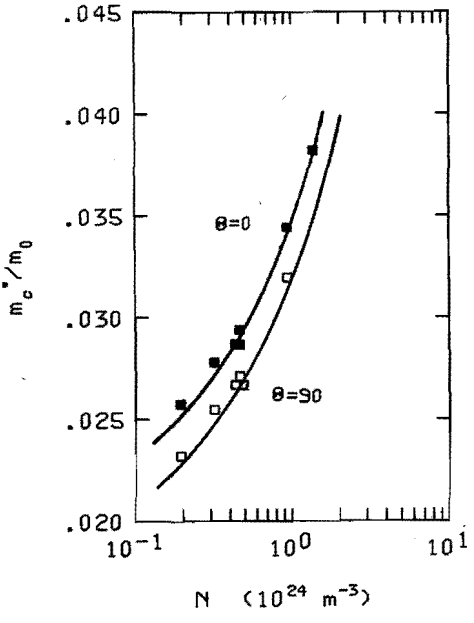

Fig.5.13.
The electron concentration dependences of the cyclotron effective masses $m_c^*(\theta = 0)$ and $m_c^*(\theta = 90)$ in conf.II. The curves have been calculated with the parameters given in the caption to fig. 5.12.

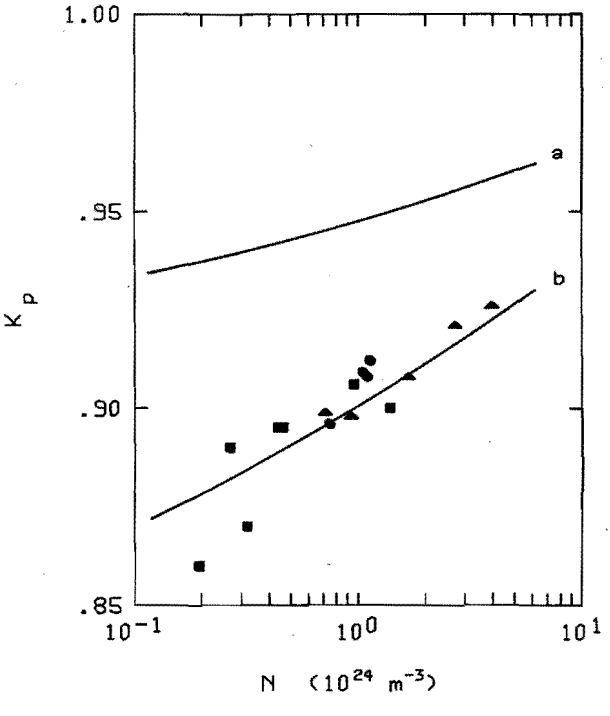

Fig.5.14.
The electron concentration dependence of the anisotropy coefficient K_p. The symbols have the same meaning as in fig.5.12. Curve a corresponds to $E_g = 0.26$ eV, $\Delta = 0.5$ eV, $\delta = -0.06$ eV, $P_{//} = P_{\perp} = 7.3 * 10^{-10}$ eVm. Curve b is calculated for the parameters given in the caption to fig. 5.12.

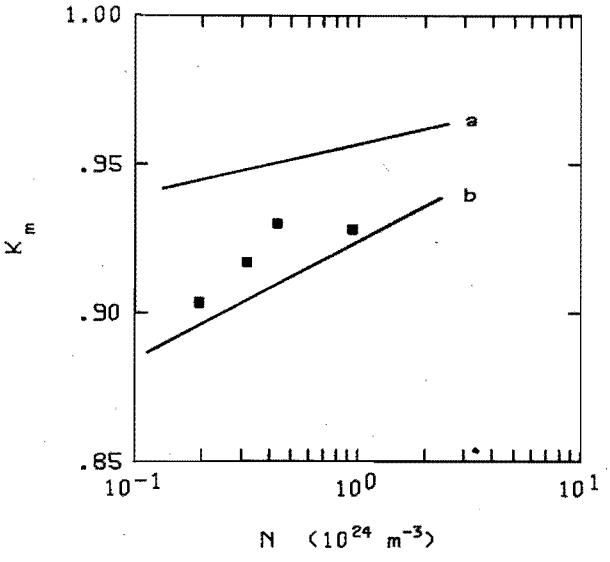

Fig.5.15.
The electron concentration dependence of the anisotropy coefficient K_m in conf.II. The results for the samples 4, 7 and 8 have been averaged. The description of the curves is given in the caption to fig. 5.14.

period measurements are more accurate than those obtained from absolute measurements of $P(\theta)$. The samples 9, 21 and 22 have also been measured in conf. III. In this configuration they showed an angular dependence of the period (see fig.5.16), $P(\theta = 90)/P(\theta = 45)$ being 1.013 ($N = 0.71 * 10^{24}$ m^{-3}), 1.015 ($N = 2.72 * 10^{24}$ m^{-3}) and 1.016 ($N = 3.97 * 10^{24}$ m^{-3}), respectively. According to the Bodnar-model one should not expect any angular dependence at all in conf. III.

Figure 5.13 presents the effective cyclotron masses, which are obtained from signals as shown in fig. 4.7, for the various samples. The anisotropy in $m_c^*(\theta)$ is even smaller than that in $P(\theta)$. The m_c^* measurements cover only a small range of electron concentrations and the resulting values of K_m (conf. II, see fig. 5.15) exhibit more scatter than those for K_p. However, for each sample of which both P and m_c^* have been measured as function of the orientation, K_m is larger than K_p. Just as in the period, the anisotropy in the effective mass decreases with increasing electron concentration.

The electron concentration dependences of K_p and K_m in $CdSnAs_2$ are much weaker than in Cd_3As_2. A variation of N from $0.2 * 10^{24}$ m^{-3} to $2 * 10^{24}$ m^{-3} for Cd_3As_2 leads to a change of K_p and K_m of approximately

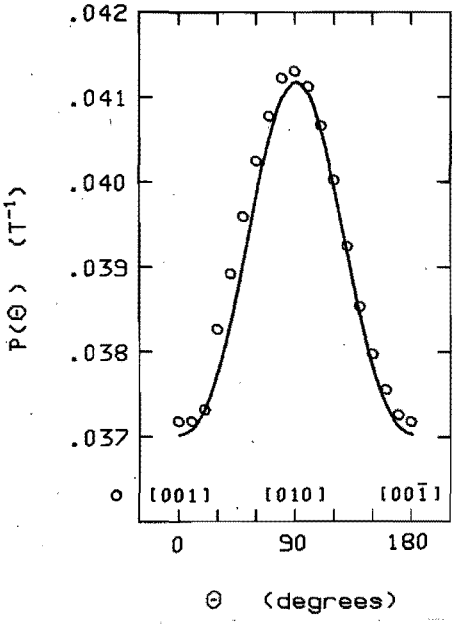
.042
.041
.040
.039
.038
.037
P(Θ) (T⁻¹)
[001]
[010]
[00$\bar{1}$]
0
90
180
Θ (degrees)

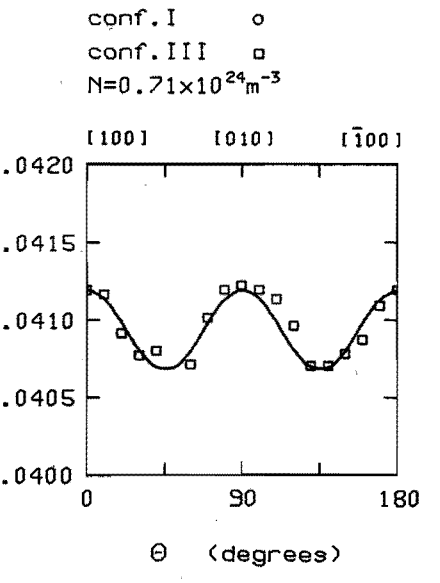
conf. I
conf. III
N=0.71x10²⁴m⁻³
[100]
[010]
[$\bar{1}$00]
.0420
.0415
.0410
.0405
.0400
0
90
180
Θ (degrees)

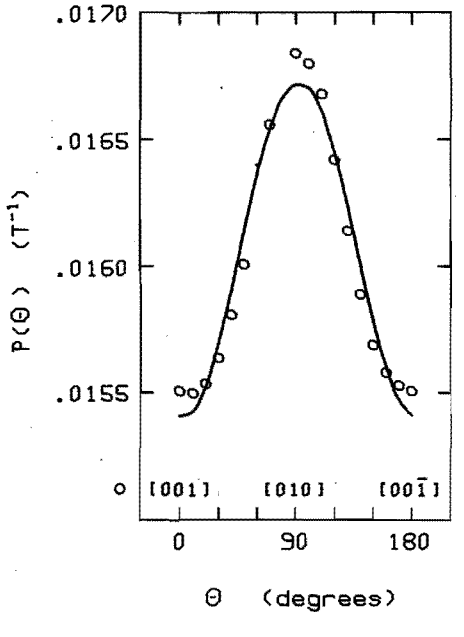
.0170
.0165
.0160
.0155
P(Θ) (T⁻¹)
[001]
[010]
[00$\bar{1}$]
0
90
180
Θ (degrees)

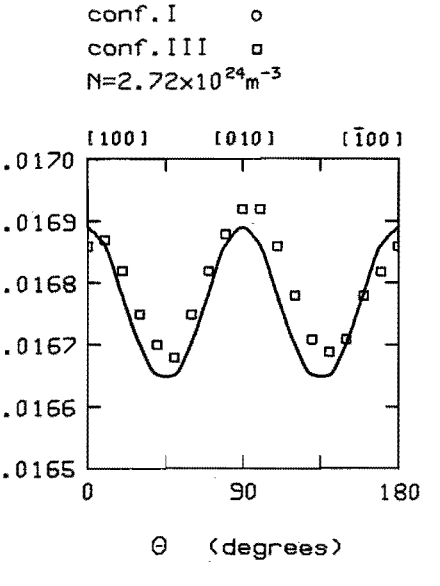
conf. I
conf. III
N=2.72x10²⁴m⁻³
[100]
[010]
[$\bar{1}$00]
.0170
.0169
.0168
.0167
.0166
.0165
0
90
180
Θ (degrees)

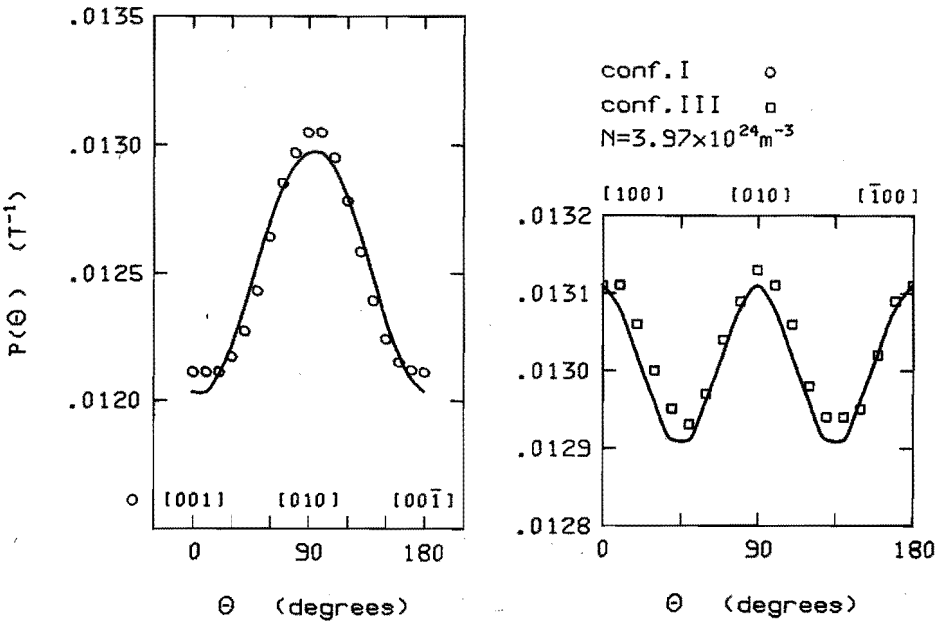

Fig.5.16. The angular dependences of the SdH-oscillation periods for the samples 9,21 and 22 in conf.I and conf.III. The curves have been obtained with the values of u_B and v_B given in the text.

17% and 7% while for $CdSnAs_2$ the change is only 4% for both K_p and K_m.

For the sample with the lowest electron concentration $N = 0.19 * 10^{24}\ m^{-3}$, we could observe the beginning of spin-splitting of the lower Landau-levels (n = 3, n = 2). Fig. 5.17 shows the experimental recordings of the SdH-signals for $\theta = 0$, $\theta = 60$ and $\theta = 90$, respectively. It can easily be seen that these oscillations are no longer sinusoidal in shape but contain considerable contributions of higher harmonics, most pronounced for $\theta = 90$. This enables us to determine the cyclotron effective mass and the g*-factor indirectly by means of the curve fitting method mentioned in §4.3.3. The results for the angular dependences of m_c^*/m_o and $|g^*|$ are shown in fig. 5.18. Concerning the g*-factor we notice that $|g^*(\theta = 0)| < |g^*(\theta = 90)|$, providing additional

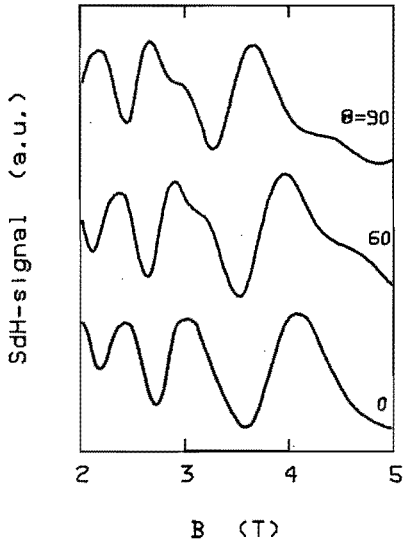

Fig.5.17.
Recorder graphs of SdH-oscillations for sample 1 ($N = 0.19 * 10^{24}\ m^{-3}$) at 4.2 K. The data were taken at the first harmonic of the modulation frequency.

information about the geometry of the Fermi-surface of $CdSnAs_2$.
From fig. 5.17 it can be seen that for this low electron concentration it is very difficult to obtain accurate values of $P(\theta)$ (and consequently of K_p) since only the first few oscillations are purely periodic. For this reason the values of K_p in fig. 5.14 for the lowest electron concentration are less accurate.
The values of $m_c^*(\theta)$ given in fig. 5.18 are not obtained from the temperature dependences of the SdH-oscillation amplitudes but result from our curve fitting routine. A variation of the $m_c^*(\theta)$-values with about 3% did not affect the resulting values of $g^*(\theta)$ seriously.

5.2.3. Interpretation of the $P(\theta)$-, $m_c^*(\theta)$- and $g^*(\theta)$ data

In earlier reported investigations of the SdH-effect on $CdSnAs_2$ [21] the author concludes from not very pronounced oscillations, that the conduction band should be isotropic. An isotropic conduction band is obtained when the crystal field splitting parameter δ equals zero and when the interband matrix elements are equal ($P_{//} = P_{\perp}$). Our measurements of the angular dependences of both period and effective mass show that $K_p < 1$ and $K_m < 1$ (see fig. 5.14 and fig. 5.15) for the investigated samples.

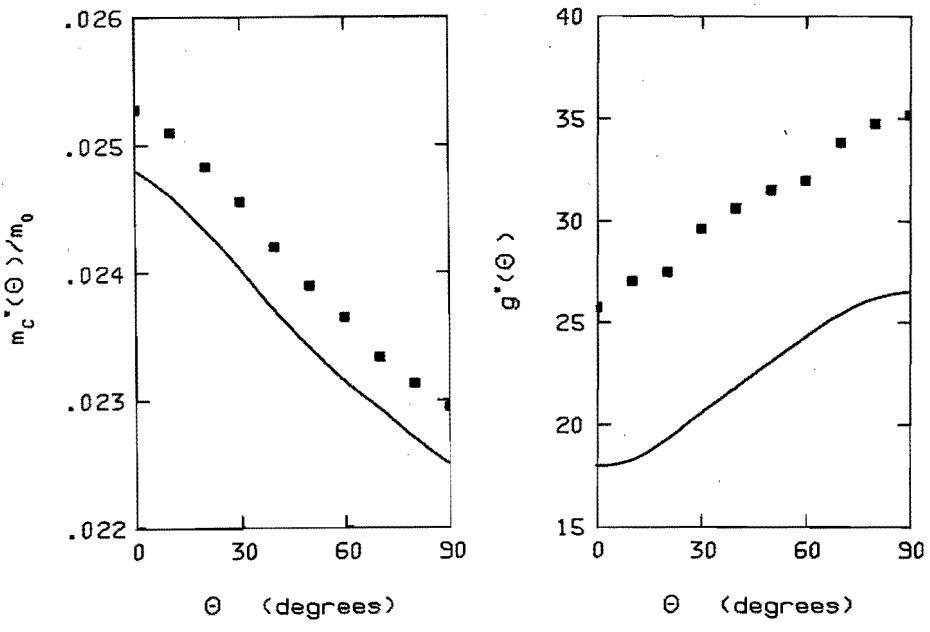

Fig.5.18. The angular dependences of m_c^* and g for sample 1 ($N = 0.19 * 10^{24}\ m^{-3}$) obtained from the g*- curve fitting routine. The curves correspond to $E_g = 0.26$ eV, $\Delta = 0.5$ eV, $\delta = -0.1$ eV, $P_{//} = P_{\perp} = 8.5 * 10^{-10}$ eVm.*

Anisotropy of period and effective mass can be described by a Fermi-surface in the form of an ellipsoid of revolution resulting from the three band Kane-model ($\delta = 0$) in which an anisotropic interband matrix element ($P_{//} \neq P_{\perp}$) is introduced.

In that case one obtains $K_m = K_p$ independent of electron concentration and the Fermi surface of $CdSnAs_2$ will be an oblate ellipsoid of revolution of which the ratio c/a (see fig. 3.2) is independent of N. Previous results from optical reflection and magnetoresistance measurements have been interpreted in this way [22-24].

Our experimental data clearly show that for each sample for which both $P(\theta)$ and $m_c^*(\theta)$ have been measured, K_m is larger than K_p. Furthermore both K_m and K_p increase (the anisotropy decreases) with increasing N. These arguments lead to the conclusion that $\delta < 0$, giving an anisotropic

conduction band with anisotropy depending on energy. This gives a Fermi-surface which is indeed an oblate ellipsoid of revolution. However, the energy dependency of the semi-axis c differs from that of the semi-axis a.

We have compared our experimental data, shown in the figures 5.12-5.15, with the theoretical predictions from the Bodnar-model for $P(\theta=0)$, $P(\theta=90)$, $m_c^*(\theta=0)$, $m_c^*(\theta=90)$, K_p and K_m respectively. Substitution of the generally accepted values of the primary bandparameters E_g (=0.26 eV), δ (=-0.06 eV), Δ (=0.5 eV) and the $CdGeAs_2$ values for the interband matrix elements $P_{//}$ and $P_{\perp}$ ($P_{//} = P_{\perp} = 7.3 * 10^{-10}$ eVm [26]) results in curves (a) in fig. 5.14 and fig. 5.15, showing far too small anisotropies (too high values of K_p and K_m).
In spite of the small anisotropies and the relatively large inaccuracies in K_p, K_m, $m_c^*(\theta)$ and $P(\theta)$, our experimental results can be reasonably well described by the four level Bodnar-model with the following set of bandparameters:

$$E_g = (0.26 \pm 0.01) \text{ eV}$$

$$\Delta = (0.50 \pm 0.05) \text{ eV}$$

$$\delta = (-0.10 \pm 0.01) \text{ eV}$$

$$P_{//} = (8.5 \pm 0.1) * 10^{-10} \text{ eVm}$$

$$P_{\perp} = (8.5 \pm 0.1) * 10^{-10} \text{ eVm} .$$

The inaccuracies in the bandparameters are obtained by tracing the influence of a systematical variation of the respective parameters. The curves (b) in the figures 5.14, 5.15 and the curves in the figures 5.12, 5.13 and 5.18 have been calculated with the above given set of bandparameters.

If we wish to compare our values of the bandparameters with those reported in the literature, we have to be aware of the different definitions used for the bandgap, spin-orbit splitting and crystal field splitting. In the literature [25,26] the results are often given as energy gaps (A, B and C) between successive bands. Using the

solutions of the secular equation 2.7 at $\vec{k} = 0$, given by $E_c = E_g$, $E_{lh} = 0$ and $E_{hh,so} = -\frac{1}{2}(\Delta+\delta) \pm \frac{1}{2}\sqrt{(\Delta+\delta)^2 - \frac{8}{3}\Delta\delta}$, we obtain for $A = E_c - E_{hh}$, $B = E_c - E_{lh}$ and $C = E_c - E_{so}$ the values 0.25, 0.26 and 0.73 eV, respectively. Taking into account that our data are obtained at liquid helium temperature, whereas the literature data (A = 0.23 eV, B = 0.26 eV, C = 0.76 eV [25]) refer to room temperature, we may conclude that they are in good agreement [26-30]. Our value of the interband matrix element $P_{//} = P_{\perp}$ of $8.5 * 10^{-10}$ eVm lies within the range of values reported in the literature viz. 7 [31], 8 [27] and $10 * 10^{-10}$ eVm [30]. One should notice that these values have been determined under different assumptions, so that a precise comparison is unrealistic.

Some values for the anisotropy of effective masses are given in the literature [22,23]. The anisotropy in these papers is defined as m_L^*/m_T^*, the ratio of the longitudinal and transverse effective mass. For the Bodnar-model we can express this ratio in terms of K_p and K_m: $m_L^*/m_T^* = K_p(2K_m - K_p)$. Substituting our values of the bandparameters we find that m_L^*/m_T^* increases from 0.77 to 0.90 for $N = 5 * 10^{23}$ m^{-3} to $5 * 10^{24}$ m^{-3}. We conclude therefore that the indirectly determined values of $0.27 < m_L^*/m_T^* < 0.64$ for the afore mentioned concentration range given by Polyanskaya et al. [23] are far too low. The individual values of $m_L^* = (0.048 \pm 0.007)\ m_o$ and $m_T^* = (0.056 \pm 0.008) m_o$ for $N = 5 * 10^{24}$ m^{-3} reported by Karymshakov et al. [22] are in good agreement with our calculated values viz. $m_L^* = 0.0509 m_o$ and $m_T^* = 0.0535 m_o$, respectively.

Concerning the effective g-factor we first of all notice that $|g^*(\theta=0)| < |g^*(\theta=90)|$, reinforcing the conclusion that we are dealing with an oblate ellipsoid of revolution which can be described by the Bodnar-model with $E_g > 0$ and $\delta < 0$. We calculated the theoretical values from the Wallace formula for $g^*(\theta)$ by substituting the given set of bandparameters. The calculated value of the anisotropy coefficient $K_g = |g^*(\theta=90)|/|g^*(\theta=0)|$ turns out to be 0.71. The experimental value $K_g = 0.73$ is in good agreement with this calculated one.
Although the angular dependence is described well by the four-level Bodnar-model, the absolute values of $g^*(\theta)$ are much too low as compared to the experimental values (see fig. 5.18). This discrepancy is often

met in NGSC (see also §5.1.3). By varying E_g, Δ, $P_{//}$, $P_{\perp}$ and δ within relatively broad regions it was impossible to find a set of bandparameters which could fit the observed angular dependences of P, m_c^* and $|g^*|$ simultaneously.

The effect of the free electron term on the g*-factor, calculated by Singh et al. [32] for NGSC and semimetals, changes the theoretical values of $|g^*|$ only slightly and cannot give an explanation for the high g^* -values obtained from our fit. The free electron contribution depends strongly on the band structure of the material. The contribution is in general considerably larger than 2 for inverted-gap ($E_g < 0$) materials and less than 2 for direct gap ($E_g > 0$) materials [32]. This is in agreement with our conclusions regarding the effect of the free electron term in $CdSnAs_2$ ($E_g > 0$) and Cd_3As_2 ($E_g < 0$).
Another possibility to explain the discrepancy in the calculated and measured g*-values could be the influence of remote bands. The g*-factor of (isotropic) NGSC can strongly depend on the effect of higher bands, while the effective mass differs only slightly from the one calculated from the three-level Kane-model [13,16]. Unfortunately, a workable theory including higher bands for tetragonal NGSC (with or without a magnetic field) is not available up to now.

5.2.4. Deviations from the Bodnar-model for $CdSnAs_2$

We carefully examined the oscillation patterns of samples with $N > 1 * 10^{24}$ m^{-3} in order to find experimental evidence for the existence of a second conduction band with its minimum 0.07 eV above the bottom of the main conduction band, as has been suggested in refs. [22,33]. The Fermi-levels of these high concentration samples lie at least 0.15 eV above the bottom of the principal conduction band, and consequently also considerably far above the minimum of this second band. Assuming the values of the effective mass and of the mobility ratio reported in [33], a simple calculation shows that the concentration of these second type of electrons cannot be neglected any longer, and we might expect the appearance of a second period in the SdH-signal. However, even for a sample with $N = 2.8 * 10^{24}$ m^{-3} the oscillations remain

perfectly periodic up to 5 T with only one single period. This result reinforces the conclusion by Daunov et al. [34] that the existence of this second subband is unlikely. Concerning a third conduction subband [22,33,34] with its minimum displaced from the centre of Brillouin zone and ΔE_{13} = 0.30-0.35 eV, our results cannot provide any information. Additional SdH-measurements on extremely highly degenerated samples, probably up to higher fields, will be necessary.

Our measurements on the samples with electron concentrations of $0.71 * 10^{24}$ m^{-3}, $2.72 * 10^{24}$ m^{-3} and $3.97 * 10^{24}$ m^{-3} respectively, clearly show an anisotropy in configuration III. This is not in accordance with the Bodnar-model, which gives an ellipsoid of revolution about the k_z-axis for the Fermi-surface. The observed deviations are very small and quite similar in shape with those observed in Cd_3As_2 (see §5.1.4). The quantities u_B and v_B (see §5.1.4 and appendix) turn out to be u_B = 0.56, v_B = -2.79 ($N = 0.71 * 10^{24}$ m^{-3}), u_B = 0.42, v_B = -2.13 ($N = 2.72 * 10^{24}$ m^{-3}) and u_B = 0.23, v_B = -1.97 ($N = 3.97 * 10^{24}$ m^{-3}). The u_B and $|v_B|$ values tend to decrease with increasing N, while for Cd_3As_2 u_B increases and v_B remains constant with increasing N. The curves in fig. 5.16 are calculated with the above given values of u_B and v_B. The agreement between points and curves is supprisingly good.

5.3 $(Cd_{1-x}Mn_x)_3As_2$: Results and Interpretation

5.3.1. Introduction

Preliminary SdH-measurements have been performed on mono- and polycrystalline $(Cd_{1-x}Mn_x)_3As_2$ samples with a low magnetic ion content ($x \leq 0.05$) and electron concentrations in the range from $3.0 * 10^{24}$ m^{-3} to $6.0 * 10^{24}$ m^{-3}. Up to now it proved to be even more difficult to affect the electron concentration in these samples than in pure Cd_3As_2. Annealing treatments in various atmospheres failed in reducing the electron concentration of the as-grown samples considerably. Due to the very narrow range of electron concentrations we are only able to give some tentative results of our SdH-measurements, which however demonstrate the influence of the exchange interaction clearly. These results

are presented and discussed in §5.3.2 for polycrystalline samples and in §5.3.3 for the single crystals.

Magnetisation measurements [35,36] showed that $\langle S_z \rangle$ may be described by eq. 4.10. The values of $S_{eff}(x)$ and $T_o(x)$ given in table 5.4 have been obtained at temperatures and fields in the range in which usually SdH-measurements are performed. The positive T_o and the small S_{eff} reflect a strong antiferromagnetic interaction between the Mn-ions, much stronger than that found in other SMSC [37-40].

x	S_{eff}	T_o (K)
0.01	1.60	1.95
0.02	1.36	3.27
0.03	1.12	3.69
0.04	0.90	4.45
0.05	0.80	5.35

Table 5.4.
The experimental values of $S_{eff}(x)$ and $T_o(x)$ obtained for $T \leq 4.2$ K and $B \leq 3$ T. After [35,36].

5.3.2. *Spin-splitting zeros in polycrystalline $(Cd_{1-x}Mn_x)_3As_2$ material*

The $(Cd_{1-x}Mn_x)_3As_2$ alloys exhibit very pronounced zeros in the SdH-signal, as is illustrated in figs. 3.3 and 5.19 for two samples with x = 0.01. Several interesting features can be seen in fig. 5.19. Looking at a fixed value of the field, for instance at B = 1.62 T, one observes with decreasing temperature first a decrease of the peak-peak amplitude, followed by an increase with opposite phase. The amplitude goes through zero between T = 1.92 K and 1.81 K. The figure also shows that this zero shifts towards lower temperature when the field is further increased: at B = 1.73 T the zero occurs between T = 1.81 K and 1.73 K. The oscillations near both zeros change their sinusoidal shape because of the rise of the second harmonic of the signal. This has been shown already more explicitly for another sample in fig. 3.4.

Fig. 5.20 presents the fundamental amplitude of the SdH-oscillations as function of temperature at B = 1.53 T for a sample with x = 0.01 and $N = 3.90 * 10^{24}$ m^{-3}. Two zeros are observed at about 2 and 6 K correspondig to $\nu = 5/2$ and 3/2, respectively (see eq. 3.18). In fig. 5.21

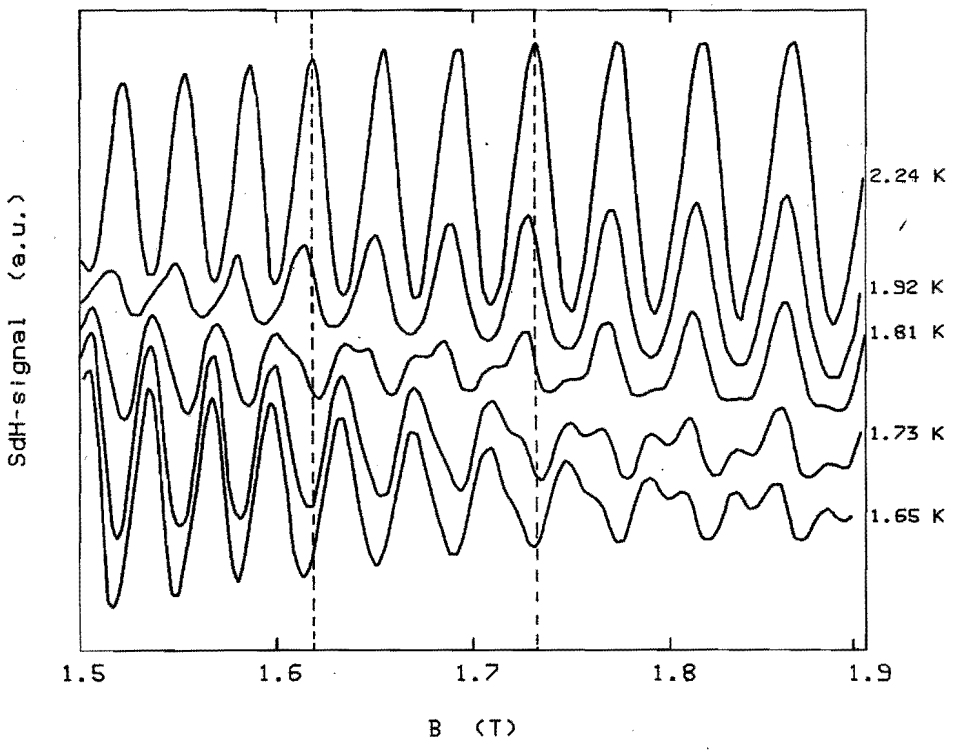

Fig.5.19. Experimental recordings of SdH-oscillations at temperatures near a spin-splitting zero.

the temperature dependences of the SdH-amplitude at B = 1.90 T are shown for two samples with N = 3.90 * 10^{24} m^{-3}(a), N = 5.45 * 10^{24} m^{-3} (b) and x = 0.02. Similar behaviour of the SdH-amplitude as function of B and T has been found for all investigated samples up to x = 0.05. It can be seen from fig. 5.21 that the zero in amplitude (ν = 5/2 in this case) shifts towards higher temperature with increasing electron concentration. In fig. 5.20 and fig. 5.21 the spin-splitting zeros with ν = 5/2 for the samples with N = 3.90 * 10^{24} m^{-3} occur at the same temperature, but different fields. Since the spin-splitting zero temperature decreases with increasing B one may conclude from these figures that the spin-splitting zero temperature increases with increasing x.

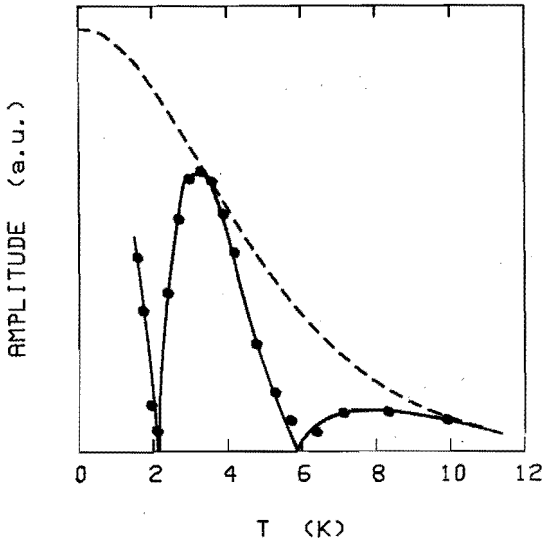

*Fig.5.20. Temperature dependences of the SdH-amplitude at B = 1.53 T for a sample with x = 0.01 and N = 3.9 * 10^{24} m^{-3}. The best fit of the experimental points is found for α = 2.08 - 1.12 β (solid curve). The dashed curve is explained in the text.*

In order to interpret the observed temperature and field dependences of the SdH-amplitude we used the theoretical model given in §2.3. For the polycrystalline samples we simplified this model to an isotropic one by substituting $\delta = 0$, $P_{//} = P_{\perp}$ and $\beta_{//} = \beta_{\perp}$. Adopting the low-temperature values of the bandparameters E_g, P and Δ of pure Cd_3As_2 and taking the magnetisation functions described by eq. 4.10, we succeeded to fit the temperature and field dependences of the observed zeros by treating α and β as adjustable parameters. This is shown in the figures 5.20 and 5.21 where the solid curves have been calculated from our model using the values of α and β found from the best fits of the zeros at T ≈ 2 K and using the Cd_3As_2 value of the effective mass. In both figures the agreement between experimental points and calculated curves is remarkably good over the whole temperature range, although only the zeros at T ≈ 2 K are used to adjust α and β.

It was impossible to determine experimentally the effective cyclotron mass values of the investigated samples with the method suggested in [40] (see §4.3.4). This is due to the fact that the absolute values of the SdH-oscillation amplitude become very small for temperatures above the last (ν = 1/2) spin-splitting zero (T ≈ 25 K). In our calculations we used the m_c^* values obtained from the Bodnar-model using

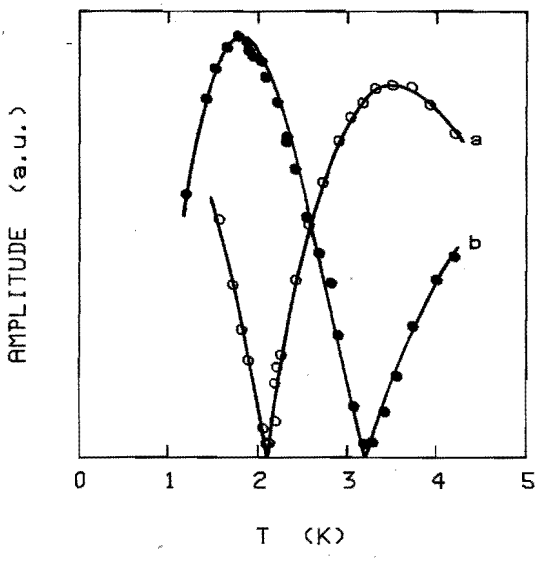

*Fig.5.21. Temperature dependences of the amplitudes at B = 1.90 T for two samples with x = 0.02, N = 3.9 * 10^{24} m^{-3} (a) and N = 5.45 * 10^{24} m^{-3} (b). The data have been fitted with α = -2.0 eV and β = 3.2 eV.*

the Cd_3As_2 values for the primary bandparameters with $\delta = 0$ and $P_{//} = P_{\perp}$. We feel justified in this choice of m_c^* since the values of the cyclotron effective mass resulting from the model including exchange interaction are practically the same as for pure Cd_3As_2 (see §2.3). Moreover, the dashed curve in fig. 5.20, which gives the temperature behaviour of the SdH-amplitude without the influence of exchange interaction, has been calculated with the m_c^*-value of Cd_3As_2 ($\delta = 0$, $P_{//} = P_{\perp}$) for the given electron concentration. Furthermore, we do not expect the m_c^* values for the given electron concentrations to change seriously with a change of the bandgap as function of x as is shown in fig. 4.9.

For each individual sample (with given N and x), it was possible to fit the experimental temperature and field dependences of the SdH-amplitude with sets of α and β which satisfy a relation $\alpha = i - s\beta$. The slope (s) and the intercept (i) of the straight line depend on the electron concentration and the bandparameters; moreover, i is a function of the Mn-ion concentration (x). Such a linear relation in α and β is predicted by our model (see §2.3.3). Due to this linear relation between α and β it is impossible to determine an unique set (α,β) from the fit of the temperature and field behaviour of the amplitude for a single sample.

The straight lines obtained from fits of the spin-splitting zeros for samples with the same Mn-ion content x but different N, should intercept in one point of the α-β plane and thus give a unique solution for α and β. We applied this procedure to the samples with x = 0.01. Because of the experimental inaccuracies in the values of B and T at the zeros, possible differences in M_n-concentration and the fact that the range of N is only very narrow, we did not find exactly one point but a conglomerate of points in the α-β plane. Averaging these values we obtained $\bar{\alpha}$ = -3.4 eV and $\bar{\beta}$ = 4.9 eV. These values were found under the assumption that for the samples with x = 0.01 the zero occurring at approximately T = 2 K and B = 1.5 T (see fig. 5.20) corresponds to ν = 5/2. The proper value of ν is selected from the positions of the zeros on the temperature scale. Our calculations show that only if the zero at $\approx$2 K corresponds to ν = 5/2 the next zero corresponding to ν = 3/2 will occur exactly at the temperature where it is observed experimentally (6.0 K). For the samples with x = 0.02 the same procedure of determining α and β resulted in averaged values $\bar{\alpha}$ = -2.0 eV and $\bar{\beta}$ = 3.2 eV. These values are less accurate, due to an even smaller electron concentration range, but deviate considerably from those for x = 0.01. Going up to x = 0.05 the values of α and β determined in this way appear to change from a negative value of $\bar{\alpha}$(-3.4 eV) and a positive value of $\bar{\beta}$(4.9 eV) for x = 0.01 to a large positive value of $\bar{\alpha}$ and a negative value of $\bar{\beta}$ for x = 0.05.

The values of α and β in most SMSC, investigated thus far, turn out to be independent of x [42,44], at least for low x. The change of α and β with increasing x may be attributed to the fact that we used the Cd_3As_2 values of the primary bandparameters, which of course are independent of x. Generally for mixed crystal systems and for SMSC in particular the bandgap varies rapidly with x [38,39,41,42]. Assuming an x-dependent bandgap in such a way that E_g becomes more positive with increasing x, it is possible to find values of $\bar{\alpha}$ and $\bar{\beta}$ which are independent of the magnetic ion content. For instance, in order to find the same values of $\bar{\alpha}$ and $\bar{\beta}$ for the samples with x = 0.01 and x = 0.02 the bandgap has to be changed from E_g = -0.095 eV for pure Cd_3As_2 to E_g = -0.077 eV and E_g = -0.060 eV for x = 0.01 and x = 0.02, respectively. The averaged values of α and β obtained in this way

turn out to be -5.2 eV and 6.8 eV, respectively. It should be stressed that the above given E_g-x relation and corresponding values of $\bar{\alpha}$ and $\bar{\beta}$ are affected with a large inaccuracy.
The inaccuracy is mainly caused by the narrow electron concentration range. The small differences in electron concentration of samples with a given x correspond to straight lines in the α-β plane with nearly the same slope, which makes an accurate determination of the values of α and β impossible. This in turn makes a determination of the E_g-x relation doubtful. This effect is enhanced by small variations in x between the individual samples. Furthermore, the higher the value of dE_g/dx, the more essential it is to know x of each sample very accurately.

5.3.3. Angular dependences of P(θ) and spin-splitting zeros in $(Cd_{1-x}Mn_x)_3As_2$ single crystals

For single crystals with $.0025 \leq x \leq .010$ and $3 * 10^{24}\ m^{-3} < N < 6 * 10^{24}\ m^{-3}$ we determined the SdH-oscillation periods in the three configurations which are defined in fig. 5.1. The angular variations of the period, which are typical for all single crystals, are presented in fig. 5.22. The angular behaviour of the period in configuration II is mainly of the Bodnar type. The anisotropy in configuration III clearly indicates that we are also dealing with warping of the Fermi-surface. The angular behaviour of the period in this configuration is quite similar in shape to that observed for Cd_3As_2 (see § 5.1.4.). Just as for Cd_3As_2 the ratio $P(\theta = 0)/P(\theta = 45)$ (conf. III) increases with increasing electron concentration. The values for $K_p = P(\theta = 0)/P(\theta = 90)$ (conf. I and II) turn out to be strongly x dependent. For $N = 4.0 * 10^{24} m^{-3}$ K_p-values of 1.06, 1.08, 1.12 (conf. I) and 1.09, 1.11, 1.15 (conf. II) were found for x = 0.01, 0.005 and 0.0025, respectively. For the given electron concentration a value of $K_p = 1.15$ is found for pure Cd_3As_2 (see fig. 5.5). An analysis of the Bodnar-model by varying the band-parameters learns that K_p is very sensitive to changes in the crystal field splitting parameter δ, but almost independent of the bandgap. This may indicate that δ decreases with increasing x, assuming the

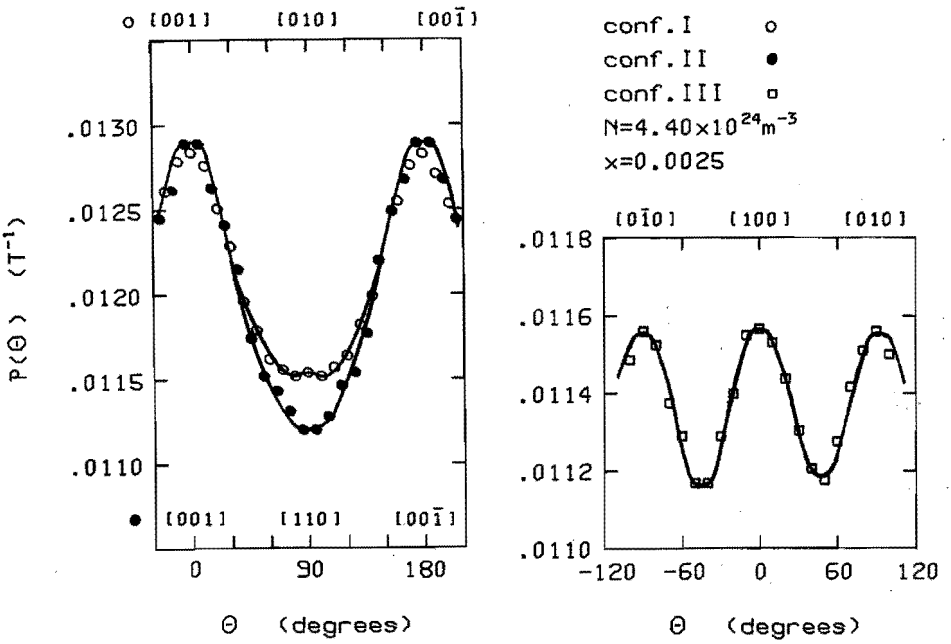

Fig.5.22. Angular dependences of the SdH-periods for a sample with $x = 0.0025$ and $N = 4.4 * 10^{24}\ m^{-3}$.
The curves are drawn to guide the eye.

values of $P_{//}$ and $P_{\perp}$ to be independent of x [40-44].

We measured the amplitudes of the SdH-oscillations for several samples in the temperature range from 1.2 K to 4.2 K in order to detect a possible angular dependence of the quantity $\nu = (1/2(m_c^*/m_o)g^*)$. A strong angular dependence of ν implies that the temperature T_Z at which the spin-splitting zeros in the SdH-amplitude occur (ν =1/2, 3/2.....) shifts considerably with the field orientation. However, we found only very small differences between the spin-splitting zero temperatures (corresponding to the same ν) for the various orientations. This is shown in fig. 5.23 which gives the amplitude near T_Z for $\theta = 0$ and $\theta = 90$ measured for samples with x = 0.01 ($N = 3.5 * 10^{24}\ m^{-3}$ and $5.3 * 10^{24}\ m^{-3}$, a and b) and for a sample with x = 0.005 ($N = 5.2 * 10^{24}\ m^{-3}$, c). We find $T_Z(\theta = 0) < T_Z(\theta = 90)$ for x = 0.01 and

$T_Z(\theta = 0) > T_Z(\theta = 90)$ for x = 0.005 corresponding with $\nu(\theta = 0) < \nu(\theta = 90)$ and $\nu(\theta = 0) > \nu(\theta = 90)$, respectively. The observed spin-splitting zeros correspond to $\nu = 5/2$ (x = 0.01) and $\nu = 3/2$ (x = 0.005). Similar results have been found for several samples with $x \leq 0.01$.

These results can be quantitatively understood from the model given in § 2.3., as is illustrated in fig. 5.24 for the sample with x = 0.01 and $N = 3.5 * 10^{24}\ m^{-3}$. Substitution of the exchange parameter values $\bar{\alpha} = -5.2$ eV and $\bar{\beta} = 6.8$ eV, found for polycrystalline samples with x = 0.01, results in too small values of ν and gives $\nu(\theta = 0) > \nu(\theta = 90)$ (curve a). By introducing a rather large anisotropy in the exchange parameter $\beta(\beta_{//} \neq \beta_{\perp})$ it is possible to obtain the correct ν-θ behaviour and larger values of ν. This is shown by curve b (T = 1.5 K), which has been calculated with $\alpha = -4.9$ eV, $\beta_{\perp} = 8.3$ eV, $\beta_{//} = 6.8$ eV, $E_g = -0.077$ eV and adopting the Cd_3As_2 values of the remaining primary bandparameters. With increasing temperature the curve shifts downwards and crosses the spin-splitting zero value $\nu = 5/2$ firstly for $\theta = 0$ and finally also for $\theta = 90$. With the above given set of exchange parameters it is also possible to describe the spin-splitting zero of sample b in fig. 5.23 satisfactorily.

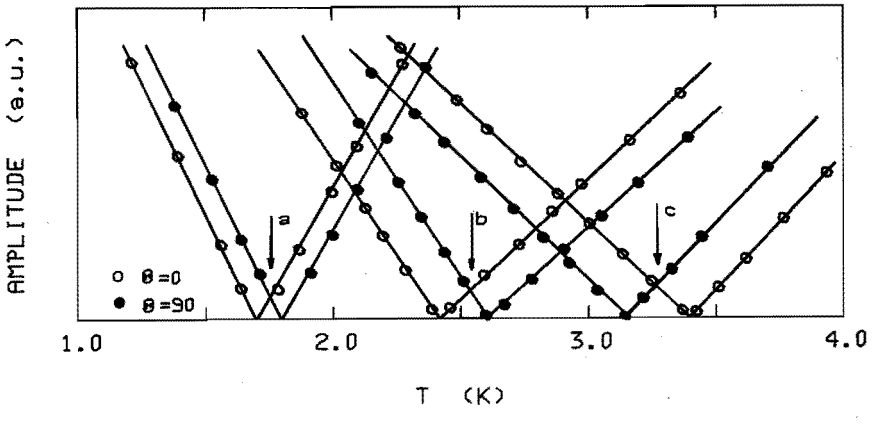

Fig.5.23. Temperature dependences of the SdH-oscillation amplitudes near a spin-splitting zero at B = 1.65 T, measured on samples with x = 0.01 (a, $N = 3.5 * 10^{24}\ m^{-3}$ and b, $N = 5.3 * 10^{24}\ m^{-3}$) and x = 0.005 (c, $N = 5.2 * 10^{24}\ m^{-3}$).

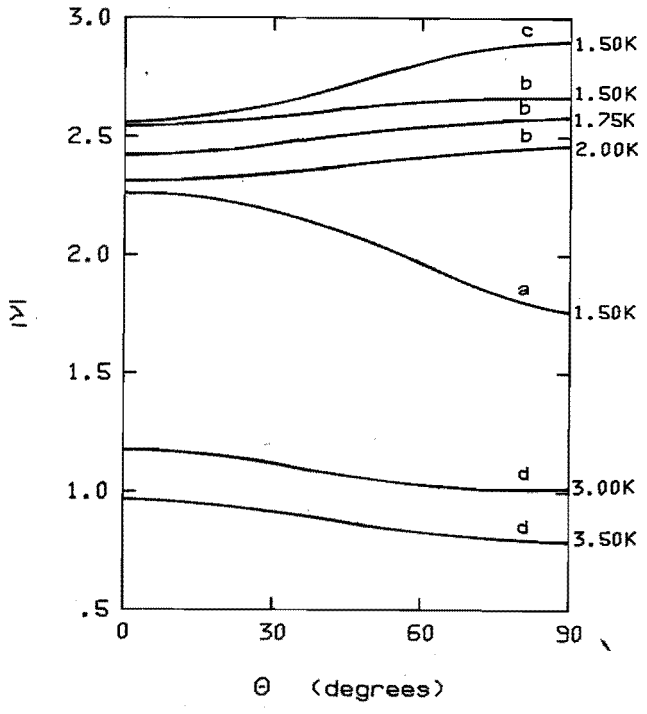

Fig.5.24. Angular dependences of $|\nu|$ *for* $x = 0.01$, $N = 3.5 * 10^{24}\ m^{-3}$, $B = 1.65\ T$ *and for* $x = 0.005$, $N = 5.2 * 10^{24}\ m^{-3}$, $B = 1.65\ T$. *The curves are explained in the text.*

It should be stressed that the curves b are mainly illustrative. The used values for α, $\beta_{//}$ and $\beta_{\perp}$ are not obtained from a systematic investigation of the field, temperature and magnetic ion content dependences of spin-splitting zeros for samples in a large electron concentration range. Furthermore, the curves a and b have been calculated using the Cd_3As_2 values of Δ, δ, $P_{//}$ and $P_{\perp}$. The absolute value and anisotropy of the theoretical ν is influenced by a change of the bandparameters which in turn influences the experimentally determined values of the exchange parameters α and β. For instance, a decrease of δ to 0.05 eV results in stronger anisotropy and higher values of ν (curve c in fig. 5.24). In order to explain the observed spin-splitting zeros in this case one has to change the values of α, $\beta_{//}$ and $\beta_{\perp}$ in such

a way that the anisotropy in β becomes smaller for decreasing δ.
For the sample with x=0.005 it is also possible to describe the observed behaviour (T_z (θ=0) > T_z (θ=90)) with our model, by choosing a different set of exchange parameters. For instance α = -4.9 eV, $\beta_{//}$ = 6.8 eV, $\beta_{\perp}$ = 7.8 eV, E_g = -0.086 eV and using Cd_3As_2 values for the other primary bandparameters, results in curve d in fig. 5.24. With increasing temperature the curve will shift downwards and passes the spin-splitting zero first for θ = 90.
The curve is once again merely illustrative. The used anisotropy in β is smaller than for the samples with x = 0.01. This is in agreement with the expected decrease of δ with increasing x as is explained above.
Here it should be noted that in the given illustrations we used the values of S_{eff} and T_o obtained for polycrystalline material. Thus far magnetisation measurements have not been performed on single crystals.

Just as in the case of polycrystalline material many more experimental data on the temperature, field, electron concentration and angular dependences of the SdH-amplitudes and spin-splitting zeros are necessary over a large range of electron concentrations in order to give an elaborate quantitative interpretation of the influence of the exchange interaction in the model given in §2.3.

REFERENCES

[1] B.L. Booth, Ph.D. Thesis, Northwestern Univ., Evanston 1967.

[2] I. Rosenman, J. Phys. Chem. Solids 30, 1385 (1969).

[3] H. Doi, T. Fukuroi, T. Fukase, Y. Muto, K. Tanaka, Sci. Rep. Inst. Tohoku Univ. A20, 190 (1969).

[4] J. Bodnar, Proc. Int. Conf. Phys. Narrow-Gap Semicond., Warsaw, 1977 (Polish Scientific Publ., Warsaw, 1978), p. 311.

[5] P.H.N.M. Monen, M.Sc. Thesis, Internal Report T.H.E. 1979 (unpubl.).

[6] F.A.P. Blom, M.J. Gelten, Proc. Int. Conf. Phys. Semicond., Edinburgh, 1978 (Institute of Physics, Bristol/London, 1979), p. 545.

[7] M.J. Aubin, A. Rambo, J.C. Portal, C. Houlbert, S. Askénazy, P.R. Wallace, Proc. Int. Conf. Phys. Narrow-Gap Semicond., Warsaw, 1977 (Polish Scientific Publ., Warsaw, 1978), p. 317.

[8] C. Houlbert, Ph.D. Thesis, INSA, Toulouse 1978.

[9] J.P. Jay-Gérin, A.A. Lakhani, J. Low-Temp. Phys. 28, 15 (1977).

[10] M.J. Aubin, L.G. Caron, J.P. Jay-Gérin, Phys. Rev. B15, 3872 (1977).

[11] L.G. Caron, J.P. Jay-Gérin, M.J. Aubin, Phys. Rev. B15, 3879 (1977).

[12] B. Dowgiallo-Plenkiewicz, P. Plenkiewicz, Phys. Stat. Solidi B87, 309 (1978).

[13] I.M. Tsidil'kovskii, Proc. Conf. on the Application of High Magnetic Fields in Semicond. Physics, Oxford, 1978, (University of Oxford, 1978), p. 138.

[14] W. Zawadzki, New Developments in Semiconductors, ed. P.R. Wallace, R. Harris, M.J. Zuckermann, (Noordhoff Internat. Publ., Leiden 1973), p. 443.

[15] M. Singh, P.R. Wallace, Solid State Commun. 45, 9 (1983).

[16] A.I. Ponomarev, G.A. Potapov, G.I. Kharus, I.M. Tsidil'kovskii, Sov. Phys.-Semicond. 13, 502 (1979).

[17] W. Zawadzki, private communication.

[18] R.R. Galazka, W.M. Becker, D.G. Seiler, Phys. of Semimetals and Narrow-Gap Semicond., ed. Carter and Bate (Pergamon Press, Oxford, 1971), p. 481.

[19] D.G. Seiler, W.M. Becker, Phys. Rev. 183, 784 (1969).

[20] J.T. Devreese, V.E. Van Doren, P.E. Van Camp, private communication. An example of such a Hamiltonian is given in: G.L. Bir, G.E. Pikus, Symmetry and Strain-Induced Effects in Semiconductors, (John Wiley and Sons, New York/Toronto 1974).

[21] R.I. Bashirov, Phys. Lett. 25A, 593 (1967).

[22] R.K. Karymshakov, Yu.I. Ukhanov, Yu.V. Shmartsev, Sov. Phys.-Semicond. 4, 1702 (1971).

[23] T.A. Polyanskya, I.N. Zimkin, V.M. Tuchkevin, Yu.V. Shmartsev, Sov. Phys.-Semicond. 2, 1215 (1969).

[24] G.A. Sikharulidze, V.M. Tuchkevich, Yu.I. Ukhanov, Yu.V. Shmartsev, Sov. Phys.-Semicond. 1, 254 (1967).

[25] J.L. Shay, J.H. Wernick, Ternary Chalcopyrite Semicond., (Pergamon Press, Oxford, 1975), p. 85.

[26] A. Shileika, Surf. Sci. 37, 730 (1973).

[27] G.F. Karavaev, S.I. Borisenko, Sov. Phys. J. 6, 712 (1978).

[28] G.F. Sikharulidze, Yu.I. Ukhanov, Phys. Stat. Solidi 26, K33 (1968).

[29] G.F. Karavaev, G.Z. Krivaite, Yu.I. Polygalov, V.A. Chaldyshev, Yu.V. Shmartsev, Sov. Phys.-Semicond. 6, 1863 (1973).

[30] R.K. Karymshakov, Yu.I. Ukhanov, Yu.V. Shmartsev, Sov. Phys.-Semicond. 5, 450 (1971).

[31] P. Leroux-Hugon, J. Phys. Chem. Solids 27, 1205 (1966).

[32] M. Singh, P.R. Wallace, S. Askénazy, J. Phys. C: Solid State Phys. 15, 6731 (1982).

[33] T.A. Polyanskaya, Yu.V. Shmartsev, Sov. Phys.-Semicond. 4, 615 (1970).

[34] M.I. Daunov, B.N. Magdiev, A.B. Magomedov, Sov. Phys.-Semicond. 9, 1147 (1975).

[35] W.J.M. de Jonge, M. Otto, C.J.M. Denissen, F.A.P. Blom, C. van der Steen, K. Kopinga, J. Magn. & Magn. Mat. 31-34, 1373 (1983).

[36] R. v.d. Linden, Internal Report T.H.E., 1981 (unpubl.).

[37] M. Jaczinsky, J. Kossut, R.R. Galazka, Phys. Stat. Solidi B88, 73 (1978).

[38] S. Takeyama, R.R. Galazka, Phys. Stat. Solidi B96, 413 (1979).

[39] J.A. Gaj, R. Planel, G. Fishman, Solid State Commun. 29, 435 (1979).

[40] M. Jaczinsky, W. Dobrowolski, Phys. Stat. Solidi B102, 195 (1980).

[41] P. Byszewski, M.Z. Cieplak, A. Mongird-Górska, J. Phys. C: Solid State Phys. 13, 5383 (1980).

[42] G. Bastard, C. Rigaux, A. Mycielski, Phys. Stat. Solidi B79, 585 (1977).

[43] P. Byszewski, K. Szlenk, J. Kossut, R.R. Galazka, Phys. Stat. Solidi B95, 359 (1979).

[44] M. Dobrowolska, W. Dobrowolski, R.R. Galazka, A. Mycielski, Phys. Stat. Solidi B105, 477 (1981).

CHAPTER VI GENERAL CONCLUSIONS AND REMARKS

This chapter summarises the conclusions that can be drawn from the work described in this thesis.

The aim of our SdH-measurements on the conduction band of Cd_3As_2 was to check the validity of the Bodnar-model and its extension to quantising magnetic fields in a relatively large electron concentration range, including electron concentrations below $N = 1 * 10^{24}\ m^{-3}$ where a considerable increase of anisotropy was predicted.
Our measurements of the energy dependent anisotropies of the SdH-period, cyclotron effective mass and effective g-factor in the electron concentration range from $0.19 * 10^{24}\ m^{-3}$ up to $7.75 * 10^{24}\ m^{-3}$ strongly confirm the dispersion relation for the conduction band according to Bodnar's model. The absolute values and angular dependences of the SdH-periods and cyclotron effective masses as well as the angular behaviour of the effective g-factor can be quantitatively described by the Bodnar-model using the following set of primary bandparameters:

$$E_g = (-0.095 \pm 0.010)\ eV$$

$$\Delta = (0.27 \pm 0.03)\ eV$$

$$\delta = (0.095 \pm 0.010)\ eV$$

$$P_{//} = (7.35 \pm 0.05) * 10^{-10}\ eVm$$

$$P_{\perp} = (7.40 \pm 0.10) * 10^{-10}\ eVm.$$

These values of the bandparameters are practically the same as those found by Bodnar from samples in a narrow electron concentration range beyond $1 * 10^{24}\ m^{-3}$ [1]. By incorporating the influence of the quantised free electron term on the effective g-factor, it is possible to obtain a good agreement between experimental and theoretical absolute values of the g*-factor.

We started our investigations of $CdSnAs_2$ by means of the SdH-effect in order to verify the applicability of the Bodnar (Kildal)-model to

$CdSnAs_2$ and to determine the anisotropy of the conduction band in more detail. The present study is as far as we know the first comprehensive one of the conduction band anisotropy of a II-IV-V_2 compound by means of the SdH-effect.
From our measurements on $CdSnAs_2$ samples with $0.19 * 10^{24}\ m^{-3} \leq N \leq 3.97 * 10^{24}\ m^{-3}$ we conclude that the anisotropy of the conduction band is energy dependent. Also for this material the anisotropies of the SdH-oscillation periods, cyclotron effective masses and effective g-factor can be described by the four level Bodnar (Kildal)-model. In this case, however, the bandgap is positive and the crystal field splitting is negative. We obtained the following set of primary band-parameters:

$$E_g = (0.26 \pm 0.01)\ eV$$

$$\Delta = (0.50 \pm 0.05)\ eV$$

$$\delta = (-0.10 \pm 0.01)\ eV$$

$$P_{//} = (8.5 \pm 0.1) * 10^{-10}\ eVm$$

$$P_{\perp} = (8.5 \pm 0.1) * 10^{-10}\ eVm \quad .$$

In contrast to Cd_3As_2, it was impossible to remove the discrepancy between the experimental and calculated values of the g*-factor by taking into account the influence of the quantised free electron term. The difference between experiment and theory might be attributed to neglecting the effect of higher bands on the conduction band. However, the angular dependences of the g*-factor in $CdSnAs_2$ have been measured for only one sample up to now.

The above mentioned results for two compounds belonging to different families, representing an inverted band structure with positive crystal field splitting and a normal level ordering with a negative δ respectively, strongly evidence the general applicability of Bodnar's model for tetragonal NGS.
Apart from a (possibly) small anisotropy in the interband matrix element

for Cd_3As_2, it is clear that the geometry of the Fermi-surface is governed by the magnitude and sign of the crystal field splitting parameter δ and the bandgap E_g. In this respect it would be interesting to investigate tetragonal semiconductors which are expected to exhibit the other two possible combinations of E_g and δ, schematically shown in fig. 2.1. Among the II_3-V_2 compounds, Cd_3P_2 is one of the few candidates combining positive values for both E_g and δ [2,3]. However, due to the wide bandgap of 0.5 eV as compared with the estimated value of $\delta = 0.02$ eV [2] we expect a nearly spherical conduction band even for the lowest attainable electron concentrations. High negative values of δ have been reported for some II-IV-V_2 compounds [4], however none of the known compounds of this family have an inverted band structure. In general semiconducting compounds obey the empirical rule that E_g decreases as the mean atomic number increases. Only a few compounds in the lower part of the periodic system show an inverted structure (i.e. α-Sn, HgTe, Cd_3As_2). $CdSnAs_2$, the "heaviest" of all direct-gap II-IV-V_2 compounds, has still a positive gap. Only $CdSnSb_2$ could be a possible candidate for a negative bandgap. However, its existence is questioned [5].

Examining the angular variation of the SdH-periods carefully we found that energy dependent ellipsoids of revolution alone are not sufficient to describe the geometry of the Fermi-surfaces of Cd_3As_2 and $CdSnAs_2$ in detail. A warping of the Fermi-surface was observed. From the increase of the deviations of the Fermi-surface with increasing electron concentration and the similarity with the deviations from a spherical surface for cubic NGS, we concluded that the warping has to be attributed to the influence of higher bands. Using the approach developed in the literature for HgSe and GaSb [6,7] we were able to explain the angular behaviour of the warping. For this reason we expected an extension of the Bodnar-model with a cubic second order $\vec{k}.\vec{p}$ perturbation to be successful in extracting the higher band-parameters from the observed warping.
An extension of the Bodnar-model to that effect has been studied [8]. It was expected that a fit of the warping data with such an extended model would give higher bandparameters which could be used in turn for

the interpretation of the experimental effective g-factor values of $CdSnAs_2$. Up to now this procedure did not give satisfactory results. Very recently quantum structure calculations by Devreese and Nachtegaele [9] showed warping of the Fermi-surface. In these calculations higher bands have not been considered at all.
Since the warping of the Fermi-surface affects also the angular dependences of the cyclotron effective mass and the effective g-factor it will be necessary to examine how the accuracy of the experimental determination of these quantities can be improved further.

Our SdH-measurements on poly- and monocrystalline samples of $(Cd_{1-x}Mn_x)_3As_2$ with low Mn content ($x \leq 0.05$) clearly show that this mixed crystal system does indeed belong to the group of SMSC.
Our measurements indicate that the primary bandparameters depend strongly on the magnetic ion content of the mixed crystal system. Although the observed anisotropy in the spin-splitting zero temperatures is only small, a rather large anisotropy in the exchange parameter β cannot be excluded from the results on the single crystals. An elaborate quantitative description of the temperature and field dependences of the band structure is hampered by the narrow electron concentration range of the measured samples. For further investigations special attention has to be given to a reduction of the electron concentration.
Measurements of the cyclotron effective mass as function of the electron concentration and the material composition by other methods than the SdH-effect, for instance by measuring the thermo-electric power in a magnetic field, are advisable. From these measurements one might obtain additional information on the primary bandparameters.

Despite the fact that we are only able to give a qualitative interpretation of the observed effects, at this stage, we may state that the system $(Cd_{1-x}Mn_x)_3As_2$ is very promising for a further study of the exchange interaction. This interaction between mobile electrons and localised magnetic ions, expressed by the parameters α and β, is much stronger than that found in other systems of SMSC, such as $Hg_{1-x}Mn_xTe$ (Se) and $Pb_{1-x}Mn_xTe$ (Se).
Recently, it appeared that in the system $Pb_{1-x}Mn_xTe$ (S) the exchange

interaction is not proportional to the macroscopic magnetisation [10,11] which needs a complicated theoretical approach [11]. In our case the electronic effective g-factor follows the macroscopic magnetisation in its dependence on temperature, magnetic field and Mn-content, which means that for the time being the simple mean field theory can be used. This feature together with a high electron mobility makes investigation of the electronic properties of this system by means of magneto-quantum transport effects very attractive.

It is worthwile to study the magnetic interactions in the system $(Cd_{1-x}Mn_x)_3As_2$, particularly how these are affected by the presence of an electron gas of intermediate density. In this respect, it should be mentioned that a spin-glass behaviour has been observed down to very low Mn-concentrations, well below the percolation limit of the system [12].

REFERENCES

[1] J. Thielemann, Ph.D. Thesis, Bayerischen Julius Maximilians Universität, Würzburg (1983).

Thielemann performed magneto-optical measurements with the strip-line technique on Cd_3As_2 samples with $1.5 * 10^{24}\ m^{-3} \leq N \leq 3.5 * 10^{24}\ m^{-3}$, which were grown and prepared in our group. He obtained values of the cyclotron effective mass anisotropy which can only be fitted with the Bodnar-model by using $P_{//} = 6.5 * 10^{-10}$ eVm and $P_{\perp} = 8.8 * 10^{-10}$ eVm. Our measurements of the SdH-period, the cyclotron effective mass and the effective g-factor cannot be described with this parameter set. The discrepancy between the cyclotron effective mass values obtained from SdH- and strip-line measurements has not been solved yet.

[2] J. Cisowski, Phys. Stat. Solidi B111, 289 (1982).

[3] M. Singh, J. Cisowski, P.R. Wallace, J.C. Portal, J.M. Broto, Phys. Stat. Solidi B114, 481 (1982).

[4] J.L. Shay, J.M. Wernick, Ternary Chalcopyrite Semicond., (Pergamon Press, Oxford, 1975), p. 85.

[5] N.A. Goryunova, The Chemistry of Diamond-Like Semiconductors, (Chapman and Hall, London, 1965), p.143.

[6] R.R. Galazka, W.M. Becker, D.G. Seiler, Phys. of Semimetals and Narrow-gap Semicond., ed. Carter and Bate (Pergamon Press, Oxford, 1971), p. 481.

[7] D.G. Seiler, W.M. Becker, Phys. Rev. 183, 784 (1969).

[8] J.T. Devreese, V.E. Van Doren, P.E. Van Camp, private communication.

[9] J.T. Devreese, private communication.

[10] H. Pasher, E.J. Fanter, G. Bauer, W. Zawadzki, M. von Ortenberg, Solid State Commun. 48, 461 (1983).

[11] M. von Ortenberg, Phys. Rev. Lett., to be published.

[12] W.J.M. de Jonge, M. Otto, C.J.M. Denissen, F.A.P. Blom, C. van der Steen, K. Kopinga, J. Magn. & Magn. Mat. 31-34, 1373 (1983).

APPENDIX WARPING OF THE FERMI-SURFACE

Warping of a spherical Fermi-surface is responsible for the observed angular dependences of the period in cubic narrow gap semiconductors. In our materials the Fermi-surface is approximated by an ellipsoid of revolution. Warping of this surface introduces small angular variations of the period in the configurations I, II and III, which in conf. I and II are superimposed on the main angular behaviour of the period described by the Bodnar-model. We treat the observed warping in Cd_3As_2, $CdSnAs_2$ and $(Cd_{1-x}Mn_x)_3As_2$ with a modified model for cubic NGSC, since the observed warping is small and similar in shape to that for spherical Fermi-surfaces.

For isotropic narrow gap materials Kane has used the $\vec{k}.\vec{p}$ method to derive the approximate energy of the conduction band. Neglecting the inversion asymmetry splitting this perturbation calculation results in

$$E = E' + u.\frac{\hbar^2k^2}{2m_o} + v.f_w(\vec{k})\frac{\hbar^2}{2m_o} \qquad (A.1)$$

where

$$u = 1 + a^2A' + b^2M + c^2L'$$

$$v = (b^2-2c^2)\,(L-M-N) \qquad (A.2)$$

$$f_w(\vec{k}) = (k_x^2k_y^2 + k_x^2k_z^2 + k_y^2k_z^2)/k^2 \ .$$

The conduction band eigenvalue E' corresponds to the undisturbed spherical Fermi-surface. The normalised coefficients a, b and c (see ref [18] section 5), which depend on the electron concentration and the primary bandparameters, give the amount of s-like and p-like basis functions in the conduction band wavefunction. The parameters A', L, M, N and L' represent the influence of higher bands. The term $f_w(\vec{k})$ produces a warping of the Fermi-surface. Applying this method to Cd_3As_2, $CdSnAs_2$ and $(Cd_{1-x}Mn_x)_3As_2$ and assuming a small distortion of the Fermi-surface we write:

$$\gamma(E) = \gamma(E') + \left(\frac{d\gamma(E)}{dE}\right)_{E'} (E'-E) \qquad (A.3)$$

with

$$\gamma(E') = f_1(E')(k_x^2 + k_y^2) + f_2(E')k_z^2$$

$$f_1(E') = P_\perp^2[E'(E' + \tfrac{2}{3}\Delta) + \delta(E' + \tfrac{\Delta}{3})] \qquad (A.4)$$

$$f_2(E') = P_{//}^2[E'(E' + \tfrac{2}{3}\Delta)]$$

and

$$(E'-E) = u_B\frac{\hbar^2k^2}{2m_o} + v_Bf_w(\vec{k})\frac{\hbar^2}{2m_o} \; . \qquad (A.5)$$

The parameters u_B and v_B depend on the electron concentration, primary bandparameters and higher bandparameters. Unfortunately the exact functional relations in a, b and c are unknown. The term $f_w(\vec{k})$ is given in eq. A.2.

In calculating the extremal cross-sectional area of the warped Fermi-surface, it is convenient to use a set of polar coordinates k_ρ, φ in the plane perpendicular to the field direction. This is illustrated for the three configurations in fig. A.1. The extremal cross-sectional area perpendicular to the field is then given by

$$S_m = \frac{1}{2}\int_0^{2\pi} k_\rho^2 d\varphi \; . \qquad (A.6)$$

It follows from eqs. A.3-A.5 that for the three configurations k_ρ^2 can be approximated by

$$k_\rho^2 = \frac{\gamma(E')}{f(E',\theta,\varphi)}\left[1 - \frac{\frac{\hbar^2}{2m_o}\left(\frac{d\gamma}{dE}\right)_{E'}(u_B + v_By(\theta,\varphi))}{f(E',\theta,\varphi)}\right] \; . \qquad (A.7)$$

The functions $f(E',\theta,\varphi)$ and $y(\theta,\varphi)$ are different for the three configurations. They are given by:

Configuration I:

$$f(E',\theta,\varphi) = f_1(E')(\cos^2\varphi + \sin^2\varphi\cos^2\theta) + f_2(E')\sin^2\varphi\sin^2\theta$$
$$y(\theta,\varphi) = \sin^2\varphi(\cos^2\varphi + \sin^2\varphi\cos^2\theta\sin^2\theta) \qquad (A.8)$$

Configuration II:

$$f(E',\theta,\varphi) = f_1(E')(\sin^2\varphi + \cos^2\varphi\cos^2\theta) + f_2(E')\sin^2\varphi\sin^2\theta$$
$$y(\theta,\varphi) = \frac{1}{4}\{\cos^4\varphi(10\cos^2\theta - 3\cos^4\theta - 1) + 2\cos^2\varphi(1 - 3\cos^2\theta) + 1\} \qquad (A.9)$$

Configuration III:

$$f(E',\theta,\varphi) = f_1(E')\cos^2\varphi + f_2(E')\sin^2\varphi$$
$$y(\theta,\varphi) = \cos^2\varphi(\sin^2\varphi + \cos^2\varphi\sin^2\theta\cos^2\theta) \qquad (A.10)$$

The SdH-oscillation frequency (or period) is obtained from

$$F(\theta) = \frac{1}{P(\theta)} = \frac{\hbar}{2e} S_m \,. \qquad (A.11)$$

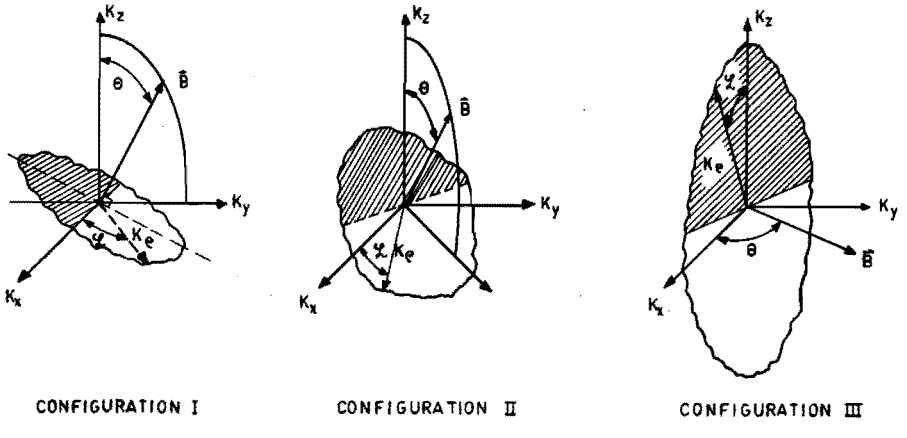

Fig.A.1. Definition of the configurations.

SAMENVATTING

Het in dit proefschrift beschreven onderzoek had tot doel na te gaan in hoeverre de anisotropie van de geleidingsband van de tetragonale gedegenereerde n-type halfgeleiders Cd_3As_2 en $CdSnAs_2$ in een groot elektronenconcentratiegebied beschreven kan worden met het door Bodnar en Kildal ontwikkelde 4-bandenmodel voor tetragonale halfgeleiders. Daartoe is door middel van het SdH (Shubnikov-de Haas)-effect de vorm van het Fermi-oppervlak van de geleidingsband van deze materialen onderzocht. Voor de mengkristallenreeks $(Cd_{1-x}Mn_x)_3As_2$ met $x \leq 0.05$ is door middel van het SdH-effect nagegaan in hoeverre deze verbindingen behoren tot de groep van de zogenaamde semi-magnetische halfgeleiders en of het voor deze materialen ontwikkelde bandenmodel voldoet.

De bandenmodellen worden in het kort in hoofdstuk II besproken. Op basis van het door Bodnar ontwikkelde 4-bandenmodel en de door Wallace gegeven uitbreiding hiervan voor quantiserende magneetvelden wordt in dit hoofdstuk een bandenmodel voor tetragonale semi-magnetische halfgeleiders voorgesteld. In dit model wordt rekening gehouden met de exchange interactie tussen de vrije ladingsdragers en de elektronen in de 3d-schillen van de mangaanionen.

In hoofdstuk III wordt summier ingegaan op de achtergronden van het SdH-effect. Onder het SdH-effect verstaat men de oscillaties in de magnetoweerstand die periodiek zijn in het reciproke magneetveld. De oscillaties worden veroorzaakt door fluctuaties in de toestandsdichtheid en de verstrooiing van elektronen in de geleidingsband. In het algemeen kan het SdH-effect worden waargenomen bij lage temperaturen in quantiserende magneetvelden aan gedegenereerde halfgeleiders. Uit metingen van de periode en de temperatuurafhankelijkheid van de amplitude van de oscillaties als functie van de oriëntatie van het magneetveld, kan de vorm van het Fermi-oppervlak van de geleidingsband worden afgeleid.

De benodigde experimentele opstellingen zijn in hoofdstuk IV beschreven. In dit hoofdstuk wordt tevens aangegeven hoe de experimentele gegevens zoals de hoekafhankelijkheid van de SdH-periode, de cyclotron effectieve massa en de effectieve g-factor uit de SdH-signalen verkregen

kunnen worden.

De resultaten van de SdH-metingen aan Cd_3As_2, $CdSnAs_2$ en $(Cd_{1-x}Mn_x)_3As_2$ worden in hoofdstuk V gepresenteerd. Het blijkt dat onze metingen aan Cd_3As_2 en $CdSnAs_2$ in het hele beschikbare elektronenconcentratiegebied uitstekend beschreven kunnen worden met het 4-bandenmodel van Bodnar (en Kildal). De door ons waargenomen afwijkingen ten opzichte van het Bodnar-model voor zowel Cd_3As_2 als $CdSnAs_2$ worden veroorzaakt door warping van het Fermi-oppervlak.
De SdH-metingen aan $(Cd_{1-x}Mn_x)_3As_2$ mengkristallen met $x \leq 0.05$ bevestigen het verwachte semi-magnetische karakter van dit materiaal. De voorlopige interpretatie van onze metingen in het bandenmodel voor tetragonale semi-magnetische halfgeleiders duidt op een opvallend sterke wisselwerking tussen de gelocaliseerde spins van de Mn-ionen en de spins van de geleidingselektronen. De primaire bandparameters lijken sterk af te hangen van de samenstelling van het materiaal. Een eventuele anisotropie van de exchangewisselwerkingsconstantes kan niet worden uitgesloten. Door de te kleine spreiding in elektronenconcentraties is het niet mogelijk in dit stadium meer uitgebreide kwantitatieve conclusies te trekken.

NAWOORD

De velen die, direct of indirect, hebben meegewerkt aan het tot stand komen van dit proefschrift, wil ik hier danken.
Mijn erkentelijkheid geldt, met excuses aan allen die onvermeld blijven, onder meer:

- *Prof.dr. M.J. Steenland voor zijn persoonlijke belangstelling in de afgelopen jaren.*
- *Frans Blom voor zijn waardevolle suggesties en zijn prettige manier van begeleiden.*
- *Cees van Es voor de vele discussies, het rekenwerk, de mooie tekeningen en zijn vriendschap.*
- *Peter Nouwens voor de vele preparaten.*
- *Jacek Kossut voor de leerzame samenwerking.*
- *Cees de Meyer, André Dommels en Cees Bouwens voor hun belangrijke bijdragen.*
- *Alle overige leden en ex-leden van de groep Halfgeleiderfysica voor de jarenlange samenwerking.*
- *Marion Rijks en Rianne van Vinken voor het typewerk.*
- *Ruth Gruyters voor het bewerken van enkele tekeningen.*

LEVENSBERICHT

8-11-1953	*Geboren te Kloosterzande*
1971	*Eindexamen HBS-B, Jansenius-lyceum te Hulst.*
1971-1979	*Studie aan de Technische Hogeschool te Eindhoven, afdeling der Technische Natuurkunde. Afgestudeerd in de groep Halfgeleiderfysica onder leiding van Prof.dr. M.J. Steenland.*
1979-1983	*Wetenschappelijk assistent aan de Technische Hogeschool te Eindhoven, in de groep Halfgeleiderfysica onder leiding van Prof.dr. M.J. Steenland.*

STELLINGEN

1. De anomale magneetveldafhankelijkheid van de amplitude van het Shubnikov-de Haas effect in HgSe en $Hg_{0.999}Mn_{0.001}Se$ wordt door Reifenberger en Schwarzkopf geïnterpreteerd in een model voor magnetic breakdown. Deze verklaring wettigt nog niet hun conclusie dat de geometrie van het Fermi-oppervlak temperatuurafhankelijk wordt door toevoeging van Mn aan HgSe.

   R. Reifenberger, D.A. Schwarzkopf, Phys. Rev. Lett. 50, 907 (1983).

2. Skok et al. verklaren het door hen bij lage magneetvelden waargenomen afwijkend gedrag van de magnetoweerstand van InSb m.b.v. magnetische quantisatie aan het oppervlak. Deze interpretatie is aan twijfel onderhevig, omdat de elektrische contacten soortgelijk afwijkend gedrag kunnen veroorzaken.

   É.M. Skok, S.A. Studenikin, H. Hefel, H. Pascher, JETP Lett. 37, 554 (1983).

3. De door Chuiko in navolging van Karavaev en Borisenko bepleite uitbreiding van het 4-bandenmodel voor tetragonale halfgeleiders door invoering van een anisotrope spin-baan koppelingsparameter, lijkt - gegeven de nauwkeurigheid waarmee deze grootheid experimenteel te bepalen is - niet zinvol.

   G.P. Chuiko, Sov. Phys. Semicond. 17, 301 (1983).
   G.F. Karavaev, S.I. Borisenko, Sov. Phys. J. 6, 712 (1978).

4. Het verdient aanbeveling de in de theoretische stromingsleer gebruikte Boussinesq-benaderingen te catalogiseren en bij gebruik te vermelden welke benadering gekozen is.

   J. Lighthill, Waves in Fluids, (Cambridge University Press, London 1978), p. 288.

5. Het feit, dat de waargenomen groottes van de renormalisatie van de soliton-rustenergie in verbindingen met duidelijk verschillende waarden van het spin-quantumgetal S vrijwel gelijk zijn, wijst niet in de richting van een interpretatie van dit verschijnsel m.b.v. quantumcorrecties.

   J.K. Kjems, M. Steiner, Phys. Rev. Lett. 41, 1137 (1978).
   J.P. Boucher, L.P. Regnault, J. Rossat-Mignod, J.P. Renard, J. Bouillot, W.G. Stirling, J. Appl. Phys. 52, 1956 (1981).
   K. Kopinga, A.M.C. Tinus, W.J.M. de Jonge, to be published in Phys. Rev. B29 (1984).

6. Het effectueren van de bij de bestelling van de Patriot-luchtdoelraketten bepleite two-way-street overeenkomsten kan leiden tot een ongewenste toename van de Nederlandse betrokkenheid bij de internationale wapenwedloop.

7. Het principiële karakter van de te nemen beslissing inzake de plaatsing van kruisraketten in Nederland wordt aangetast door de discussie over het aantal raketten.

Eindhoven, 10 april 1984 J.J. Neve